ABSTRACT

MCFARLAND, DANIEL CLINTON. Spatial Dependency of Muscular and Joint Loading During Dynamic Submaximal Pushing and Pulling. (Under the direction of Drs. Katherine Saul and Scott Ferguson).

This dissertation evaluates how workspace design impacts muscular demand and joint loading during dynamic submaximal push-pull tasks. Work involving extensive pushing and pulling is associated with higher frequency of shoulder complaints. While reports of shoulder muscle demand during submaximal isometric tasks are abundant, dynamic submaximal push-pull exertions are not well understood. First, the effects of task type and task target on muscle demand (weighted EMG average) of surface glenohumeral muscles were evaluated. Seventeen healthy young adults performed unimanual and bimanual pushes and pulls to 3 thoracohumeral elevations (20º, 90º, 170º) and 4 elevation planes (0º, 45º, 90º, 135º) with loading at 15% of isometric push-pull capacity. Pulling required less demand than pushing ($p<0.0001$). Muscle demand varied more with elevation than elevation plane. The lowest target had highest demand for pulling ($p<0.01$), and the most elevated target had highest demand for pushing ($p<0.0001$). Working above the shoulder is known to increase demand during isometric tasks, however, these results suggest that for dynamic tasks working against gravity has a larger effect on demand than task target.

Next, experimental data was used to inform computational simulations of push-pull tasks to evaluate the spatial dependency of glenohumeral stability. Degenerative wear to the glenoid from repetitive loading can reduce effective concavity depth and lead to future instability. Therefore, workspace design should consider glenohumeral stability to prevent initial wear. While glenohumeral stability has been previously explored for activities of daily living including push-pull tasks, whether stability is spatially dependent is unexplored. A subset of the bimanual

and unimanual push-pull tasks were simulated including tasks to 4 horizontal targets (planes of elevation: 0º, 45º, 90º, and 135º) at 90º thoracohumeral elevation and 3 elevation targets (thoracohumeral elevations: 20º, 90º, 170º) at 90º plane of elevation. The lateral 45º horizontal target was most stable regardless of exertion type and would be the ideal target placement when considering stability. This target is likely more stable because the applied load acts essentially perpendicular to the glenoid, limiting shear force production. The cross-body 135º horizontal target was particularly unstable for unimanual pushing, and the applied force direction for this task is essentially parallel to the glenoid, likely creating shear forces. Pushing was less stable than pulling (all targets except sagittal 170º for both unimanual and bimanual and horizontal 45º for bimanual) ($p<0.01$), which is consistent with prior reports. There were limited stability benefits to task placement for pushing, and larger stability benefits may be seen from converting push tasks to pull rather than optimizing task layout. There was no difference in stability between bimanual and unimanual tasks, suggesting no stability benefit to bimanual operation.

Lastly, a comparison was made among modeling techniques that attempt to account for active glenohumeral stabilization in inherently stable musculoskeletal models. Most upper extremity musculoskeletal models represent the glenohumeral joint with an inherently stable ball-and-socket, but the biological joint requires active muscle coordination for stability. Sensitivity of common predicted outcomes (net glenohumeral reaction force, rotator cuff activations, and instability) to different implementations of active stabilizing mechanisms (constraining net joint reaction direction and incorporating surface EMG) were evaluated. Both EMG and reaction force constraints successfully reduced joint instability, however other

outcomes were more sensitive to EMG constraints, which also tended to overconstrain the model, leading to poor tracking and simulation failure. Therefore, force constraints may be more robust when representing stability.

This dissertation provides new information characterizing the spatial dependency of muscular demand and glenohumeral stability during dynamic submaximal push-pull tasks. Furthermore, the evaluation of modeling techniques lays the foundation for future studies evaluating glenohumeral instability for other functional tasks.

Spatial Dependency of Muscular and Joint Loading During Dynamic Submaximal Pushing and Pulling

by
Daniel Clinton McFarland

A dissertation submitted to the Graduate Faculty of
North Carolina State University
in partial fulfillment of the
requirements for the degree of
Doctor of Philosophy

Mechanical Engineering

Raleigh, North Carolina

2018

APPROVED BY:

_____	_____
Dr. Katherine Saul Co-Chair of Advisory Committee	Dr. Scott Ferguson Co-Chair of Advisory Committee
_____	_____
Dr. Matthew Bryant	Dr. Chang Nam

DEDICATION

To my parents, Audrey S. and Daniel D. McFarland, thank you for all the support and guidance you gave me over the years.

BIOGRAPHY

Daniel C. McFarland was born in Mesa Arizona and grew up in Charlotte, North Carolina. Daniel was homeschooled until high school where he attended David W. Butler High School. Upon graduation, he attended and graduated Northwestern University in 2013 with his B.S. in Mechanical Engineering. Subsequently, he began his graduate studies at North Carolina State University in the department of Mechanical and Aerospace Engineering as part of the direct-track PhD program in 2014. He will complete the requirements for his Ph.D. in Mechanical Engineering in July 2018.

ACKNOWLEDGMENTS

First and foremost, I would like to thank Dr. Katherine Saul. Without your support and guidance, I would have abandoned my graduate education long ago. Thank you for your patience and guidance as you helped me become the researcher I am today. I would also like to thank all the member of my committee for their continual support and guidance. I would like to thank the CFD Research corporation for funding much of the research presented here.

I would like to thank all my lab mates throughout the years. Emily McCain and Michael Poppo, thank you for making science fun. Nikhil Dixit, it has been a pleasure working with you, and I will always remember the fun we had on our conference trips. Matthew Berno, it has been fun getting to know you and your unique hobbies over the last year. And Alex Brynildsen and Lauren Levine, thank you for helping post-process much of the data that comprises this work.

Lastly, I would like to thank my friends and family who were there for me along the way. Mom and Dad, without your support throughout the years none of this would be possible. My sisters, Jennifer and Kelley McFarland, thank you for continually encouraging me to be a better person. Ryan McFarland and Martin Romo, I could not ask for better roommates. Thank you for distracting me from work and keeping me sane. And Scout, thank you for being the best dog in world. Lastly, Alison Ashe, thank you for your continual love and support.

TABLE OF CONTENTS

LIST OF TABLES

LIST OF FIGURES

CHAPTER 1

Background

Work-related Musculoskeletal Disorders

Work-related musculoskeletal disorders (WMSD) are a group of painful disorders to muscle, nerve and tendon that develop gradually due to overuse of the musculoskeletal system. These disorders do not include traumatic injuries such as tearing muscle or tendon during a workplace accident. WMSD is a broad category of disorders, and in this work, we will focus on WMSD that occur at the shoulder such as sprains, strains, and rotator cuff tendonitis.

Physically demanding occupations such as military service have high occurrence of musculoskeletal disorders, with active duty non-deployed service members having an injury rate of 62.8% per person-years (Hauret et al., 2010). In general, repetitive motion, excessive force, and working in awkward postures are associated risk factors for WMSD; however, each type of WMSD has different risk factors associated with it (da Costa and Vieira, 2010). For the shoulder, working at or above shoulder height is a well-documented risk for muscle fatigue and musculoskeletal disorders (Fredriksson et al., 2002; Grieve and Dickerson, 2008; Hagberg and Wegman, 1987; Roquelaure et al., 2009; Wiker et al., 1989).

WMSD place a large burden on the economy and workers' health, accounting for 29-35% of all occupational injuries and illnesses involving days away from work in private industries (Bhattacharya, 2014). The Bureau of Labor Statistics reports the number of WMSD cases in the United States was 335,390 in 2007 (Bhattacharya, 2014), and it is estimated that 20% of disabling injuries and 35% of non-disabling injuries go unreported, suggesting that the actual number of WMSD is much higher (Leigh et al., 2001). Annual direct costs of musculoskeletal disorders including non-work-related disorders have been estimated at $215 billion (National

Academy of Science, 2001), and estimates of total cost from work-related MSD range between $45 and $54 billion (National Academy of Science, 2001). As a result of these high costs, WMSD is the most expensive form of work disability (Thiehoff, 2002). Of these disorders, shoulder injuries in particular are taxing on worker health and the economy. A study of worker compensation claims found that shoulder claims resulted in the second highest total cost behind lumbar spine claims and that 30.6% of claims involving the shoulder resulted in over seven days of lost work (Dunning et al., 2010).

Ergonomics of Pushing and Pulling

In ergonomics, pushing is traditionally defined as an exertion in which the majority component of the resultant force is directed horizontally away from the body whereas pulling is defined in the same manner except the force is directed toward the body (Hoozemans et al., 1998). Pushing and pulling are frequently performed in many different professions (Hoozemans et al., 2002). According to the Bureau of Labor Statistics, 1/3 of employees in the USA are exposed to push-pull tasks at work (Lind, 2018). Baril-Gringras and Lortie (1995) estimate that push-pull exertions are present in nearly half of all manual material handling tasks, i.e. moving or handling objects. Pushing and pulling, however, have been identified as problematic exertions for the musculoskeletal system. Ergonomics research suggests that 9-18% of low back injuries are associated with pushing and pulling (Hoozemans et al., 1998). Furthermore, frequency of push-pull tasks in the workplace has been linked with shoulder complaints (Hoozemans et al., 2002). Therefore, to prevent the occurrence of push-pull related musculoskeletal disorders, effort has been made to characterize the biomechanical demand of push-pull tasks. Here we provide a summary of these efforts.

Strength Capacity

Determining strength capacity for a task can help ergonomists develop workplace guidelines for maximum acceptable forces, such as Snook tables (Snook and Ciriello, 1991). Some workplace guidelines, like Snook tables, are based on psychophysical methods of determining maximal capacity, where subjects self-select workloads that they could sustain for 8 hours without straining themselves (Boocock et al., 2006; Snook and Ciriello, 1991). More recently, ergonomic tools like 3DSSPP (University of Michigan, Ann Arbor, MI) have been based off quantitative strength measurements rather than psychophysical evaluations. To help inform such tools and guidelines, several studies have characterized one-handed manual force capacity in diverse scenarios (Das and Wang, 2004; Fischer et al., 2013; La Delfa et al., 2014; La Delfa and Potvin, 2016; J. Lin et al., 2013; MacKinnon, 1998; Roman-Liu and Tokarski, 2005). The majority of strength literature focuses on isometric strength capacity rather than isokinetic strength capacity, and relevant findings from these isometric studies are summarized here. Inferiorly directed forces have been reported to be the strongest exertion direction for both males and females (Chow and Dickerson, 2009; Fischer et al., 2013; La Delfa et al., 2014; La Delfa and Potvin, 2016). Chow and Dickerson (2009) suggest that mass of the arm is a contributing factor in increasing strength capacity in this direction. After the inferior direction, those studies reported that strength capacity was greatest in either the anterior (pushing) or posterior (pulling) direction. Studies directly comparing isometric push and pull strength, however, have reported mixed results on which exertion is stronger (Chaffin et al., 1983; Chow and Dickerson, 2016; Das and Wang, 2004; Kumar, 1995; La Delfa and Potvin, 2016). Das and Wang (2004) and Kumar (1995) have reported stronger pull strength; however, in Kumar (1995) pushing and pulling were measured in a standing posture with the legs stabilized, while Das and Wang (2004)

used seated tests without a torso restraint. On the other hand, Chaffin et al. (1983) and Chow and Dickerson (2016) both evaluated standing push-pull capacity without external stabilization of the lower limb and found push strength to be greater. Experimental task conditions vary between these studies, and different task conditions are known to influence strength capacity (Chow and Dickerson, 2009; Das and Wang, 2004; Fischer et al., 2013; La Delfa and Potvin, 2016); therefore, strength data needs to be interpreted in context of the experimental conditions.

Since experimental conditions can vary greatly between studies, knowledge of what factors influence strength is critical when interpreting results. Posture and task location have a strong influence on isometric strength capacity (Chow and Dickerson, 2009; Das and Wang, 2004; La Delfa and Potvin, 2016; J. Lin et al., 2013). La Delfa and Potvin (2016) suggest that maximal capacity is higher when the direction of applied force is parallel to the vector from the shoulder to the knuckles and weakest when the direction of force is perpendicular to this vector. For standing pulling, strength capacity is related to handle height, decreasing with increased handle height (J. Lin et al., 2013). Effects of sitting or standing on strength capacity have been reported with mixed results (Chow and Dickerson, 2009; Das and Wang, 2004). Chow and Dickerson (2009) report only marginal differences in strength capacity between sitting and standing whereas Das and Wang (2004) report standing strength as 79% of seated strength. These differing results may deal more with stability rather than strength, as Chow and Dickerson (2009) had participants sit in a stool without back support whereas Das and Wang (2004) had subjects sit in a chair. Stability and foot placement in standing exertions are known to influence strength capacity (Fischer et al., 2013). For example, when balance was removed as a biomechanical constraint in standing pull exertions, strength capacity increased by 3 folds (Fischer et al., 2013). Therefore, stability may also influence strength capacity in seated

exertions as well. Other experimental factors including handle stability, orientation, and friction have been shown to influence strength (Seo and Armstrong, 2009; Seo et al., 2010). For example, handles oriented perpendicular to applied force direction result in greater strength capacity than handles oriented parallel to the applied force direction (Seo et al., 2010).

Additionally, differences in isometric unimanual strength capacity exist between genders (Das and Wang, 2004; J. Lin et al., 2013). Studies agree that female strength capacity is less than that of males, however, the degree of reported strength difference varies. Lin et al. (2013) report female pulling strength was 70% of male pulling strength, whereas Das and Wang (2004) report female strength capacity was 56% of male strength capacity when considering both pushing and pulling.

These studies summarized thus far have all been isometric unimanual tasks; however, task speed also affects strength capacity during dynamic tasks (Calé-Benzoor et al., 2016a; Garg and Beller, 1990; Imrhan and Ramakrishnan, 1992; Mital et al., 1995). Several studies show that pull strength decreases with increased task speed (Garg and Beller, 1990; Imrhan and Ramakrishnan, 1992; Mital et al., 1995). Calé-Benzoor et al. (2016a) compared both dynamic pushing and pulling strength at 2 task speeds (12.22 cm/s and 36.67 cm/s) and found similar strength capacity between pushing and pulling at the low task speed. However, at the high task speed, pulling capacity was higher than pushing.

Furthermore, strength differences exist between bimanual and unimanual exertions (Chaffin et al., 1983; Warwick et al., 1980). Chaffin et al. (1983) report that one-arm push and pull strength was 73% of bimanual strength, which suggests that push-pull force capacity does not depend solely on arm strength. Warwick et al. (1980) also report unimanual strength greater than 50% of the bimanual capacity. It is important to note that both these studies evaluated

standing exertions, so lower limb contributions may influence these results. To the author's knowledge, however, no other studies have directly compared bimanual and unimanual strength capacity. Other studies evaluating only bimanual exertions suggest that strength capacity for bimanual tasks follows similar trends to unimanual exertions. For example, like unimanual tasks, there are mixed results whether bimanual pushing or pulling capacity is stronger. On one hand, several studies report that bimanual push strength is greater than pull strength (Chaffin et al., 1983; Chow and Dickerson, 2016; Warwick et al., 1980). The most recent study by Chow and Dickerson (2016) report that total hand force for bimanual pulling was 68% of pushing. On the other hand, other studies report that pulling resulted in greater strength than pushing (Kumar et al., 1995; Kumar, 1995). These studies, however, stabilized the lower extremity of subjects whereas the other studies did not. Bimanual strength is also affected by task conditions, and absolute strength capacity results need to be interpreted in context of the experimental condition. Several studies show that task location and posture also affect bimanual strength capacity (Chow and Dickerson, 2016; Kumar et al., 1995). Both studies show that a 100cm handle height is associated with higher manual force capacity when compared with 150cm handle height, which agrees with unimanual results of Lin et al. (2013) that show increased height reduces unimanual capacity. Task speed influences bimanual strength capacity, with isokinetic strength being less than isometric (Kumar et al., 1995). Unimanual studies did not compare isometric strength capacity with isokinetic strength capacity but do report decreasing capacity with increased task speed (Garg and Beller, 1990; Imrhan and Ramakrishnan, 1992; Mital et al., 1995). Handle orientation, however, has limited to no influence on bimanual strength capacity, in contrast to unimanual results (Chow and Dickerson, 2016; J. Lin et al., 2012; Okunribido and Haslegrave, 2008).

Differences in strength capacity between sexes also exist for bimanual tasks with females having less absolute strength capacity than male counterparts (Chaffin et al., 1983; Chow and Dickerson, 2016; Kumar et al., 1995). Chow and Dickerson (2016) report that female push strength was 65% of male push strength and female pull strength was 70% of male pull strength, whereas Kumar et al. (1995) report less striking differences with female strength ranging from 1-29% lower than male strength capacity depending on task conditions.

Electromyography and Muscle Demand

Electromyography (EMG) is a tool frequently used by ergonomists to characterize task demand at the muscular level, since increases in muscular demand are linked with shoulder pain and discomfort (Wiker et al., 1989). Demand on individual muscles (Bennett et al., 2011; Kao et al., 2015; MacKinnon and Vaughan, 2005) and total muscle demand (Chopp et al., 2010; McDonald et al., 2012; Meszaros et al., 2018) during push-pull tasks have been evaluated using EMG; total muscle demand is typically calculated as a sum or average of individual EMG signals (Nadon et al., 2016). Frequently, averaged muscular demand is calculated as a weighted average of individual EMG signals, with physiological cross-sectional area (PCSA) as the weighting factor (Chow et al., 2017; Meszaros et al., 2018; Nadon et al., 2016).

$$\sum_{i=1}^{n} Norm\_EMG_i \left[\frac{PCSA_i}{\sum_{i=1}^{n} PCSA_i}\right]$$

PCSA is the cross-sectional area of muscle perpendicular to muscle fibers and is related to a muscle's maximum capacity through specific tension of muscle. By weighting individual EMG signals according to PCSA, the average demand accounts for differences in force-generating capacity between each muscle.

Muscle demand has been previously reported for push-pull tasks with mixed results, but differences between studies may be explained by muscle selection. Multiple muscles and muscle compartments span the shoulder complex, but experimental EMG studies often only measure a subset of muscles due to experimental constraints such as number of available EMG channels. Selecting more muscles that are involved in pushing than pulling, for example, will artificially raise the demand of pushing, skewing the comparison; therefore, it is important to consider muscle section when evaluating results of EMG studies. Several studies on dynamic cart pushing report that pushing requires less demand at the muscular level than pulling (Bennett et al., 2011; Kao et al., 2015; C. Lin et al., 2010). However, these studies evaluated a limited selection of upper limb "push" muscle. For example both Bennett et al. (2011) and Lin et al. (2010) only measure anterior deltoid and no other push muscles such as pectoralis major or triceps brachii. In a full-body two-handed maximum push-pull study, Chow et al. (2017) evaluated a more extensive selection of upper limb muscles (pectoralis major, biceps brachii, middle deltoid, middle trapezius, and triceps brachii)and found that pushing resulted in 82% higher EMG activation in comparison to pulling. These studies highlight the importance of evaluating muscle selection when comparing muscular demand results.

Although many push-pull tasks in the workplace are performed while standing or unstabilized, prior work reports that nevertheless the upper limb muscles are still the primary muscles engaged during these tasks. In the examination by Bennett et al. (2011), EMG signals of both lower limb and upper limb muscles, and reported that changes in push-pull technique had a greater impact on muscle demand of the upper limb muscles, highlighting the importance of evaluating upper extremity muscles rather than lower limb muscles during push-pull tasks even when standing. Furthermore, in a study of submaximal dynamic pulling without stabilization of

the torso, MacKinnon and Vaughan (2005) reported that shoulder complex muscles worked at a higher percent of the maximum voluntary capacity (MVC) than did trunk muscles. Therefore, muscle demand of the shoulder complex during pushing and pulling is critical under a variety of performance conditions.

Muscle demand for the shoulder complex is influenced by both exertion direction and task location, but exertion direction has a stronger influence on demand than does task location (Chopp et al., 2010; Cudlip et al., 2016; Meszaros et al., 2018). . Two prior studies that focused solely on overhead isometric exertions of 30 and 40N found that backward (posteriorly directed pull) exertions resulted in highest muscular demand (Chopp et al., 2010; Cudlip et al., 2016) whereas Meszaros et al. (2018) evaluated more spatially varied task targets at varying loads between 20 and 60N and report that upward exertions were the most demanding. All three studies, however, concurred that downward exertions were the least demanding which agrees with isometric strength capacity studies that report inferiorly directed exertions are the strongest (Chow and Dickerson, 2009; Fischer et al., 2013; La Delfa et al., 2014; La Delfa and Potvin, 2016). Furthermore, Meszaros et al. (2018) found that increasing submaximal loading increased muscle demand regardless of exertion direction, but exertion direction had a dominant influence on demand, that is, downward exertions at the highest load were less demanding than upward exertions at the lowest load. Therefore, more benefits in reducing muscular demand may be seen by first considering task direction if possible rather than just optimizing task location.

Muscular demand during seated isometric exertions is spatially dependent on task location (McDonald et al., 2014; McDonald et al., 2012; Meszaros et al., 2018; Nadon et al., 2016), with superior tasks generally increasing muscular demand (McDonald et al., 2014; McDonald et al., 2012; Meszaros et al., 2018; Nadon et al., 2016). Downward and right exertions

for right-handed subjects, however, did not show an increase in demand with more elevated targets (McDonald et al., 2014; Nadon et al., 2016). Lateral location also affects demand, with increased demand for pushing, pulling, and upward exertions as task location moved laterally to either side of the subject (McDonald et al., 2012; Nadon et al., 2016); horizontal task placement influenced muscular demand more than superior/inferior and anterior/posterior target location during pushing and pulling (McDonald et al., 2012). When contextualizing these results, it is important to note that pushing and pulling are defined as purely anterior and posterior forces in this study. Another noteworthy finding from this study was that pulling was more spatially influenced than pushing. Similarly, upward exertions showed more spatial dependency than downward exertions (Nadon et al., 2016). These studies evaluated the effects of spatial location throughout the reachable workspace; other studies have considered the effects of task location in purely overhead work (Chopp et al., 2010; Cudlip et al., 2016). From Cudlip et al. (2016), it was concluded that overhead work should remain within 15 cm in the medial/lateral direction of their pelvis since substantial changes in muscular activity occurs beyond this threshold. This is consistent with isometric exertions (pushing, pulling, upward, downward, and leftward exertions for right handed subjects) when evaluated over the entire reachable workspace (McDonald et al., 2014; McDonald et al., 2012; Nadon et al., 2016). Furthermore, both of these overhead studies found that targets placed farther in front of subjects reduced muscular demand for pulling, but increased demand for upward exertions which is consistent with results from Nadon et al. (2016) and McDonald et al. (2012) who evaluated these exertions as part of evaluation of the entire reachable workspace. Furthermore, Chopp et al. (2010) found that workspaces scaled to subject anthropometry reduced muscle demand. While the work discussed thus far evaluated seated tasks, spatial dependency also affects demand during full body isometric maximal exertions. In

one such report, pulling with a handle at waist height and pushing with the handle at shoulder height were less demanding than other handle heights (Chow et al., 2017).

Lastly, sex differences exist in muscle demand for push-pull tasks (Chow et al., 2017; Cudlip et al., 2015). Both of these studies report that females require higher activations to perform the same tasks. Chow et al. (2017) accounted for differences in strength capacity between men and women by dividing EMG averages by maximal force capacity; however, differences in activation still persisted, indicating that women were less efficient at converting muscular activity to force. Chow et al. (2017) did note that tasks were performed at fixed handle heights, and differences in anthropometry between males and females may contribute to these differences. Lin et al. (2013) also compared sex differences for cart pushing tasks, but found no significant difference between sexes; however, their sample size was much smaller than the other studies, and this report may be limited due to statistical power.

In summary, the majority of the muscle demand studies reviewed here emphasized isometric exertions or full body dynamic tasks. Loading under these conditions cannot be directly applied to isolated arm dynamic push-pull tasks since EMG and force exertion under dynamic conditions can be much different from those recorded isometrically (Antony and Keir, 2010; Kumar, 1995), and foot placement influences pushing force (Rancourt and Hogan, 2001). Therefore, there is still a need to evaluate muscle demand during isolated arm dynamic push-pull tasks. Dynamic tasks that could benefit from this ergonomic analysis include assembly line work or machine operation where objects and/or levers are pulled or pushed. While workers are typically unconstrained in industrial setting and may rely on torso movement to complete tasks, isolating the upper extremity isolates the contributions of those muscles crossing the shoulder, which are most likely to be injured in the workplace. Prior work has also reported that even when

the torso and lower limb are unconstrained, upper limb muscle demand is most affected by task requirements. Further, isolated shoulder movement will require more extreme motion that may represent the worst-case scenarios if operators were constrained, i.e. by a seatbelt during machine operation.

Joint Loading

Overuse and repetitive joint stress can lead to joint wear and disease such as glenohumeral arthritis; therefore, ergonomic design should consider how tasks influence joint loading. Analysis of joint loading during push-pull tasks, however, is studied less extensively in ergonomics literature. Several of the studies that evaluate joint loading during pushing and pulling tasks focus solely on loading of the low back (Knapik and Marras, 2009; Lett and McGill, 2006; Resnick and Chaffin, 1995; Weston et al., 2017). Net joint moments at the shoulder have been evaluated for a few push-pull studies (Chow and Dickerson, 2016; La Delfa and Potvin, 2016; Laursen and Schibye, 2002). From these studies, resultant shoulder moments have been shown to correspond moderately with manual arm strength (Chow and Dickerson, 2016; La Delfa and Potvin, 2016). Furthermore, shoulder moments - like manual strength - are also influenced by task conditions such as force direction, handle height, and handle orientation (Chow and Dickerson, 2016). Whether pushing or pulling causes higher shoulder moments, however, appears to depend on task conditions (Chow and Dickerson, 2016; Laursen and Schibye, 2002). Chow and Dickerson (2016) found that shoulder moments were higher during pushing than pulling for bimanual isometric tasks. On the contrary, Laursen and Schibye (2002) reported pulling resulted in higher shoulder torques when comparing dynamic pulling and pushing of two-wheeled containers. These studies, however, only consider net joint moments,

and do not consider how the net reaction force acts at the glenohumeral joint. The direction of the net joint reaction force is critical to glenohumeral stability (see section 1.3). Nimbarte et al. (2013) evaluated the resultant joint reaction force at the glenohumeral joint during dynamic cart pushing tasks, and found that higher transverse to compressive forces act at the glenohumeral joint, indicating stability risks for cart pushing tasks. Additionally, they found that reaction forces at the glenohumeral joint were influenced by task conditions including cart weight and walkway gradient. Marchi et al (2014) calculated a stability index related to the direction of the net reaction force for hand positioning tasks and report that pushing resulted in less stable reactions than pulling. Furthermore, Vidt et al. (2014) found that the net joint reaction force was directed within the glenoid for entire duration of a functional pull tasks, further suggesting that pulling is a stable motion. Future work evaluating how task conditions such as task location influence the net joint reaction at the glenohumeral joint would provide valuable information to improve the design of workspaces.

Applications of Ergonomic Analyses

Strength capacity studies have been applied to the design of workplaces by informing guidelines for maximum acceptable forces for particular tasks (Snook and Ciriello, 1991). These studies take the approach of evaluating a range of specific tasks and developing tables of maximum acceptable forces based on task condition. Many of these studies are based on psychophysical methods of determining capacity, where subjects self-select workloads that they feel that they sustain. More recently, ergonomic software packages have been developed that incorporate quantitative strength measurements. One powerful and commonly used tool is 3DSSPP (University of Michigan, Ann Arbor, MI) (Chaffin, 1997). This software package

predicts static strength requirements for tasks such as pushes and pulls based on input data of posture, force parameters and subject anthropometry. Outputs include percentages of men and women who have the strength to perform the tasks and data comparisons to NIOSH guidelines. Such software packages are useful when designing workspaces to determine if novel tasks are too demanding, but 3DSSPP is most useful for analysis of slow movements in heavy material handling tasks, since the computations assume effects of acceleration and momentum are negligible. Characterization of submaximal tasks throughout the reachable workspace is needed to expand the relevance of these types of tools to dynamic repetitive tasks that also pose a risk for injury.

Muscle demand studies have also been used to refine workspace and task design. Several authors have developed 3-dimensional spatial maps of muscle activities for a variety of submaximal isometric exertions (McDonald et al., 2014; McDonald et al., 2012; Nadon et al., 2016). Data from these studies were used to develop predictive equations to extrapolate demand of individual muscles to all hand locations within the reachable workspace. These predictive relationships demonstrate the complex non-linear relationship between hand location and individual and overall muscle demand. Such predictive equations can be beneficial to ergonomists when designing novel workspaces, but there still remains a need to characterize dynamic exertions and loading on other musculoskeletal structures, such as joint loading and stability.

Glenohumeral Stability

The glenohumeral joint is the most mobile joint in the human body due to a lack of an intrinsically stable osseous socket like the acetabulum of the hip joint. Despite the shallow glenoid fossa, the humeral head remains centered throughout motion, exhibiting kinematics similar to a ball-and-socket (Howell et al., 1988). Even under anterior loading during abduction, in-vivo humeral head translations are on the order of millimeters (Cereatti et al., 2014). When excessive or symptomatic translations of the humeral head occur, however, the joint is said to be clinically unstable, and normal function of the shoulder complex is inhibited (Pagnani and Warren, 1994; Soslowsky et al., 1997) Glenohumeral stability is provided through a combination of passive structures and active contributions of muscles, with muscle contributions acting as the primary stabilizers during motion. Here we provide a summary of both active and passive stabilizers.

Passive Stability Mechanisms

The glenohumeral joint is the articulation of the humeral head and the glenoid fossa of the scapula (Figure 1). The osseous contour of glenoid fossa is relatively flat; however, the cartilage surface is thicker peripherally than in the center, creating a radius of curvature that matches the humeral head closely (Flatow et al., 1991). Furthermore, the labrum, fibrocartilage that attaches to the rim of the glenoid, provides an additional extension to the glenoid concavity. Howell and Galinat (1989) reported in a dissection study that the labrum provides approximately 50% of the total depth of the glenoid. Resection of the labrum reduces the average effective depth of the glenoid concavity under a constant compressive load from 4.0±1.1mm to 3.2±0.8 mm (Halder et al., 2001). Glenoid concavity depth is directionally dependent, with the superior-

inferior having increased depth over the anterior-posterior direction (Halder et al., 2001; Lippitt et al., 1993).

In addition to the labrum providing additional depth to the glenoid concavity, the passive capsuloligamentous structures surrounding the glenohumeral joint provide a critical component of glenohumeral joint stability (Lippitt and Matsen, 1993; Terry et al., 1991). Major ligaments include the coracohumeral ligament and inferior, middle, and superior glenohumeral ligaments (Figure 2). The function of these ligaments is highly dependent on the position of the humerus relative to the scapula, and several cadaveric studies have evaluated their role in stability in different postures (Bigliani et al., 1996; Burkart and Debski, 2002; Felli et al., 2012; Terry et al., 1991). The inferior glenohumeral ligament is the major static stabilizer of the abducted glenohumeral joint against anterior instability (Bigliani et al., 1996; Felli et al., 2012; Terry et al., 1991). The superior glenohumeral ligament and the coracohumeral ligament act as stabilizers in the inferior direction (Burkart and Debski, 2002). Furthermore, the superior glenohumeral ligament works with the middle glenohumeral ligament to stabilize the joint in adducted postures (Felli et al., 2012). The middle glenohumeral ligament also provides anterior stability in abducted postures (Burkart and Debski, 2002; Felli et al., 2012). Ligaments, however, are passive elements and can only provide stabilizing forces when under tension, and these structures are only under tension at the end-range of motion in these postures (Harryman et al., 1990; Terry et al., 1991). During the mid-range of motion, these structures are lax, therefore stability must be provided through active contributions of muscles such as the rotator cuff (Bigliani et al., 1996).

Active Stability Mechanisms

Muscles act to stabilize the glenohumeral joint by controlling the direction of the resultant joint reaction force. The rotator cuff is the primary active stabilizer of the glenohumeral joint and is comprised of four muscles (infraspinatus, supraspinatus, subscapularis, and teres minor) (Figure 3). Rotator cuff muscles originate on the scapula, and the four tendons connect with each other prior to insertion on the humeral head to form a common cuff (Sonnabend and Young, 2009). Rotator cuff muscles lie under the deltoids, and their activity is typically measured with fine-wire EMG since surface measurements of these muscles can be inaccurate (Rajaratnam et al., 2014).

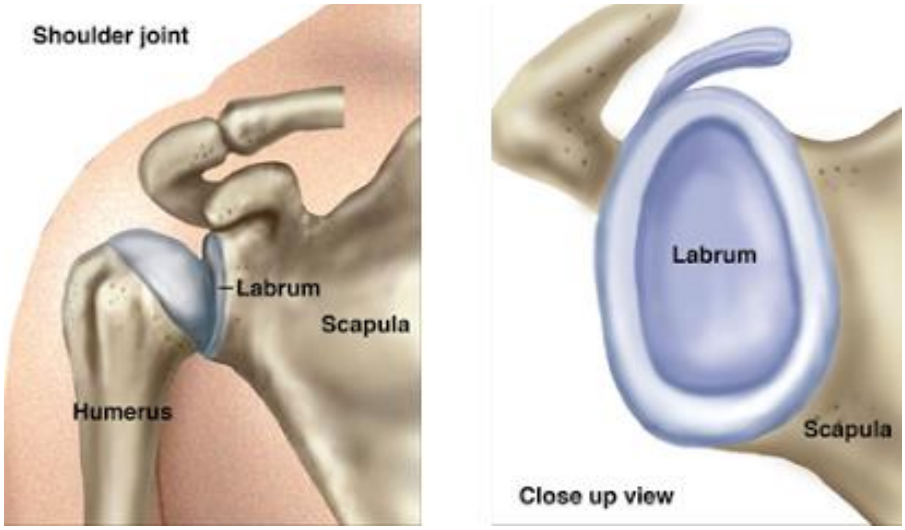

Figure 1.1: Glenohumeral joint.

The glenohumeral joint is the articulation of the humeral head with the glenoid fossa of the scapula. The glenoid fossa is a shallow concavity whose depth is extended by the glenoid labrum. Concavity depth is directionally depended with the superior-inferior direction having increased depth over the anterior-posterior direction. (adapted from https://sgbonedoctor.com/shoulder/glenoid-labrum-tear/).

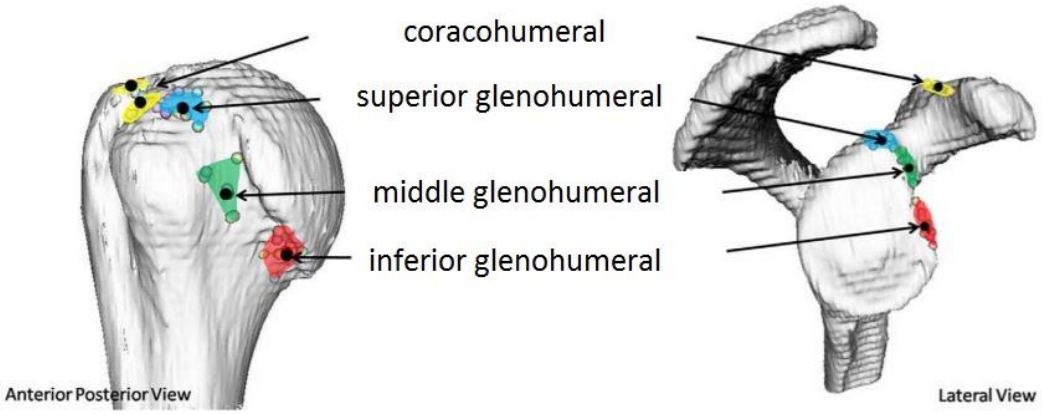

Figure 1.2: Coracohumeral and glenohumeral ligaments.

Ligaments are passive stabilizers that provide additional stability under tension. Attachment and insertion points of the coracohumeral and glenohumeral ligaments are displayed. (adapted from (Yang et al., 2010)).

Active stabilization is provided through muscles by two mechanisms: concavity compression (pressing the humeral head into the glenoid fossa) and scapulohumeral balance (the principle that the humeral head is balance if the net joint reaction passes through the glenoid fossa). Previous cadaveric studies have evaluated stability from concavity compression by applying a fixed compressive load through the humeral head into the glenoid fossa and determining the transverse load required to dislocate the humeral head over the glenoid rim (Halder et al., 2001; Lazarus et al., 1996; Lippitt et al., 1993). Stability from concavity compression is thus quantified as the ratio of the transverse to compressive forces. These experiments revealed that concavity compression stability is directionally dependent with the superior-inferior direction being the most stable and the anterior-posterior direction being the least (Halder et al., 2001; Lippitt and Matsen, 1993). This increase in stability in the inferior-

superior direction corresponds to the increased concavity depth in the superior-inferior plane (Lippitt and Matsen, 1993).

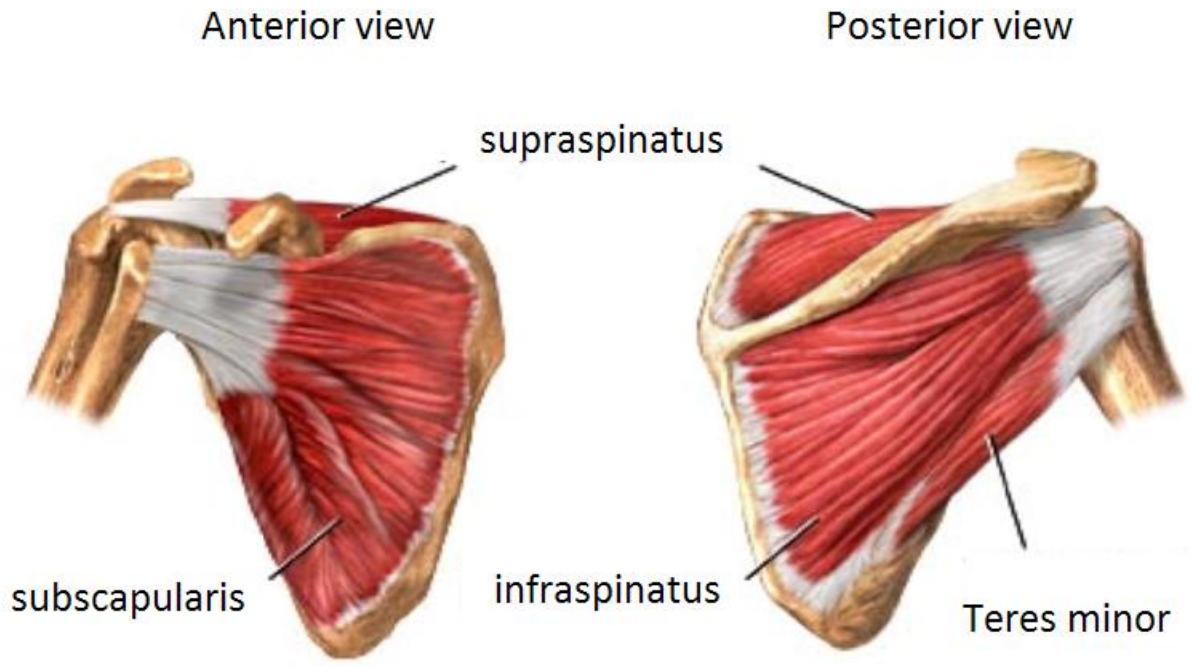

Figure 1.3: Rotator cuff muscles.

The rotator cuff consists of four muscles (supraspinatus, infraspinatus, subscapularis, and teres minor) and is the primary active stabilizer of the glenohumeral joint. (adapted from http://www.drtylermarshall.com/rotater/).

The other active stability mechanism, scapulohumeral balance, requires that the net joint reaction force pass through the glenoid; therefore, the larger the arc of the glenoid concavity, the larger the range of net forces that can be balanced by the glenoid fossa. This range of stable net reaction force vectors can be estimated through geometric calculations; however, the glenoid fossa does not have a symmetric concavity, but rather a complex 'inverted-comma' shape (Lippitt and Matsen, 1993). Furthermore, the labrum and cartilage surrounding the glenoid are deformable, which affect the shape of the concavity under compression. As a result, the range of

reaction forces stabilized by scapulohumeral balanced have been estimated by coaxially loading the humeral head and incrementing glenoid angulation until the humeral head dislocates (Lippitt and Matsen, 1993). The range of stability from scapulohumeral balance was greater in the superior-inferior direction than anterior-posterior direction, which again correlates with the greater concavity depth in this direction.

Recurrent Instability and Degenerative Wear

Damage and wear to the glenohumeral joint are often linked with traumatic injury such as a such as a fall on an outstretched arm or direct blow to the shoulder; however, repetitive use and recurrent stress on the glenohumeral joint can also lead to degenerative wear. Furthermore, previous instability, such as static posterior subluxation, is often associated with joint wear such as glenohumeral arthritis (Gerber et al., 2009). Regardless of the cause, damage to active and passive structures of the glenohumeral joint can limit the ability to stabilize the glenohumeral joint (Lazarus et al., 1996; Lippitt and Matsen, 1993; Steenbrink et al., 2009; van Drongelen et al., 2013). Several studies have evaluated the effect of damage to the glenoid concavity on concavity compression stability ratios (Halder et al., 2001; Lazarus et al., 1996; Lippitt and Matsen, 1993). Resection of the labrum reduces the required force to dislocate the humeral head at a given compressive force (Halder et al., 2001; Lippitt and Matsen, 1993), and this reduction in dislocation threshold was statistically significant in all directions except the posterior and posterosuperior directions (Halder et al., 2001). While a resection of the labrum would not occur naturally, Lippitt and Matsen (1993) concluded that any reduction in the glenoid concavity from injury or wear would result in reduction of stability. Furthermore, Lazarus et al. (1996) simulated a more realistic chondral-labral defect in a cadaveric model, which caused a reduction in the

stability ratio in the direction of the defect by 65%. Therefore, wear to the glenoid concavity from overuse or atraumatic instability can lead to further instability. Furthermore, Marchi et al. (2014) reported reduction in the stability index, a measure of transverse to compressive forces calculated using a musculoskeletal model (informed with experimental force, EMG and kinematic data), for subjects with prior dislocation when compared against healthy controls. If damage to the glenohumeral joint is severe, recurrent instability can occur and surgical intervention may be needed to restore stability and function. Surgical intervention can restore functional stability with a high success rate; for example, a postoperative follow up of Bankart repairs, a procedure in which the torn labrum and ligaments are reattached, showed that 90% of subjects did not experience a recurrent instability at the follow up at least 4 year later (Saper et al., 2017). While surgical intervention can be successful at restoring glenohumeral instability, preventing initial instability by preventing wear to the joint would be a preferable solution.

Computational Musculoskeletal Modeling

Computational musculoskeletal modeling is an effective framework to perform exploratory studies that would not be possible experimentally. Through modeling and simulations, researchers can augment experimental findings by exploring features of movement that cannot be evaluated experimentally, such as muscle forces and overall joint reactions. Furthermore, computational studies allow researchers to evaluate what-if scenarios to help provide a foundation for clinicians to design or implement surgical interventions and potential rehabilitation strategies.

Upper Extremity Model

A previously developed and validated three-dimensional upper extremity model will be used in this work to characterize joint reaction forces during unimanual and bimanual pushing and pulling (Holzbaur et al., 2005; Saul et al., 2015). This model was developed in OpenSim (OpenSim, Stanford University, Palo Alto, CA) (Delp et al., 2007). OpenSim is an open-source musculoskeletal modeling and simulation platform capable of performing and analyzing muscle driven simulations of motion. The unimanual upper extremity model contains 7 degrees of freedom including 3 at the shoulder (plane of elevation, thoracohumeral elevation, axial rotation) as well as elbow flexion, forearm pronation/supination, and wrist flexion and deviation as defined by the International Society of Biomechanics (Wu et al., 2005). Scapular and clavicle movement are constrained to move with scapulohumeral rhythm through regression equations developed by de Groot and Brand (2001). We will employ an implementation of the model with expanded internal shoulder rotation range of motion (Vidt, 2014).

The model contains 50 muscles and muscle compartments spanning the shoulder, elbow, forearm, and wrist joints. The upper extremity model employs Hill-type muscle actuators (Figure 4), a lumped parameter muscle-tendon model that accounts for nonlinear force production in muscle (Zajac, 1989). The Hill-type muscle incorporates a contractile element, a passive elastic element, and a series elastic element.

The contractile element is activation dependent and represents the force-velocity and force-length relationships of muscle (Figure 5). Active force production in muscle has a force-length relationship where muscle fibers can produce their maximal force at their optimal fiber length. As the muscle fiber length deviates from the optimal length in either direction, muscle force production decreases. Active muscle force production is also dependent on the shortening

velocity of muscle fibers. Isometric force production occurs when muscle fiber remains at a constant length and fiber velocity is 0. When the muscle contracts, muscle fiber length decreases, and as the shortening velocity increases muscle force production decreases. As a muscle lengthens, the force that a muscle produces is greater than the isometric force. Force production increases with increasing lengthening velocity in a non-linear manner until the force plateaus (Zajac, 1989). This plateau in force production occurs because muscle tissue begins to fail mechanically at this fiber-velocity. In musculoskeletal models, muscle excitation and activation continuously vary from 0 (unexcited) to 1 (fully excited). At full activation, the contractile element of the Hill-type muscle model can achieve its maximal force, but as activation decreases peak force on the force-length and force-velocity curves also decreases.

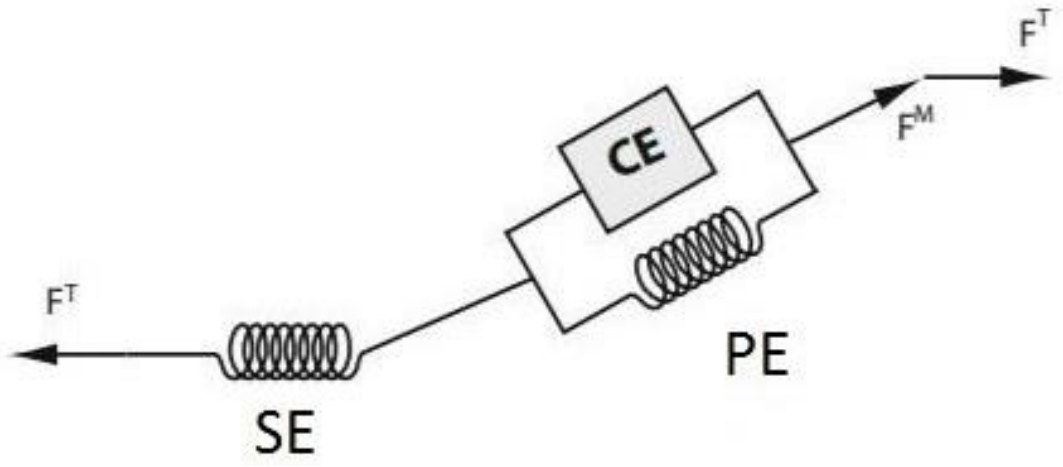

Figure 1.4: Hill-type model of skeletal muscle.

Mechanical model of skeletal muscle, developed by A.V. Hill (Hill, 1938). The contractile element (CE) represents active force production in muscle and is dependent on muscle fiber length and contraction velocity. The passive elastic element (PE) is modeled as an elastic spring in parallel to the contractile element. The passive element represents titin and connective tissues. The series elastic element (SE) is an elastic spring acting in series to the CE and PE and represents the elasticity of tendon. (adapted from (Arnold et al., 2010)).

The passive elastic element represents passive stretch in muscle. Passive force production occurs in muscle when the fiber length stretches beyond the optimal fiber length and has nonlinear behavior as described by the passive force length curve (Figure 5). Passive force production only depends on stretch in muscle fiber and is not dependent on muscle activation. Total force production of muscle is the combined force of the active and passive components. The serial elastic element represents tendon and is modeled as a non-linear spring, and acts in series to the contractile element and the passive elastic element which act in parallel to each other.

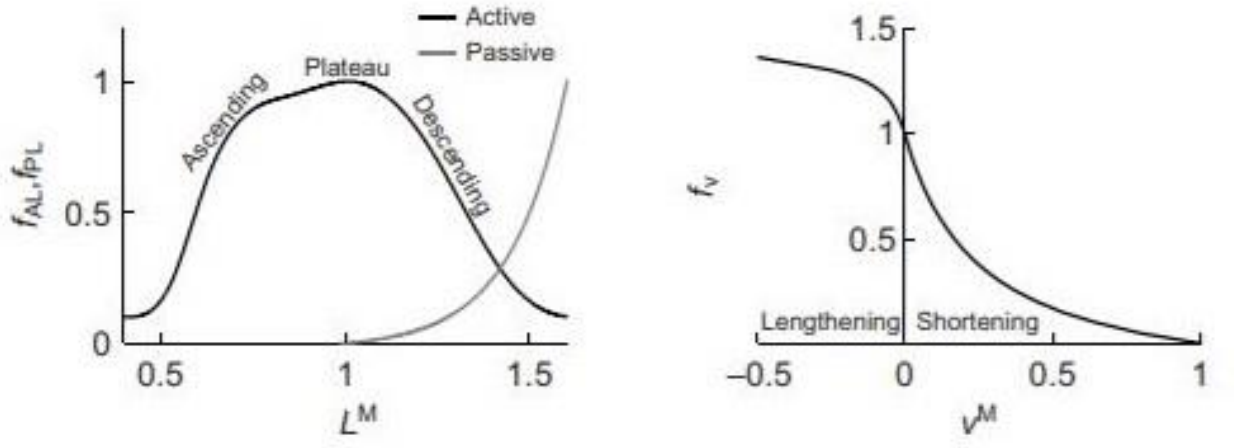

Figure 1.5: Force-length and force-velocity relationships.

Force-length relationship of muscle represents an isometric contraction of a muscle fiber where contraction velocity is held constant. Active force production is maximal at optimal fiber length ($L^M = 1$), and force production tapers off as muscle fiber strays in either direction from the optimal length. Passive force production does not depend on activation and occurs when muscle fiber stretches beyond the optimal fiber length. Force-velocity relationship of muscle considers the force of a muscle when the length of the muscle is held constant (adapted from (Arnold et al., 2013)).

The lumped parameters in the Hill-type muscle model (pennation angle, maximum isometric force, optimal fiber length and tendon slack length) can be adjusted to represent specific muscles. Pennation angle is the angle between the muscle fibers and the tendon and alters how much force is transmitted to the line of action of the muscle. Maximum isometric force is the maximum force the muscle is capable of producing at its optimal fiber length and is related to the physiological cross-sectional area of muscle through specific tension of muscle. In musculoskeletal modeling, specific tension of muscle of 50.8 N/cm^2 is typically used for upper limb muscles (Saul et al., 2015). Optimal fiber length is the length where muscle can produce its' peak force. Tendon slack length is the length at which the tendon must be stretched to before it can produce force. In the upper extremity model that we will employ, these parameters have been defined for each muscle and muscle compartment to represent a 50^{th} percentile male (Holzbaur et al., 2005; Saul et al., 2015). Maximum isometric force can be altered to represent individual's strength profiles.

Modeling Glenohumeral Stability

Upper limb musculoskeletal models typically model the glenohumeral joint as an ideal ball-and-socket joint, ignoring translations of the humeral head within the glenoid concavity (Chadwick et al., 2009; Dickerson et al., 2007; Holzbaur et al., 2005). Quental et al. (2016) developed a 6 degree of freedom model of the glenohumeral joint and compared to an ideal ball-and-socket joint with a concavity compression-based stability constraint (Quental et al., 2015). Their study concluded that the ideal ball-and-socket was an appropriate model for the glenohumeral joint since muscle forces and glenohumeral reactions were similar between both models. Ideal ball-and-socket joints are inherently stable; therefore, incorporation of stability

constraints into dynamic simulations can improve calculation of muscle activations by forcing the model to account for active stabilization of the joint that occurs in-vivo. Stability constraints at the glenohumeral joint have been modeled using both mechanisms of active glenohumeral stability, i.e. scapulohumeral balance and concavity compression (Chadwick et al., 2009; Dickerson et al., 2007; van der Helm, 1994a). These stability criteria constrain the resultant joint reaction force at the glenoid, thereby guaranteeing that the humerus would not theoretically dislocate.

The Delft Shoulder and Elbow Model (DSEM) (Chadwick et al., 2009) uses a scapulohumeral balance type stability criteria requiring that the resultant force remains within the curvature of the glenoid. The glenoid concavity is modeled as an ellipse and stability is defined according to the following equation

$$GH_{stab} = \left(\frac{\theta}{\theta_a}\right)^2 + \left(\frac{\varphi}{\varphi_a}\right)^2$$

where θ and φ are the angles of the joint reaction force away from the normal of the glenoid along the major and minor axis of the ellipse and θ_a and φ_a are the angles of that vector as it reaches the rim of the glenoid. As the value of the criteria approaches 1, the joint reaction force approaches the rim of the ellipse indicating instability. Nikooyan et al. (2010) evaluated the DSEM model against in-vivo glenohumeral joint contact forces measured with an instrumented shoulder endoprosthesis. The model predicted joint reaction forces similar to the measured reactions, but generally underestimated peak reaction for dynamic tasks and overestimated peak reaction for force modulation tasks. Incorporating EMG into the simulations allowed the model to better account for co-contraction and improved the predicted glenohumeral joint reaction up to 45% (Nikooyan et al., 2012). Applications of the DSEM model include simulating varying

degrees of rotator cuff tears to determine how different tear types influence glenohumeral stability (Steenbrink et al., 2009; van Drongelen et al., 2013).

On the other hand, concavity compression has been incorporated in the models by Dickerson et al. (2007) and Blache et al. (2017) which employ multi-directional dislocation force thresholds from cadaveric studies to constrain the resultant joint reaction. The stability dislocation force thresholds were calculated in eight directions around the glenoid by determining the amount of transverse force required to dislocate the humeral head when a fixed compressive force was applied (Lippitt and Matsen, 1993). Dickerson et al (2007) evaluated the effect of this constraint by scaling the reported dislocation thresholds by factors ranging from 0.4 to 1.0 and found that more restrictive constraints resulted in increased muscular force. In a sensitivity analysis of this model, Chopp-Hurley et al. (2014) concluded that predicted rotator cuff muscle forces were more sensitive to origin-insertion locations of the rotator cuff muscles than these glenohumeral stability thresholds. However, the inferior stability threshold influenced predicted rotator cuff forces when the model was abducted, and an internal or external rotation force was applied at the hand. The concavity compression constraint has also been evaluated in a different model during a lifting task (Blache et al., 2017). Blache et al (2017) ran static optimizations of lifting with and without the concavity compression constraint, and report that without the constraint the model predicted an unstable reaction 74% of the time. Incorporating the constraint cause the supraspinatus force to increase by 107% to stabilize the predicted joint reaction. While the effect of the concavity compression has been evaluated qualitatively, this style of constraint has not been evaluated against in-vivo glenohumeral joint reaction forces like the DSEM model (Nikooyan et al., 2010; Nikooyan et al., 2012). The model by Dickerson et al. (2007) has, however, been validated with EMG-data (Dickerson et al., 2008). They found that

predicted muscle forces for primary movers correlated well with experimental data while predicted muscle forces for secondary muscles were less accurate (Dickerson et al., 2008). Direct comparison of both styles of glenohumeral stability constraint against experimental data could provide valuable insight into modeling glenohumeral stability.

Computed Muscle Control

Computed muscle control (CMC) is a previously developed algorithm to determine muscle activations while tracking experimental kinematic (Thelen et al., 2003). In this algorithm, CMC considers time dependent properties of muscle force generation (Figure 6).

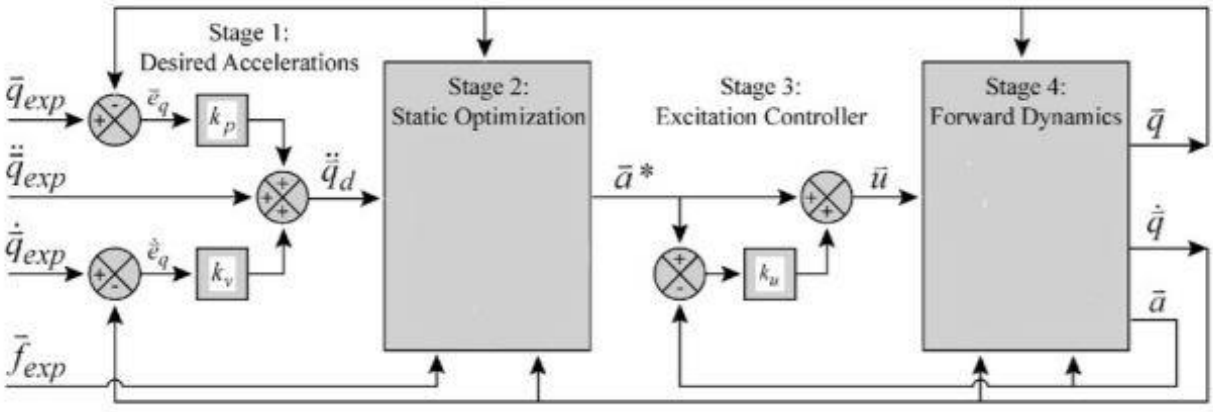

Figure 1.6: Computed Muscle Control Algorithm.

Computed muscle control algorithm (CMC) calculates muscle activations required to track experimental kinematics. CMC is a dynamic simulation that considers time dependent activation dynamics of muscle force production. CMC incorporates error dynamics, static optimization, a muscle excitation controller and a forward dynamic simulation. (adapted from (Thelen et al., 2003)).

Muscles are not capable of producing force instantaneously, and time delays exist between converting neural excitations to muscle activations. The relationship between muscle excitation and muscle activation is modeled through the following first order differential equation (Zajac, 1989).

$$\frac{da(t)}{dt} + \left[\frac{1}{\tau_{act}} * \left(\frac{\tau_{act}}{\tau_{deact}} + \left[1 - \frac{\tau_{act}}{\tau_{deact}}\right] * u(t)\right)\right] * a(t) = \frac{1}{\tau_{act}} * u(t)$$

Where a(t) is activation, u(t) is excitation, and τ_{act} represents physiological activation time delays, and τ_{deact} represents physiological deactivation time delays.

CMC incorporates a static optimization with feedforward and feedback algorithms to determine required muscle activations while tracking kinematics. Unlike a static optimization which optimizes muscle activation at a singular time point, CMC takes into account muscle activation dynamics by including feedforward and feedback components. CMC first calculates desired joint accelerations that when achieved drive the model to track the experimental joint kinematics through the following error dynamics equation:

$$q''_{des} = q''_{exp} + k_v\left(q'_{exp} - q'\right) + k_p(q_{exp} - q)$$

Where q''_{des} is the desired acceleration, q''_{exp} is the experimental acceleration, $q'$and q are the model's coordinates' velocities and positions respectively, q'_{exp} and q_{exp} are the experimental coordinate velocities and positions, and k_v and $k_p$are critically damped feedback gains. The next step in CMC, is to perform a static optimization that computes muscle activations that will achieve the desired accelerations. The optimization is static in that the optimization criterion is dependent only on the current time instant. The default static optimization criterion for CMC is

$$\sum_{i=1}^{n} {x_i}^2 + \sum_{j=1}^{m} (q''_{des} - q'')^2$$

Where x_i represents the forces of the actuators and $q''_{des} - q''$ represents error between the model's acceleration and the desired acceleration for each tracked joint. This criterion can be altered to incorporate additional criteria such as a stability constraint for the glenohumeral joint. The final step in CMC is to use the computed controls to drive a forward dynamic simulation, advancing forward in time by a small timestep. Typically, 0.01 seconds is used such that the time step is still small, but long enough for activation dynamics to change force production in the muscle models. These steps are repeated until time advances to the end of the desired movement.

CMC has been shown to generate required muscle activations to track input kinematics within 1º of experimental kinematics (Thelen et al., 2003; Thelen and Anderson, 2006). CMC has been validated against experimental kinematics and EMG recordings for cycling, walking, and forward reaching (Saul et al., 2015; Thelen et al., 2003; Thelen and Anderson, 2006).

Specific Aims

Appropriate workplace design is critical to maximizing productivity and minimizing work-related musculoskeletal disorders. Since most modern industrial workspaces are characterized by predominantly light repetitive work (Das and Sengupta, 1996), there is a need to understand biomechanical demands during submaximal work. Among manual work tasks, push-pull tasks in particular have been shown to be significantly related to shoulder complaints (Hoozemans et al., 2002). In order to effectively design workplaces for these tasks, knowledge of the demands placed on muscles and joints is needed. While much is known on mechanical loading of the low back during push-pull tasks, less is known regarding shoulder loading (Hoozemans et al., 1998). Recent studies have attempted to fill these gaps (Calé-Benzoor et al., 2016; McDonald et al., 2012; Nimbarte et al., 2013); however, these studies focused on full-body

cart pushing, isometric tasks, and strength. Loading under these conditions cannot be directly applied to isolated arm dynamic submaximal push-pull tasks since EMG and force exertion under dynamic conditions can be much different from those recorded isometrically (Antony and Keir, 2010; Kumar, 1995), and foot placement influences pushing force (Rancourt and Hogan, 2001). Therefore, the objective of this research is to quantify mechanical loading of muscles and joints during dynamic push-pull tasks. This objective will be accomplished through the following specific aims:

Specific Aim 1: Determine the effect of task and task target on muscle activation during dynamic push-pull tasks. Task target has been shown to influence muscle demand during lifting (Blache et al., 2015) and isometric push-pull tasks (McDonald et al., 2012). Knowledge of muscle loading under dynamic push-pull tasks is needed to develop a more complete understanding of workspace design for preventing fatigue and injury. **Methods:** We will collect EMG data of healthy young subjects performing unimanual and bimanual dynamic push-pull tasks in the sagittal and horizontal planes. **Hypothesis 1:** (*i*) Superior and lateral task locations will increase muscle activation levels. (*ii*) Task type will influence muscle activation levels.

Specific Aim 2: Evaluate how joint reaction forces vary with changes in task and task target during dynamic push-pull tasks. Dynamic cart pushing results in larger translational forces than compressive forces at the glenohumeral joint (Nimbarte et al., 2013). Dynamic isolated upper extremity push-pull tasks may also destabilize the glenohumeral joint and thereby increase the risk of shoulder musculoskeletal disorder with cumulative exposure. **Methods:** We will use the extended CMC algorithm with the OpenSim upper extremity model (merged) to

calculate joint reaction forces at the shoulder during push-pull tasks across the workspace. **Hypothesis 2:** (*i*) Task target will influence the ratio of translational and compressive forces acting at the shoulder. (*ii*) Pushing will result in less stable joint reactions than pulling.

Specific Aim 3: Evaluate how incorporating EMG and glenohumeral joint reaction stability constraints affects prediction of resultant joint reaction force and rotator cuff activations during CMC. Most musculoskeletal models of the upper extremity use an ideal ball-and-socket for the glenohumeral joint (Chadwick et al., 2009; Dickerson et al., 2007; Quental et al., 2015; Saul et al., 2015; van der Helm, 1994b); however, the glenohumeral joint requires active coordination of muscles to limit translations and stabilize the joint. Several methods have been proposed to incorporate active stabilizing mechanisms into computational simulations and thereby improve predicted outcomes, but direct comparison of these methods on multiple predicted outcomes have not been previously made. **Methods:** We will perform a sensitivity analysis of common predicted outcomes (net glenohumeral reaction force, calculated rotator cuff activations, and predicted instability) to different techniques of modeling active stabilizing mechanisms. We will evaluate 2 styles of stability constraint that control the direction of the net joint reaction and several styles of constraints that incorporate surface EMG signals into the optimization. **Hypothesis 3:** (*i*) Inclusion of the experimental surface EMG will stabilize the glenohumeral joint and result in higher calculated joint reaction forces and predicted rotator cuff activations than when no EMG constraints are applied. (*ii*) Inclusion of stability constraints will stabilize the glenohumeral joint and result in higher calculated joint reaction forces and predicted rotator cuff activations than when no stability constraint is applied, but constraint type will not have a significant impact on the calculated joint reaction.

CHAPTER 2

Spatial Dependency of Shoulder Muscle Demand during Dynamic Unimanual and Bimanual Pushing and Pulling (In review for *Applied Ergonomics*)

Daniel C. McFarland, Michael N. Poppo, Emily M. McCain, and Dr. Katherine R. Saul

Abstract

Work involving extensive pushing and pulling is associated with higher frequency of shoulder complaints. While reports of shoulder muscle demand during submaximal isometric tasks are abundant, dynamic submaximal push-pull exertions are not well understood. We evaluated how muscle demand (weighted EMG average) of surface glenohumeral muscles varies with task type and target. Seventeen healthy young adults performed seated unimanual and bimanual pushes and pulls to 3 thoracohumeral elevations (20º, 90º, 170º) and 4 elevation planes (0º, 45º, 90º, 135º) with loading at 15% of isometric push-pull capacity. Pulling required less demand than pushing ($p<0.0001$). Muscle demand varied more with elevation than elevation plane. The lowest target had highest demand for pulling ($p<0.01$), and the most elevated target had highest demand for pushing ($p<0.0001$). Working above the shoulder is known to increase demand during isometric tasks, however, these results suggest that for dynamic tasks working against gravity has a larger effect on demand than task target.

Introduction

Work-related musculoskeletal disorders (MSD) place a large burden on the economy and workers' health, with MSD accounting for 29-35% of all occupational injuries and illnesses involving days away from work in private industries (Bhattacharya, 2014). Physically demanding occupations such as military service have high occurrence of musculoskeletal

disorders, with active duty non-deployed service members having an injury rate of 62.8% per person-years (Hauret et al., 2010). Annual total cost from work-related MSD in the United States ranges between $45 and $54 billion (National Academy of Science, 2001). Shoulder injuries, in particular, are taxing on worker health and the economy. A study of worker compensation claims found that 30.6% of claims involving the shoulder resulted in over seven days of lost work and that shoulder claims resulted in the second highest total cost behind lumbar spine claims (Dunning et al., 2010).

Ergonomics research has identified push-pull tasks as related to shoulder complaints (Hoozemans et al., 2002). Since Hoozemans et al. (1998) identified a lack of knowledge regarding the biomechanical demands placed on shoulder muscles and joints as a result of these exertions, numerous efforts have been made to characterize such tasks. Much of the push-pull literature considers how various conditions including exertion direction and task location influence strength capacity (Calé-Benzoor et al., 2016; Chaffin et al., 1983; Chow and Dickerson, 2016; Chow and Dickerson, 2009; Das and Wang, 2004; La Delfa et al., 2014; La Delfa and Potvin, 2016; MacKinnon, 1998). When designing workspaces to prevent MSD, it is important to evaluate demand at the muscular level in addition to overall strength capacity. Since most modern industrial workspaces are characterized by predominantly light repetitive work (Das and Sengupta, 1996), several studies have characterized total muscular demand, a sum or average of individual EMG signals, during submaximal isometric tasks (Chow et al., 2017; McDonald et al., 2014; McDonald et al., 2012; Meszaros et al., 2018; Nadon et al., 2016). These studies report that muscular demand during these isometric tasks including pushing and pulling are spatially dependent. In general, superiorly located tasks increase muscle demand, although exertion direction also plays a large role in determining muscular demand (Meszaros et al., 2018)

and the resulting spatial dependency (McDonald et al., 2014; McDonald et al., 2012; Meszaros et al., 2018; Nadon et al., 2016). All these studies, however, evaluated isometric tasks and the results may not be directly applicable to dynamic exertions since EMG and force exertion under dynamic conditions frequently differ (Antony and Keir, 2010; Kumar, 1995). There has been some effort to characterize muscular loading during dynamic tasks (Bennett et al., 2011; Kao et al., 2015; Lin et al., 2010), but these studies involve full-body cart pushing and may not be applicable to seated or stationary dynamics tasks, such as work on an assembly line or opening and closing hatches on military equipment, since foot placement is known to influence push-pull capacity (Rancourt and Hogan, 2001).

Therefore, to effectively design workplaces involving dynamic force tasks to minimize work-related shoulder MSD, additional understanding of the demands placed on shoulder muscles during these tasks is needed. To characterize a workspace, a combination of task targets, i.e. target hand location at the end of motion, covering the entire space is needed. One obvious solution to reduce muscular demand at the shoulder is to perform task bimanually and split the loading over two shoulders; however, studies comparing unimanual to bimanual strength capacity report unimanual capacity as greater than 50% of bimanual capacity (Chaffin et al., 1983; Warwick et al., 1980), suggesting that there may be limited muscular demand benefits seen by switching to bimanual operation. While muscle demand during bimanual pushing and pulling has been previously evaluated (Chow et al., 2017), to the author's knowledge no study has directly compared muscular demand between bimanual and unimanual pushing and pulling. Therefore, our objective was to quantify how muscle demand, a measure of the overall load placed on the muscular system, of superficial muscles crossing the glenohumeral joint varies with both task type (unimanual and bimanual pushing and pulling) and task target for dynamic

tasks. This research aims to expand understanding of how task design contributes to overuse injuries, thereby enabling the development of preventive measures to reduce risk of shoulder MSD and lower the associated economic burden.

Methods

Experimental Protocol

Seventeen healthy young adults (8 males/9 females) between the ages of 20 and 32 years participated in this study. A power analysis (power: 0.8, α=0.05) was used to estimate the number of required subjects. Effect size for the power analysis was informed by previously reported weighted demand results for upward exertions (Nadon et al., 2016). Required subjects ranged from 9 to 22 depending on how conservative an estimate of effect size was used. The participants were recruited from the local community using the following inclusion criteria: 1) no history of injury or pathology of the upper limb, 2) no neuromuscular impairments, and 3) no physical impediments to performing the required physical exertions. Fifteen of the subjects were right-dominant, and two were left-dominant. Hand dominance was self-reported by subjects, and their dominant hand was used for all unimanual tasks. All subjects provided written informed consent in accordance with North Carolina State University Institutional Review Board. Each subject completed the testing protocol in a single session on a single day.

Unimanual surface electromyographic (EMG) recordings of the anterior, middle, and posterior deltoid, biceps brachii, lateral head of triceps brachii, latissimus dorsi, and pectoralis major were collected. The skin overlying the location of markers was shaved and cleaned with alcohol prior to electrode placement. Electrodes were placed over each muscle belly in line with muscle fibers using published placement locations (Cram and Criswell, 2011). Recordings were

made at 2000 Hz using 1-cm Ag/AgCl dual electrodes with 16-channel capacity (Noraxon Telemyo DTS system, Noraxon, Scottsdale, AZ) (input impedance >100Mohm, CMRR>100dB, gain 500).

Subjects performed a series of isometric joint moments on a Biodex System 4 Quick Set (Biodex, Shirley, NY), and EMG data collected during these trials was used in subsequent EMG normalization. Maximum isometric joint moments of shoulder abduction and elbow flexion for the dominant hand were collected following a previously described standard protocol (Holzbaur, Delp et al., 2007). Subjects were seated with their torso restrained in a vertical posture with straps to prevent changes in posture during the trials. At the shoulder, maximum isometric abduction moment was assessed with the shoulder abducted to 60º and the elbow braced in full extension. At the elbow, maximum isometric flexion moment was assessed with the shoulder in neutral abduction and the elbow flexed to 90º. Three trials of each moment were obtained, and participants received standardized verbal and visual feedback to encourage MVC. To minimize the effects of fatigue, 60 seconds of rest was provided in between trials.

Additionally, maximal isometric push-pull capacity with the arm in 90º forward flexion was determined for each participant using a closed-chain attachment for the Biodex. This location was chosen for maximal push-pull testing as it represents a neutral baseline task location for the subsequent testing protocol. Six trials using the dominant hand were collected (three push/three pull) where subjects received standardized visual and verbal feedback to encourage maximum force production (Holzbaur, Delp et al., 2007). EMG recordings during these trials were also used in subsequent EMG normalization. Force production was only measured along the single axis aligned with the task. The maximal push-pull force sustained for at least 0.5 seconds, determined by a custom Matlab script (The Mathworks, Natick, MA), during these six trials was

used to determine loading for the testing protocol. Studies of sustained isometric, continuous dynamic, and intermittent isometric contractions have reported fatigue thresholds ranging from 7-25% maximum isometric strength (Bjorksten and Jonsson, 1977; Hagberg, 1981; Rohmert, 1973), with intermittent contractions associated with higher thresholds. Therefore, loading was set at 15% of the maximal push-pull force in the tested baseline posture to avoid participant fatigue. This load was applied as a set weight to a pulley system that allowed resistance for each task to be explicitly controlled. This load did not change between task targets or task type (unimanual or bimanual pushing and pulling) in the testing protocol.

A series of unimanual and bimanual push and pull tasks were performed by subjects. Tasks were performed to a combination of 3 thoracohumeral elevation angles (20º, 90º, 170º) and 4 planes of elevation (0º/abduction, 45º, 90º/flexion, and 135º) as defined by the International Society of Biomechanics (Wu et al., 2005) for a total of 12 task targets (Figure 2.1). These task targets represent the angle of the dominant arm at the end of the push task and start of the pull task. Subjects performed both unimanual and bimanual pushes and pulls at each task target for a total for 48 unique tasks. Three repetitions of each unique task were performed for a total of 144 exertions per subject. To prevent fatigue, participants were provided with a rest period of one minute between each task. For each task, all three repetitions were performed consecutively without a rest period. The order of tasks was randomized to avoid any ordering effects.

Participants performed tasks in a seated position (chair height: 0.53m) with their torso restrained by straps to standardize incline across participants. Tasks were performed on a custom pulley resistance system (Figure 2.2) to reduce variability in the direction of applied force between participants and trials. Details on device components and assembly are provided in Appendix C. The custom device has a resistance pulley system employing a linear track that

allows for height adjustments and locks at 3 angles to achieve the thoracohumeral elevation angle targets (Powertec Strength, Powertec Fitness, Long Beach, CA). Plane of elevation angle selection was achieved by rotating the seat. For pulling, participants held a fixed-length handle in the dominant hand (unimanual tasks) or both hands (bimanual tasks). The handle was mounted on a carriage that slides along a linear track. Handle orientation was perpendicular to the linear track. Hand trajectory was controlled by the linear tack, but other joint angles were not controlled to encourage natural movement choices. For pulling, subjects began with the handle away from the body along the desired trajectory at approximately 80% of full limb length (Figure 2.2A) and pulled until the humerus was in a neutral posture (Figure 2.2B), approximately 0º thoracohumeral elevation. Pushing tasks were accomplished in a similar manner. Subjects received instructions on desired timing, approximately 1 sec (60bmp) although task speed was not explicitly controlled with a metronome to prevent jerky movement. Trials that deviated noticeably from these instructions were repeated.

Following the experimental protocol, subjects performed a two-minute isometric elbow flexion test on the Biodex to evaluate subject fatigue. Fatigue is typically studied in isometric contractions at a predefined percentage of maximum isometric capacity, which can range from 25 to 80% (Bonato et al., 2003; Hawkes et al., 2015). In this study, subjects were situated in the same posture as the isometric elbow flexion moment and were encouraged to maintain 60% of their elbow flexion moment for the duration of fatigue test. Elbow flexion was chosen for evaluation because biceps brachii was engaged heavily in all pulling tasks and to a lesser degree in pushing tasks during the experimental protocol. Because triceps brachii was heavily engaged in pushing tasks during the experimental protocol, co-contraction during the elbow flexion test was also monitored.

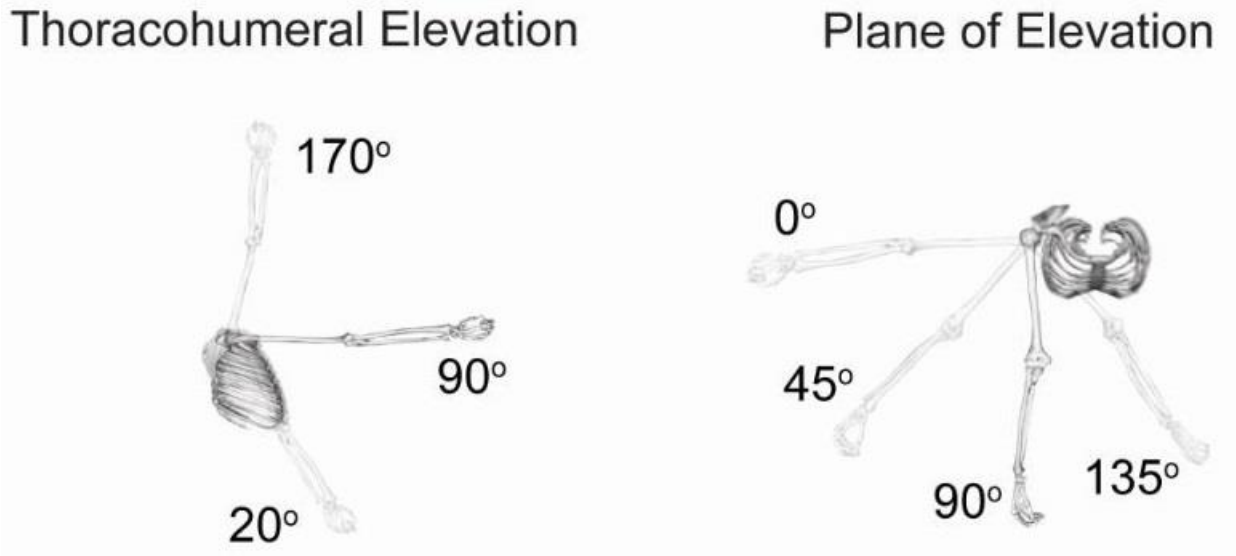

Figure 2.1: Task targets.

Subjects reached to a combination of 3 thoracohumeral elevations (20º, 90º, and 170º) and 4 planes of elevation (0º, 45º, 90º, and 135º) for a total of 12 distinct task targets.

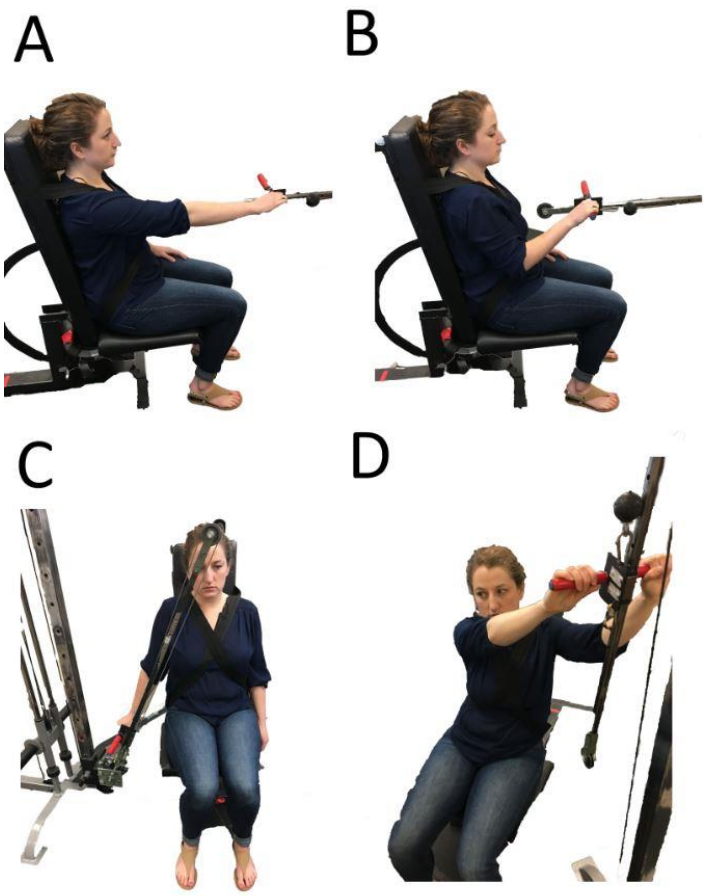

Figure 2.2: Custom pulley resistance system**.**

Subjects performed push-pull tasks on a custom device designed to reduce variability in force applied between participants and trials. The custom device has a resistance pulley system employing a linear track that allows for height adjustments and locks at the 3 angles to achieve the thoracohumeral elevation targets. Planes of elevation selection were achieved by rotating the seat. The start (A) and stop (B) for a pull task at the baseline target (90º thoracohumeral elevation/0º plane of elevation). The final position (C) for a unimanual push task at the 20º thoracohumeral elevation/0º elevation target. The starting position (D) for a bimanual pull trial at the 170º thoracohumeral elevation/135º plane of elevation target.

Data Analysis

To evaluate subject fatigue at the end of the testing protocol, median frequency analysis of biceps brachii and triceps brachii was conducted on EMG data from the isometric elbow flexion joint moment and the fatigue test (Potvin and Bent, 1997). Median frequency was chosen over mean frequency because it is less susceptible to noise (Hof, 1991). Raw EMG data was post-processed for evaluation by removing DC offset, bandpass filtering with cutoff frequencies of 30 and 300 Hz to remove signal noise (Shair et al., 2017) and dividing data into non-overlapping epochs of 0.5 seconds (Hawkes et al., 2015). Median frequency was calculated for each epoch excluding the first and last 2.5 seconds. For the isometric elbow flexion joint moment (rested condition), average median frequency for the trial was calculated. For the fatigue trial, a linear regression of the changes in median frequency over the time course of the fatigue trial was performed to calculate slope and intercept (Hawkes et al., 2015). Initial and final median frequency for the fatigue trial were calculated from the linear regression. A one-way ANOVA ($\alpha<0.05$) and Tukey's honest significant difference post-hoc test were performed to analyze changes in median frequency, since decrease in median frequency is an indicator of localized muscle fatigue (Cifrek et al., 2009; Shair et al., 2017).

Raw EMG data from the push/pull testing protocol were post-processed by removing the DC offset, highpass filtering with a 4^{th} order Butterworth filter with a cutoff frequency of 30 Hz, full-wave rectifying, and RMS filtering with a 200 msec window. Cutoff of 30 Hz was used to eliminate electrocardiogram contamination from EMG signals (Drake and Callaghan, 2006). Data for each muscle in the dominant arm were normalized to the peak value recorded for that muscle during the maximum isometric trials including the maximal push-pull capacity trials.

Muscle demand of the superficial glenohumeral muscles evaluated was calculated for each task as an average of each participant's weighted total of normalized EMG output (Nadon et al., 2016). Physiological cross-sectional areas (PCSAs) were used to determine weightings for EMG signals. Deltoid, bicep brachii, triceps, latissimus dorsi, and pectoralis major PCSA were as reported by Holzbaur et al. (2007), and the deltoid weighting was divided into anterior, middle and posterior components using PCSA fraction from Langenderfer et al. (2004).

$\sum_{i=1}^{7} Norm\_EMG_i \left[\frac{PCSA_i}{\sum_{i=1}^{7} PCSA_i}\right]$.

Statistical Analysis

Differences in peak muscle demand were analyzed across thoracohumeral elevation angles, plane of elevation angles, and task type (unimanual and bimanual pushing and pulling) using a three-way ANCOVA ($\alpha<0.05$) with sex as a covariate. When interactions were not present, they were removed from the model and a Tukey's honest significant difference post-hoc test was used to analyze results. If an interaction was present, simple main effect test was performed at each factor level using a Bonferroni correction to adjust the α.

Results

Fatigue

Average rested median frequency was 69.38±10.81 Hz and 61.25±6.18 Hz for biceps brachii and triceps brachii respectively. Average median frequency at the start of the fatigue trial was 66.74±9.19 Hz and 62.75±5.37 Hz for biceps brachii and triceps brachii respectively. Average final median frequency at the end of the fatigue trial calculated from the slope of the regression line was 58.77±14.00 Hz and 49.70±7.32 Hz for biceps brachii and triceps brachii

respectively. For biceps brachii, time of measurement influenced median frequency (p=0.0173). Rested condition and final median frequencies were significantly different from each other (p=0.0171), but rested and start of the fatigue trial were not (p=0.7593) (Figure 2.3). Start of the fatigue trial and final median frequency were also not significantly different (p=0.0928). For triceps brachii, time of measurement influenced median frequency (p<0.0001). Rested condition and the start of the fatigue trial were not significantly different from each other (p=0.7488), but the final median frequency was significantly different from both rested (p<0.0001) and start of fatigue trial conditions (p<0.0001) (Figure 2.3).

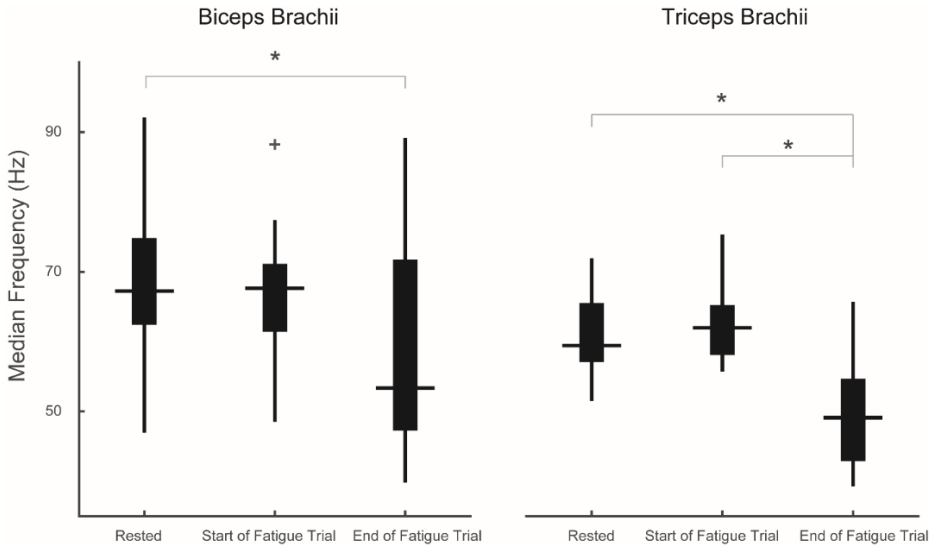

Figure 2.3: Fatigue analysis.

For biceps brachii (left), rested and start of the fatigue trial were not different (p=0.7593) indicating that subjects were not fatigued at the end of testing protocol. Rested condition and final median frequencies were significantly different from each other (p=0.0171) indicating subjects were fatigued at end of the fatigue trial. For triceps brachii (right), rested and start of the fatigue trial were not different (p=0.7488), but the final median frequency was significantly different from both rested (p<0.0001) and start of fatigue trial conditions (p<0.0001). These results indicate that fatigue in triceps brachii did not occur until the end of the fatigue test.

Muscle Demand

Isometric push strength was greater than isometric pull strength (Table 1). This was true for all subjects; therefore, the constant task loading was higher than 15% of subjects' isometric pull capacity, but exactly 15% of their push capacity. Demand during the isometric pull trial was 0.41 whereas demand during the isometric push trial was 0.55. Task duration for a subset of the trials was evaluated to confirm that subjects performed the trials at similar speeds. Task duration for this subset of task was 0.96 ± 0.3 seconds. During the testing protocol, one subject was unable to complete the push trial at the 170º thoracohumeral elevation/135º plane of elevation target. For another subject, the pull trial at the 170º thoracohumeral elevation/135º plane of elevation target was not collected successfully and had to be removed.

All factors were present as main effects ($p<0.0001$) for thoracohumeral elevation and task type, ($p=0.0148$) for plane of elevation. Post hoc analysis of the main effect for plane of elevation revealed that only the 0º and 45º target were significantly different from each other, with the most lateral 0º target being more demanding (Figure 2.4), although difference in demand between these targets was only 0.03. The only interaction present was between task type and thoracohumeral elevation angle ($p<0.0001$); therefore, the interaction rather than the main effects for these factors were analyzed with a simple main effects tests at each level of the interaction.

Table 2.1: Subject push-pull strength capacity and demographic information.

Age	Height (in)	Weight (lbs)	Isometric Pull (lbs)	Isometric Push (lbs)	Dynamic Loading (lbs)	Dynamic Loading (lbs)
24.0±3.4	68.8±3.3	173.3±24.9	75.5±24.5	99.5±30.4	19.1±3.5	11.9±2.4

For pulling, elevation targets below the shoulder were most demanding, but for pushing, elevation above the shoulder was most demanding. When pulling, the 20º elevation target was more demanding than other targets ($p<0.0001$) (Figure 2.5). Moving the task target to a low elevation from baseline 90º elevation resulted in an average increase in demand of 111% and 103% for unimanual and bimanual pulling, respectively (0.22 and 0.13 increase in weighted demand, respectively). When pushing, the 170º elevation target required the most demand ($p<0.0001$) (Figure 2.5). Moving the task target to a high elevation from baseline 90º elevation resulted in 45% and 51% average increase in demand for unimanual and bimanual pushing, respectively (0.16 and 0.13 increase in weighted demand, respectively). Additionally, for bimanual pushing, the 90º target was more demanding than the 20º target ($p=0.0014$). Moving the task target to a low elevation from baseline 90º elevation for bimanual pushing resulted in an average 21% reduction in demand (0.06 reduction in weighted demand).

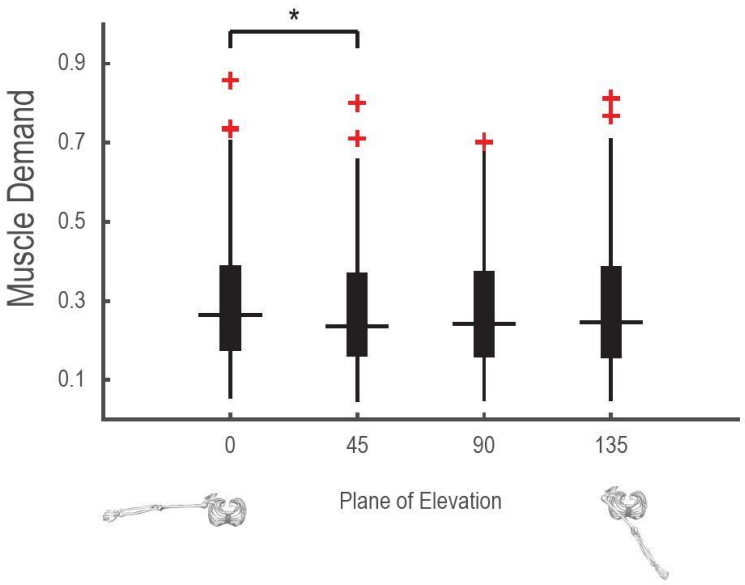

Figure 2.4: Main effect of plane of elevation.

Post hoc analysis revealed that only the 0º and 45º target were significantly different from each other ($p=0.0148$), with the most lateral 0º target being more demanding.

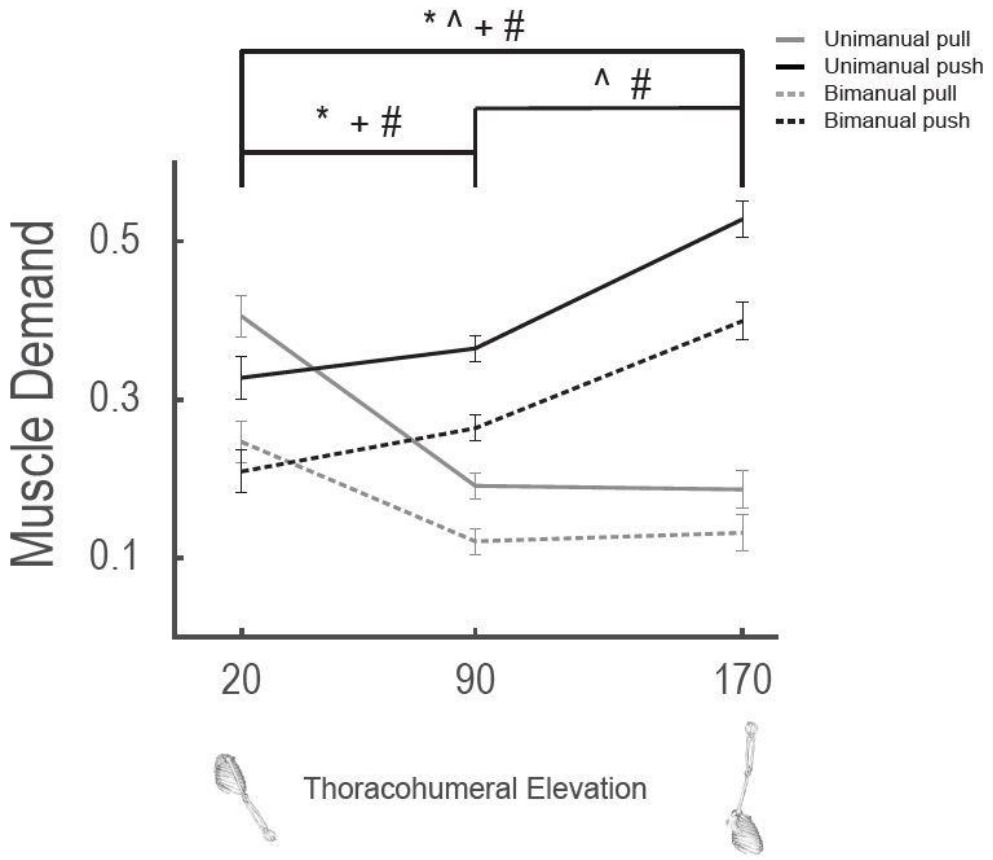

Figure 2.5: Task type by thoracohumeral elevation interaction.

Low elevation angle increased demand for pull tasks ($p<0.0001$) whereas high elevation increased demand for push tasks ($p<0.0001$). Unimanual tasks were always more demanding than their bimanual counterpart at every elevation target, and in general pushing required more demand than pulling. All task types are significantly different from each other for the 90º and 170º elevation, ($p<.0001$) for all comparisons except bimanual and unimanual pulling at 170º elevation ($p=0.0068$). For 20º elevation, bimanual pushing and pulling were not significantly different. All other task type comparisons at 20º were significantly different ($p<0.001$). Significance among elevation angles is denoted by * for unimanual pulling, ^ for unimanual pushing, + for bimanual pulling, and # for bimanual pushing. Error bars represent 95% confidence interval for adjusted means.

Unimanual tasks were always more demanding than their bimanual counterpart at every elevation target, and in general pushing required more demand than pulling. At targets at or above shoulder height (90º and 170º elevation), when pulling, bimanual operation resulted in a 36% ($p<0.0001$) and a 29% ($p=0.0068$) average reduction in demand compared to unimanual operation, respectively; when pushing, bimanual operation resulted in a 28% and a 24% average reduction in demand, for 90º and 170º elevation, respectively ($p<0.0001$). Overall differences in demand between bimanual and unimanual demand at these targets were less than 0.15 (Figure 2.5). For both of these elevation targets, both pushing task types were more demanding than both pulling task types ($p<0.0001$). Unimanual pulling required 47% and 65% average lower demand compared to unimanual pushing for elevations of 90º and 170º respectively (0.18 and 0.34 decrease in weighted demand, respectively). Bimanual pulling required 54% and 67% average lower demand compared to bimanual pushing for elevations of 90º and 170º respectively (0.15 and 0.27 decrease in weighted demand, respectively). At targets below shoulder height (20º elevation), when pulling, bimanual operation resulted in a 39% average reduction in demand and when pushing resulted in a 36% reduction in demand ($p<0.001$). Overall differences in demand between bimanual and unimanual demand at these low targets were less than 0.16 on average (Figure 2.5). At the low targets, unimanual pulling was more demanding than unimanual pushing ($p=0.0004$), but there was no difference between bimanual tasks. Unimanual pushing resulted in a 19% average reduction in demand from unimanual pulling (overall demand difference 0.08) (Figure 2.5).

Discussion

Fatigue

Fatigue analyses suggest that the task evaluations were not affected by muscle fatigue. Neither biceps nor triceps median frequency were significantly different between the rested condition at the start of the assessment and start of the fatigue protocol following assessment. This supports the claim that subjects were not fatigued at the end of the testing protocol, since localized muscle fatigue is associated with a shift in median frequency to lower values (Cifrek et al., 2009; Shair et al., 2017). Potvin and Bent (1997) reported similar rested mean frequencies for biceps brachii of 72.6±8.4 Hz compared with this study's rested and start of fatigue trial median frequencies of 69.38±10.81 Hz and 66.74±9.19 Hz respectively. Mean frequencies are always slightly higher than median frequencies because of the skewed shape of the EMG power spectrum (Knaflitz et al., 1990). In addition, the fatigue analysis suggests we were able to induce and detect fatigue in our participants during the fatigue trial, as evidenced by the shift to a lower median frequency from the rested condition to the final condition for both biceps and triceps. In addition, Potvin and Bent (1997) reported fatigued mean frequencies for bicep brachii of 53.0±9.9 Hz similar to this study's final median frequency of 58.77±14.00 Hz.

Muscle Demand

We evaluated the effects of task target and task type (unimanual and bimanual pushing and pulling) on muscle demand of superficial glenohumeral muscles during dynamic tasks. Muscular demand for superficial glenohumeral muscles was primarily dependent on the interaction between thoracohumeral elevation target and task direction (e.g. push or pull). Pushing to the highest thoracohumeral elevation target increased muscular demand, whereas

pulling from the lowest thoracohumeral elevation target increased muscular demand. Demand during both of these exertions neared the respective push-pull demand of the maximal isometric capacity trials suggesting certain task target and task type interactions for low load dynamic tasks can be as demanding as maximal isometric exertions. Furthermore, pushing was more demanding than pulling at all elevation angles except the low target, suggesting that exertion direction with respect to gravity plays a larger role in determining demand than task target or task, i.e. pushing or pulling, alone. Working against gravity to elevate the handle during the pull from the lowest target and the push to the highest target likely makes these tasks more demanding. Prior work with isometric force exertions suggest that, in general, more elevated tasks increase muscular demand (McDonald et al., 2014; McDonald et al., 2012; Meszaros et al., 2018; Nadon et al., 2016), although task direction plays an integral role in determining spatial dependency. Contextualizing our results against the spatial dependency for a given exertion in these studies is somewhat difficult as their exertion directions are defined relative to a fixed axis and our exertions are defined relative to the torso. Of these isometric studies, Meszaros et al. (2018), however, directly evaluated the effect of task direction, reporting that downward exertions were the least demanding over a range of task targets whereas upward exertions were the most demanding. Despite differences in task definition, our current study agrees with this isometric study that working against gravity increases demand. The results from the current dynamic study are also consistent with isometric strength data that has found inferiorly directed force to be the strongest for both males and females (Chow and Dickerson, 2009; La Delfa et al., 2014; La Delfa and Potvin, 2016). While it is well documented that maintaining elevated postures is a risk for fatigue and MSD (Grieve and Dickerson, 2008; Hagberg and Wegman, 1987), this present study highlights that shoulder loading during dynamic conditions is more

dependent on exertion direction with respect to gravity than actual location of the task target or task type alone. With this in mind, workspaces involving dynamic tasks can be designed to make better use of the whole reachable workspace without compromising safety conditions for shoulder loading by requiring that elevated tasks move with gravity rather than against it.

Plane of elevation was only present as a main effect and had a limited effect on muscular demand for superficial glenohumeral muscles. Only the lateral 0º target was significantly more demanding than the 45º target and differences in demand values between these task targets were minimal (less than 0.03). Previous studies of isometric anterior/posterior pushing and pulling have reported increased total muscular activity at both horizontal extremes (McDonald et al., 2012). Studies of upward isometric exertions showed similar increases in total muscle activity with more lateral targets (Nadon et al., 2016); however, studies of downward (Nadon et al., 2016) and lateral (McDonald et al., 2014) isometric exertions did not show the same trend. These additional studies support the claim that exertion direction can influence how muscle demand varies across horizontal targets throughout the workspace. For the dynamic tasks in this study, our exertion direction (pushing/pulling) was defined as away from/towards the torso, while the isometric studies used exertions relative to a fixed frame. Meszaros et al. (2018) evaluated 6 force exertion directions (anterior/posterior, upward/downwards, and medial/lateral) and found no influence of medial/lateral targets on muscle demand. The results of this current dynamic study lie between the single direction isometric studies and the multidirectional study, since we saw limited horizontal dependency, but only at the lateral extreme. This makes sense, since our task direction is most similar to a combination of the isometric exertion directions. Furthermore, a study of isometric strength by La Delfa et al. (2016) suggested that maximal capacity is higher when the direction of applied force is parallel to a vector for the shoulder to the knuckles. All of

our exertions in the current study were in this direction and may contribute to why there was limited effect of elevation plane. One explanation for why the 0º target required slightly more demand than the 45º target is that subjects have reduced stability from the backrest of the chair for this test target. These results highlight that task definition needs to be considered before generalizing results to workspace design for a specific task.

Pushing, in general, resulted in higher demand than pulling except for the low thoracohumeral elevation target. Even at the neutral elevation angle 90º in which motion with respect to gravity was not in play, pulling required 47% and 54% lower demand compared to pushing for unimanual and bimanual tasks respectively. This is true even though pulling tasks occurred at a higher percentage of isometric capacity because the resistance was defined based on 15% max push-pull exertion (which for these participants was always a push exertion; Table 1). Two primary factors explain this result. First, differences in dynamic strength capacity between pushing and pulling may contribute. Previous studies of strength capacity report varying results as to whether pushing or pulling is stronger depending on experimental conditions (Calé-Benzoor et al., 2016; Chaffin et al., 1983; Chow and Dickerson, 2016; Das and Wang, 2004; Kumar, 1995). In the current study, isometric strength was measured in a seated posture with the torso restrained. Other work by Das and Wang (2004) and Kumar (1995) have reported stronger pull strength, in contrast to our results; however, in Kumar (1995) pushing and pulling were measured in a standing posture with the legs stabilized, while Das and Wang (2004) used seated tests without a torso restraint. Our strength results agree with the isometric results of Chaffin et al. (1983) and Chow and Dickerson (2016) which both evaluated standing push-pull capacity without external stabilization of the lower limb. Importantly, dynamic measures of strength suggest that isometric push-pull relative strength may change with movement. Calé-Benzoor et

al. (2016), measured isokinetic strength ratio between pushing and pulling in a similar seated and restrained manner as the testing protocol in this present study. They found push:pull ratios for dominant and non-dominant arm to be near 1 at a slower velocity 12.22cm/s. However, at a faster speed of 36.67cm/s these ratios decreased to 0.81 and 0.82 for dominant and non-dominant arms. This decrease in push strength relative to pull strength at speeds similar to the dynamic tasks in the present study could account for some of the increase in muscle demand between task direction. A second factor influencing comparisons of push to pull task types is the selection of muscles evaluated in the present study. Because our interest was with muscles crossing the glenohumeral joint, we chose a balanced selection of antagonist pairs of muscles that play important roles in the actuation of the glenohumeral joint. However, other muscles, such as trapezius which plays an important role in pull tasks at close reach distances (MacKinnon and Vaughan, 2005), were omitted and not included in the demand calculation. If more omitted muscles play important roles in pulling than in pushing, this may artificially lower the pulling demand measured. Evidence from other work nevertheless supports that pushing may be more demanding than pulling. For example, a prior study of submaximal isometric anterior/posterior pushing and pulling (McDonald et al., 2012) did not directly compare total muscle demand between two task directions, but similarly reported that muscle activity as a percentage of MVC was greater in pushing than pulling. The increase in muscle demand during dynamic pushing may make it more likely to cause fatigue and lead to MSD than pulling.

Bimanual operation of a task can reduce the demand placed on a single shoulder, but these improvements were less than 50%. Our results show that bimanual tasks reduced muscle demand on a single shoulder by 32% on average, although reductions depended on task target. Our results support the claim that bimanual tasks can reduce the risk of MSD, however,

improvements in muscle demand may be undermined if overall loading is increased for bimanual tasks since reduction in demand is less than 50%. In a study of non-seated push pull forces, Chaffin et al. (1983) reported one arm strength averages were approximately 73% of the two arm values. This study demonstrates that push-pull capacity is only partially dependent on arm strength which may contribute to the limited decrease in muscle demand we saw when switching from unimanual to bimanual operation. Another potential reason for the limited reduction in demand is uneven load sharing between dominant and non-dominant arms. Chow et al. (2017) evaluated muscle demand on both arms during bimanual pushing and pulling. Their statistical analysis did not directly compare left and right demands, but they report different interactions between sex and handle height for left and right weighted EMG and show differences in weighted EMG divided by hand force, suggesting that demand during bimanual tasks may not be evenly distributed. Therefore, this limited reduction in demand in the current study may be a combination of uneven load sharing and differences of strength between unimanual and bimanual operation.

Study limitations should be considered when interpreting these results. Participant history of upper limb injury was self-reported, and subjects were not screened for the presence of an asymptomatic injury. The presence of asymptomatic injury can alter strength capacity (Kim et al., 2009). Altered strength capacity in the dominant arm would have resulted in lower loading for the testing protocol, and thereby introduced confounding factors into analysis. Additionally, asymptomatic rotator cuff tears alter muscle activity patterns (Kelly et al., 2005), although these injuries are primarily present in older adults and our population was young healthy adults. The objective of this study was to analyze muscle demand in a healthy population and altered muscle activation strategies resulting from injuries would confound results of this study. Our study

population included both left and right dominant subjects, and hand dominance could be a potentially confounding factor; however, all task targets were defined relative to the dominant shoulder and we present data by the dominant side to mitigate any confounding effects. While other muscles play a role in push-pull tasks, we chose a balanced subset of push-pull muscles crossing the glenohumeral joint, since MSD at the shoulder often manifests at the glenohumeral joint (e.g. impingement and bursitis). Additionally, we acknowledge that many dynamic force exertions have variable force profiles, but in order to isolate the effects of task target and task type (unimanual and bimanual pushing and pulling) a constant force profile was used. Neither isometric individual muscle MVC (Cram and Criswell, 2011) nor dynamic MVC (Hodder and Keir, 2013) were collected; rather, we normalized EMG data to isometric joint moments and maximal push-pull exertions. These four maximal exertion trials were chosen to elicit contraction in our selected muscles in an efficient manner, but the lack of individual muscle MVC data may have altered normalized peak values, as we saw some peaks above 1.0. Our analysis, however, was intended to identify how demand varies according to task location rather than absolute value per se. Since EMG data of the maximal push-pull exertions were taken at a neutral location, the spatial dependency observed should be unaffected by the normalization scheme. In addition, EMG recordings were made with surface EMG which limited our selection of muscle to superficial glenohumeral muscles. Rotator cuff muscles also cross the glenohumeral joint but were not included in our muscle selection since they are more accurately recorded with intramuscular recordings of EMG signals (Rajaratnam et al., 2014). The primary function of the rotator cuff is joint stabilization; therefore, demand of these muscles should be related to demand of superficial glenohumeral muscles. A single PCSA ratio was used for all subjects since muscle volume distribution is highly conserved across adults (Holzbaur, Murray et al., 2007; Saul et al.,

2015; Vidt et al., 2012). Muscle volume distribution among subjects in this study may have been different from reported values in the literature, which would influence muscle demand calculations; however, we did not have imaging data available to evaluate this. One subject was unable to complete the push trial at 170º thoracohumeral elevation/135º plane of elevation. Other subjects, however, did not struggle with this target. Subjects were free to choose their own coordination strategies to complete tasks, and this subject may have made kinematic choices that made this task target particularly difficult for them. Excluding this task for this subject underestimates the average demand of this task target. Task speed was not explicitly controlled during the testing protocol, although subjects received instructions regarding approximate trial timing, and trials were reperformed if they noticeably deviated from instructions. During study development, we explored the use of a metronome to control task speed; however, when using a metronome, subjects tended to perform the tasks less smoothly which was undesirable. By not controlling for task speed we introduce another variable into the analysis; however, workers typically perform tasks at a self-selected speed and thus this approach may be more representative of industrial settings. Lastly, participants performed tasks in a seated posture with their torso restrained to isolate the effects of task target and task direction on shoulder muscle demand. In an industrial setting, workers are typically unconstrained and may rely more heavily on back muscles to complete tasks or employ altered movement strategies. Our task definition in this study was necessary to isolate the effects of task target and task type on glenohumeral muscles, but future work should consider contributions of the back as well.

Conclusion

Submaximal dynamic pushing and pulling are common industrial tasks whose muscle demand has been previously unexplored. In particular, we found that elevating the limb during dynamic pushing and pulling results in increased muscle demand for superficial glenohumeral muscles. Thus, workspace design involving dynamic pushing and pulling should avoid tasks that result in motion against gravity. Plane of elevation, however, appears to have reduced influence on muscle demand, and is thus a less important constraint. Furthermore, priority should be given to locating push tasks at low demand locations since pushing is in general more demanding than pulling. Additionally, where possible workspaces should be designed to enable bimanual operation of tasks since dividing load over two-hands reduces muscle demand placed on a single shoulder and can help reduce worker fatigue and prevent MSD. Single shoulder demand was reduced by 32% on average as a result of bimanual operation, suggesting that while task type can greatly reduce demand on a single shoulder, this reduction is somewhat limited by factors such as uneven load sharing. The current study found that dynamic pushing and pulling tasks have different muscle demand and workspace location dependence compared to previous studies of spatial dependence using isometric tasks and various exertion directions, although both isometric and dynamic exertions require increased demand when working against gravity. Thus, care should be used when generalizing from isometric to dynamic tasks and across exertion directions for workplace design.

CHAPTER 3

Spatial Dependency of Glenohumeral Joint Stability During Dynamic Unimanual and Bimanual Pushing and Pulling (In preparation for *ASME Journal of Biomechanical Engineering*)

Daniel C. McFarland, Emily M. McCain, Michael N. Poppo and Dr. Katherine R. Saul

Abstract

Degenerative wear to the glenoid from repetitive loading can reduce effective concavity depth and lead to future instability. Therefore, workspace design should consider glenohumeral stability to prevent initial wear. While glenohumeral stability has been previously explored for activities of daily living including push-pull tasks, whether stability is spatially dependent is unexplored. We simulated bimanual and unimanual push-pull tasks to 4 horizontal targets (planes of elevation: 0º, 45º, 90º, and 135º) at 90º thoracohumeral elevation and 3 elevation targets (thoracohumeral elevations: 20º, 90º,170º) at 90º plane of elevation. The 45º horizontal target was most stable regardless of exertion type and would be the ideal target placement when considering stability. This target is likely more stable because the applied load acts perpendicular to the glenoid, limiting shear force production. The 135º horizontal target was particularly unstable for unimanual pushing (143% less stable than the 45º target), and the applied force for this task acts parallel to the glenoid, likely creating shear forces. Pushing was less stable than pulling (all targets except sagittal 170º for both task types and horizontal 45º for bimanual) ($p<0.01$), which is consistent with prior reports. There were limited stability benefits to task placement for pushing, and larger stability benefits may be seen from converting tasks from push to pull rather than optimizing task layout, e.g. unimanual pushing at the 90º horizontal target was

197% less stable then unimanual pulling. Lastly, there was no difference in stability between bimanual and unimanual tasks, suggesting no stability benefit to bimanual operation.

Introduction

The glenohumeral joint is the most mobile joint in the human body due to a lack of an intrinsically stable osseous socket, like that of hip joint acetabulum. As a result, this joint relies on a combined effort of passive structures and active contributions of muscles, with muscles acting as the primary stabilizers during motion. Damage to these active and passive structures can limit the ability to stabilize the glenohumeral joint (Lazarus et al., 1996; Lippitt and Matsen, 1993; Steenbrink et al., 2009; van Drongelen et al., 2013), and reduction in stability is often linked to prior episodes of instability (Marchi et al., 2014). For example, Marchi et al. (2014) reported a reduction in stability index, a measure of computed transverse to compressive forces, for subjects with prior dislocation when compared against healthy controls Furthermore, atraumatic instability (Lazarus et al., 1996; Rowe et al., 1978) and/or degenerative wear to the glenoid concavity from repetitive loading can compromise the glenoid concavity. Lippitt and Matsen (1993) performed a cadaveric study on glenohumeral stability and reported reductions in stability after resection of the labrum, concluding that any wear or damage that reduces the depth of this concavity would result in a reduction to stability. Active stabilization from muscles is provided through concavity compression, compressing the humeral head into the glenoid cavity, and scapulohumeral balance, balancing the net joint reaction force through the glenoid fossa (Lippitt and Matsen, 1993). Therefore, joint reaction forces composed of large ratios of transverse to compressive forces destabilize the joint and pose greater risk for shoulder instability and degenerative wear to the joint.

To prevent initial damage to these joint structures, workspace design should consider glenohumeral joint reaction force to avoid motions that naturally place the shoulder at higher risk for instability. Pushing and pulling are frequently performed occupational tasks (Baril-Gingras and Lortie, 1995; Lind, 2018), and while muscular demand during isometric (McDonald et al., 2012) and dynamic (McFarland et al., In review; McFarland et al., 2017) push-pull tasks have been shown to be spatially dependent, whether this spatial dependency extends to stability is unclear. Furthermore, unimanual and bimanual operation during dynamic pushing and pulling result in differing muscle demands (McFarland et al., In review), and these differences may also apply to joint stability. Previous studies, however, have reported differences in stability between pushing and pulling (Marchi et al., 2014). Pushing results in unstable joint reaction forces for both cart pushing (Nimbarte et al., 2013) and hand positioning tasks (Marchi et al., 2014) whereas pulling results in stable joint reaction during a functional pull from in front of the body (Vidt et al., In review; Vidt, 2014) and hand positioning tasks (Marchi et al., 2014). The stability index during activities of daily living (Klemt et al., 2018) has been shown to depend on shoulder posture, but such this index has not been used to evaluate workspace layout. Knowledge of whether these risks are spatially dependent with task target, i.e. hand location at the end of the task, is necessary to inform safer workspace design that incur less wear to the glenohumeral joint.

This research aims to expand understanding of how task design affects glenohumeral joint instability, and whether smarter workspace design can reduce loading associated with risk for degenerative wear and subsequent instability issues. The objective of the present study was to evaluate how task target and task type (unimanual and bimanual pushing and pulling) influence stability at the glenohumeral joint. Our hypotheses for this study were that (i) task target would

influence the ratio of transverse to compressive forces acting at the shoulder and (ii) pushing would result in larger ratios of transverse to compressive forces than pulling. Since the modern industrial workspace is typically characterized by light repetitive work (Das and Sengupta, 1996), submaximal loading was evaluated.

Methods

Experimental Protocol

Experimental data was previously recorded from 14 healthy young adults (6 males/8 females) 20 to 32 years old while performing unimanual and bimanual push-pull tasks (McFarland et al., In review; McFarland et al., 2017); these data informed the computational simulations evaluated here. The participants had the following inclusion criteria: 1) no history of upper limb injury or pathology, 2) no neuromuscular impairments, and 3) no physical impediments to performing the required exertions. All subjects were self-reported right-dominant, and the right hand was used for all unimanual tasks. All subjects provided written informed consent in accordance with North Carolina State University Institutional Review Board. A brief summary of the pertinent experimental data collected in the previous study is provided here, as well as a summary of additional data obtained at the time of data collection but not previously reported.

Maximum isometric joint moments for shoulder abduction and elbow flexion of the dominant arm were collected (Biodex System 4 Quick Set, Biodex, Shirley, NY) following a previously described standard protocol (Holzbaur, Delp et al., 2007). Maximum isometric shoulder abduction moment was assessed with the shoulder abducted to 60º and the elbow braced in full extension. Maximum isometric elbow flexion moment was assessed with the shoulder in neutral abduction and the elbow flexed to 90º. Three trials of each exertion were obtained;

participants received standardized verbal and visual feedback to encourage maximum isometric moments. The maximum moment was determined as the peak isometric moment of the three trials sustained for at least 0.5 seconds. To minimize fatigue, 60 seconds of rest were provided between trials.

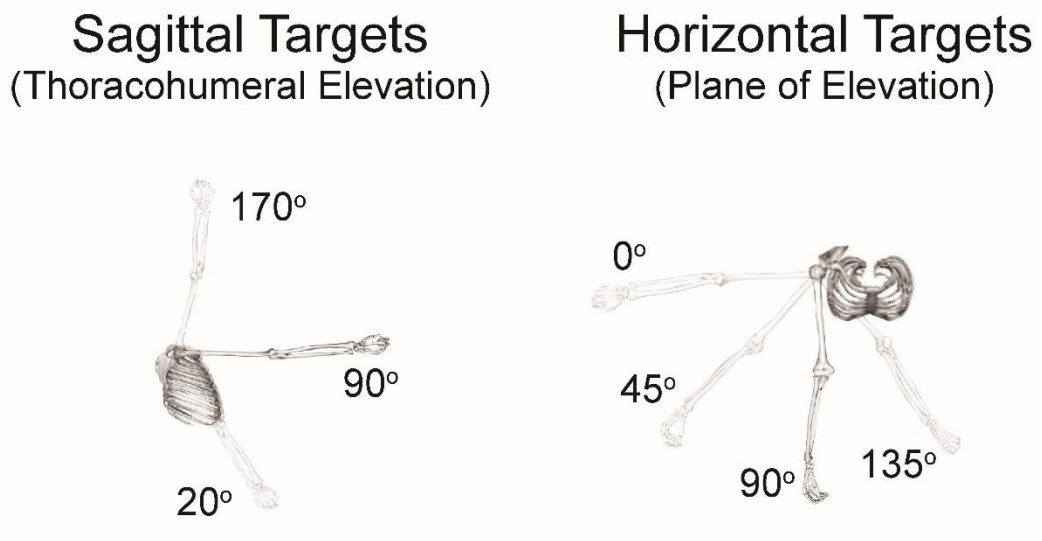

Figure 3.1: Task targets

Unimanual and bimanual push and pull simulations were performed for 4 horizontal targets defined by the plane of elevation angle achieved at the target (0º, 45º, 90º, and 135º) at thoracohumeral elevation of 90º and 3 sagittal targets defined by the thoracohumeral elevation angle achieved at the target (20º, 90º, 170º) at plane of elevation of 90º, for a total of 6 independent task targets. Bimanual tasks to the lateral 0º horizontal target were not simulated due to the extremely restricted handle motion and joint rotations observed.

A series of submaximal unimanual and bimanual push and pull tasks were performed by subjects. Task loading for all tasks was 15% of subject maximum push-pull capacity measured with the arm in 90º forward flexion determined with a closed-chain Biodex attachment using the same protocol as for the isometric joint moments. Tasks were performed to targets located at 4

horizontal positions, defined by the plane of elevation angle achieved at the target (0º, 45º, 90º, and 135º) at 90º thoracohumeral elevation and 3 sagittal positions, defined by the thoracohumeral elevation angle achieved at the target (20º, 90º, 170º) at 90º plane of elevation, for a total of 6 independent task targets (Figure 3.1). Bimanual pushes and pulls to the lateral 0º horizontal target resulted in extremely restricted handle motion and joint rotations and were, therefore, not simulated. This resulted in a total of 22 unique simulated tasks for each subject.

Bilateral surface electromyographic (EMG) recordings of the anterior, middle, and posterior deltoid, biceps brachii, lateral head of triceps brachii, latissimus dorsi, and pectoralis major were collected during the testing protocol. Recordings were made at 2000 Hz using 1 cm Ag/AgCl dual electrodes with 16-channel capacity (Noraxon Telemyo DTS system, Noraxon, Scottsdale, AZ). Electrodes were placed on the skin overlying the muscle belly following recommendations of Cram and Criswell (2011). EMG recordings were normalized to maximal voluntary contractions obtained during the isometric moment-generating capacity tests (McFarland et al., In review). Kinematics data were simultaneously collected at 200Hz using 7 Hawk and 4 Kestral cameras (Motion Analysis Corporation, Santa Rosa, CA) tracking 1 cm retroreflective markers placed on anatomical landmarks (Figure 3.2) (Vidt et al., 2016). Data was post-processed and smoothed with a 6 Hz Butterworth filter (Cortex, Motion Analysis Corporation, Santa Rosa, CA).

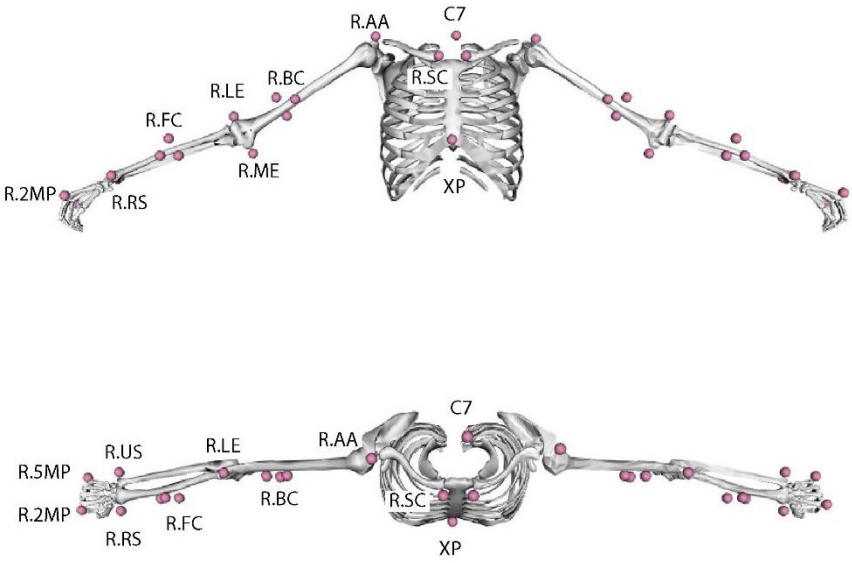

Figure 3.2: Upper limb marker set.

Retro-reflective motion capture markers (pink spheres) were placed on anatomical locations. Only the right side (denoted by R.) and neutral markers are labeled in the figure; left markers are mirrored from right side. Markers include the 7th cervical vertebra (C7), the most ventral aspect of the sternoclavicular joint (SC), xiphoid process (XP), the most lateral aspect of the acromial angle (AA), a biceps cluster of three markers (BC), the lateral epicondyle of the humerus (LE), the medial epicondyle of the humerus (ME), a forearm cluster of three markers (FC), the styloid process of the radius (RS), the styloid process of the ulna (US), the 2nd metacarpophalangeal joint (2MP), and the 5th metacarpophalangeal joint (5MP).

Musculoskeletal Modeling

Simulations of these tasks were performed using a previously developed and validated unimanual upper extremity musculoskeletal model (Saul, Hu et al., 2015) implemented in OpenSim (v.3.3) (Delp et al. 2007) as a foundation. The model was extended to a bimanual model by mirroring joint definitions, muscle paths, and muscle properties to the contralateral

side. Shoulder kinematics are defined according to the ISB standard (Wu et al. 2005), and the shoulder rotation coordinate was expanded to -90º to 120º to allow full range of motion observed during the experimental testing protocol (Vidt et al., In review; Vidt, 2014). Muscle force-generating behavior was represented using the muscle model described by Millard and colleagues (Millard et al., 2013) with force-length, force-velocity, and tendon curves described by Binder-Markey and Murray (2017) to reflect the force profiles implemented in the nominal model (Saul, Hu et al., 2015). Tendon compliance for the clavicular component of pectoralis major was neglected to improve simulation stability since this muscle-tendon unit had a small ratio of tendon slack length to optimal muscle fiber length (Millard et al., 2013). Ligament models representing the coracohumeral ligament and the superior, middle, inferior portions of the glenohumeral ligament were included, with attachment points approximated from mean insertion and origin data obtained in an anatomical study (Yang et al., 2010). Mechanical properties of the ligament models were defined from previous tensile strength studies (Bigliani et al., 1992; Boardman et al., 1996).

Individualized models representing the participants were developed by scaling the generic model to subject anthropometry and strength. Models were scaled to participants' anthropometry using static motion capture trials. Peak muscle forces of the muscle actuators were scaled to match experimental strength data of shoulder abduction and elbow flexion. The model's muscles were grouped by the joint of primary action (Daly et al., 2012), and muscles within a group were scaled together to preserve muscle distribution within a functional group (Holzbaur, Murray et al., 2007; Saul, Vidt et al., 2015; Vidt et al., 2012). Muscle force scaling was determined by a custom optimization that minimized the difference between experimentally measured maximum voluntary joint moments and the model's isometric capacity in the

corresponding posture. To preserve proportionate muscle strength at joints for which strength data was not available, wrist muscles were scaled to an average of the elbow and shoulder scale factors. Symmetry was assumed, and dominant-side scale factors were applied to the non-dominant side.

Computational Simulations

Scaled models were used to obtain joint angle trajectories consistent with observed joint marker positions for each task using inverse kinematics. Resultant kinematics were filtered with a zero-phase filter (Matlab, The Mathworks, Natick, MA). Experimental task loading was applied as an external force to the model, directed along a vector from the initial hand position to the final position in the plane of the task performance. For unimanual tasks, this force was applied to the hand's center of mass. To allow uneven load distribution during the bimanual tasks, external force was applied to the center of a handle body added to the model, with 5 degrees of freedom (rotation about the axis along the handle's length was excluded) linked to each hand's center of mass through point constraints.

Computed muscle control (CMC) (Thelen et al., 2003; Thelen and Anderson, 2006) was used to determine muscle activations required to track the experimental joint kinematics. Briefly, the CMC algorithm incorporates error dynamics to determine joint accelerations required to track experimental kinematics, a static optimization to calculate required muscle activations to produce the desired joint accelerations, and an excitation controller to drive a forward dynamic simulation which creates simulated joint kinematics that feedback into the error dynamics. The EMG recordings were used to inform on/off timing of the respective muscle actuators. When the normalized EMG signal was below 0.1, the muscle was considered off and calculated excitation

was limited to 0.1. Otherwise, the muscle was considered on, and calculated excitation was not constrained. To prevent theoretical glenohumeral joint subluxation (Chadwick et al., 2009; Dickerson et al., 2007; van der Helm, 1994), an additional penalty term was included during the optimization to constrain the resultant joint reaction force to fall within experimental limits of joint stability (Halder et al., 2001). Halder et al. (2001) characterized multidirectional concavity compression stability ratios (transverse to compressive force ratios) at 4 levels of shoulder abduction and 3 force levels; the average stability ratio reported was used as the limits for the penalty function. When the resultant joint reaction was beyond these experimental limits, a penalty term proportional to the amount over the limit was applied. Reserve actuators were permitted to provide up to 10Nm of joint torque to track the kinematics (Hicks et al., 2015).

Joint reaction forces at the glenohumeral joint were determined using the joint reaction analysis tool in OpenSim. Resultant joint reaction forces were decomposed into components in the transverse plane (i.e. superior/inferior and anterior/posterior forces) and compressive direction (medial forces). Because cadaveric studies of concavity compression report stability ratios that depend on transverse orientation (Halder et al., 2001; Lippitt and Matsen, 1993), as related to the depth of the glenoid concavity (Halder et al., 2001; Lippitt and Matsen, 1993), calculated peak ratios of transverse to compressive forces were adjusted by the stability limit in the direction of the resulting transverse force. Differences between the stability ratio and stability limit were analyzed across task target and task direction (push and pull) for bimanual and unimanual data sets using a two-way ANCOVA ($\alpha<0.05$) with sex as a covariate. Differences between the stability ratio and stability limit were analyzed across exertion type (unimanual vs bimanual) with a one-way ANCOVA ($\alpha<0.05$) with sex as a covariate. For analysis of exertion type, unimanual data for the lateral 0^{o} horizontal target was excluded since bimanual simulations

for this task target were not performed. When interactions were not present, they were removed from the model and a Tukey's honest significant difference post-hoc test was used to analyze results. If an interaction was present, simple main effect test was performed with a one-way ANCOVA at each factor level using a sequential Bonferroni correction to adjust the α. SAS software (v. 9.4, SAS Institute, Inc, Cary, NC) was used for statistical analyses.

Results

Simulation Performance

Average applied external force was 68.95±22.45 N. When separated by sex, applied external force was 54.21±12.25 N for females and 88.59±17.71 N for males. A total of 4.22% of the simulations were removed from the analysis (1.79% of the unimanual tasks and 7.14% of the bimanual tasks). Simulations were removed when the optimization was unable to converge on a solution within the set convergence criteria or when tracking error between input kinematics and simulated kinematics was greater than 5º for shoulder degrees of freedoms. Of the removed simulations, 2.92% were removed because the optimization failed, and 1.30% resulted in tracking error above 5º for shoulder degrees of freedoms. Removed simulations are reported in Table 1. Mean root mean squared (RMS) error between input kinematics and CMC results for the remaining simulations was less than 1º for all degrees of freedom. Maximum RMS reserve torque used was 5.04 Nm for any of the simulated trials. This maximum occurred for the shoulder elevation degree of freedom during a unimanual push to the sagittal target of 20º.

Table 3.1: Removed simulations.

task type	task target	subject	reason
unimanual pull	horizontal 0º	F7	optimization did not converge
unimanual push	sagittal 20º	M4	plane of elevation tracking error of 16.2º
unimanual pull	sagittal 20º	M5	plane of elevation tracking error of 10.9º
bimanual push	sagittal 20º	F1	optimization did not converge
bimanual pull	sagittal 20º	F2	optimization did not converge
bimanual push	horizontal 45º	F2	optimization did not converge
bimanual pull	horizontal 45º	F2	optimization did not converge
bimanual push	sagittal 170º	F2	optimization did not converge
bimanual push	sagittal 20º	F4	optimization did not converge
bimanual pull	sagittal 20º	F4	plane of elevation tracking error of 7.1º
bimanual push	sagittal 20º	F7	plane of elevation tracking error of 9.1º
bimanual pull	horizontal 135º	M2	optimization did not converge
bimanual pull	sagittal 20º	M4	optimization did not converge

Stability

Both task direction and task target were main effects for unimanual and bimanual tasks ($p<0.0001$); however, an interaction between task direction and task target was also present ($p=0.0003$ for unimanual and $p=0.0234$ for bimanual). Therefore, the interaction was analyzed with a simple main effects test at each level of the interaction.

In general, unimanual pushing was less stable than unimanual pulling, and responded differently to target location. Unimanual pushing was less stable than unimanual pulling ($p<0.001$) at all task targets except the most elevated: sagittal 170º ($p=0.0503$). For unimanual pulling, glenohumeral stability was most sensitive to sagittal target placement. The horizontal targets at 90º and 45º were significantly more stable than sagittal targets of 20º (low) and 170º (high)($p<0.001$) (Figure 3.3). The horizontal 45º target tended to be more stable than the more lateral 0º target ($p=0.048$), but this was not significant due to sequential Bonferroni adjustment. For unimanual pushing, however, horizontal target placement had the largest impact. The cross-body 135º horizontal target was significantly less stable then the forward 90º and the lateral 45º

horizontal targets ($p=0.0095$ and $p<0.0001$ respectively) and the elevated sagittal target of 170º ($p=0.0003$) (Figure 3.3). Additionally, for pushing, the lateral 45º horizontal target was more stable than the lateral 0º horizontal target ($p=0.0058$) and the sagittal 20º target ($p=0.0133$). However, for unimanual pushing all mean peak stability indexes were near experimental limits of stability determined through concavity compression (Halder et al., 2001).

For the dominant limb during bimanual tasks, pushing, in general, was again less stable than pulling, but both bimanual task types had similar response to target location. Bimanual pushing was significantly less stable then bimanual pulling at all targets ($p<0.01$) except for horizontal 45º ($p=0.289$) and sagittal 170º ($p=0.1947$) (Figure 3.4). For bimanual pulling, the lateral 45º horizontal target was significantly more stable than sagittal targets (20º and 170º) and the cross-body 135º horizontal target ($p<0.0001$). Bimanual pushing showed a similar response with the lateral 45º horizontal target being significantly more stable than all other targets ($p<0.001$). However, for bimanual pushing, peak stability indexes for all targets except horizontal 45º target were near the experimental limits of stability. Comparison between unimanual and bimanual tasks revealed no difference in stability at the glenohumeral joint ($p=0.5836$).

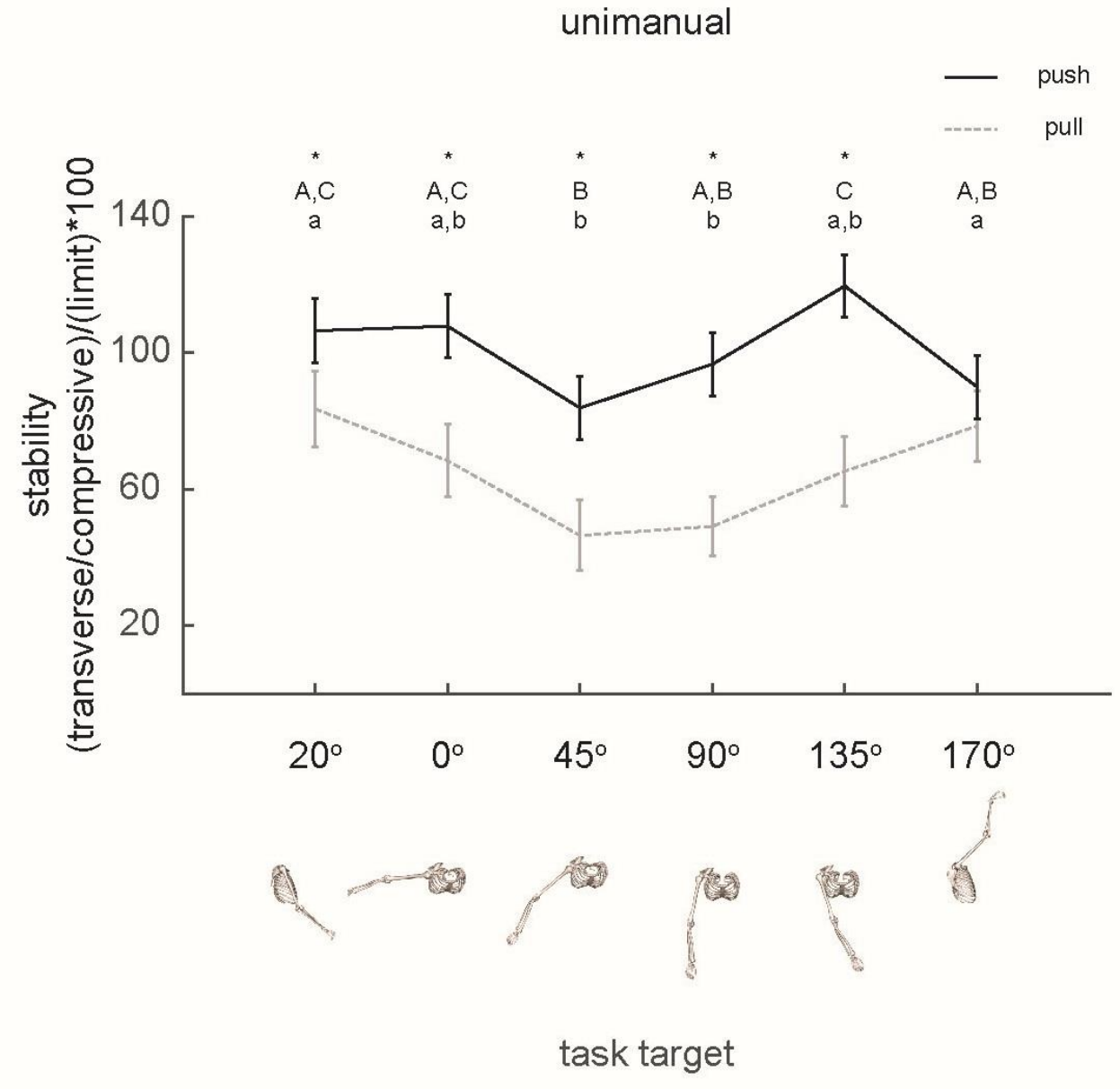

Figure 3.3: Unimanual task direction by task target interaction**.**

In general, pushing was less stable than pulling, and had a different spatial dependency from pulling. Unimanual pushing was less stable than unimanual pulling (indicated by *) ($p<0.001$) at all task targets except the most elevated: sagittal 170º ($p=0.0503$). For pushing, targets with different capital letters are significantly different. For pulling, targets with different lowercase letters are significantly different. Error bars represent 95% confidence interval for adjusted means.

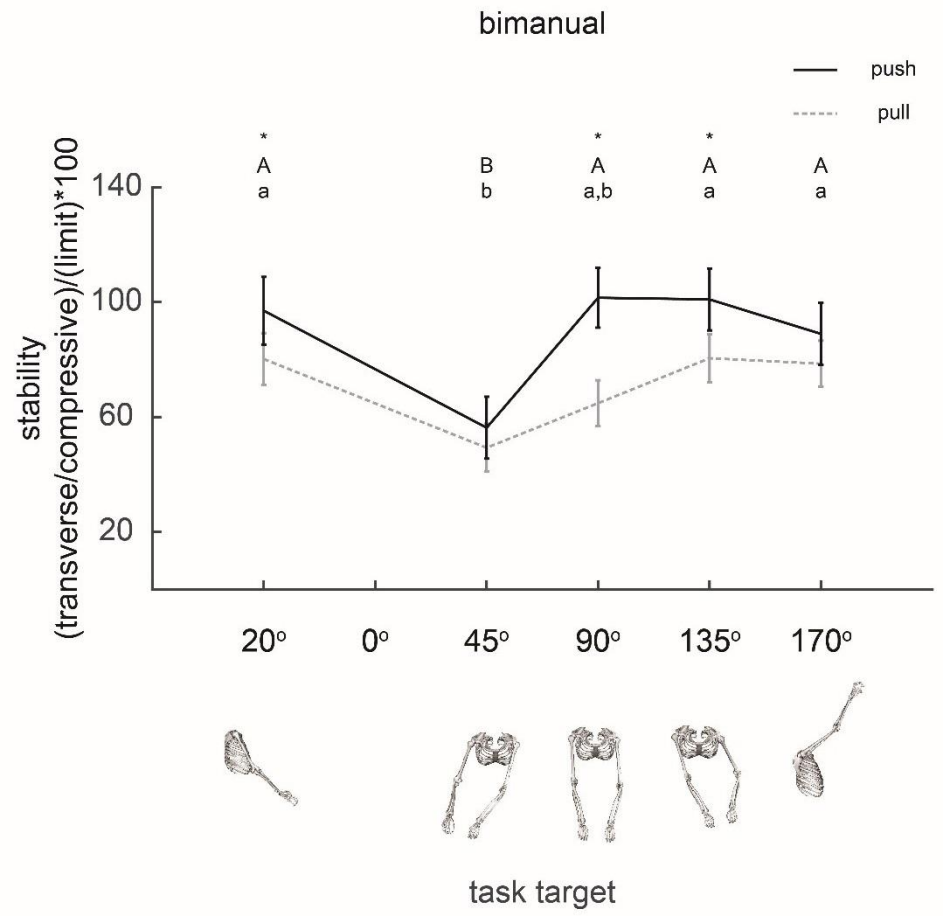

Figure 3.4: Bimanual task direction by task target interaction.

For bimanual tasks when considering only the dominant shoulder, pushing, in general, was again less stable than pulling, but both bimanual task types had similar response to spatial location of tasks. Bimanual pushing was significantly less stable then bimanual pulling at all targets (indicated by *) ($p<0.01$) except for horizontal 45º ($p=0.3059$) and sagittal 170º ($p=0.1947$). For pushing, targets with different capital letters are significantly different. For pulling, targets with different lowercase letters are significantly different. Error bars represent 95% confidence interval for adjusted means.

Discussion

This work demonstrated that glenohumeral stability during both pushing and pulling was spatially dependent, with the lateral 45º horizontal target favoring stability most across exertion types. In general, pushing was less stable than pulling for both unimanual and bimanual tasks. We detected no difference in stability between bimanual and unimanual tasks, suggesting there may be no stability benefit to bimanual operation at low loading.

For unimanual pulling, sagittal targets had the biggest impact on glenohumeral stability with the low and high sagittal targets being significantly less stable than horizontal targets (specifically, 90º and 45º). Other researchers have reported that transverse loading depends on shoulder elevation for other types of tasks as well (Blache et al., 2017; Klemt et al., 2018). For example, similar to our pull from the low target, Blache et al. (2017) evaluated glenohumeral reaction forces during an experimentally-driven simulation of a sagittal lifting task from hip level to shoulder level. They reported increased shear force at the beginning and final phase of the motion. Furthermore, they ran their simulations with and without a joint stability constraint (Dickerson et al., 2007), and found that shear/compressive forces were near empirical limits when constrained and well over these limits when unconstrained. Additionally, similar to the decreased stability seen at our high target, Klemt et al. (2018) found that reaching to head height with a 0.5kg weight was less stable than reaching far ahead with the same weight. In the current study, there was no significant dependence for unimanual pulling on horizontal target location, although the most lateral target (0º) tended to be less stable than the 45º target. The lack of statistical difference may be due to statistical power, since lateral targets during unimanual pulling had wide variability in stability ratios. For unimanual pushing, the cross-body horizontal target of 135º was the least stable target. For the cross-body target, the applied force direction at

the hand is essentially parallel to the glenoid fossa. Therefore, force production for this task target likely results in increased shear forces along the anterior-posterior plane of the glenoid fossa contributing to instability. Furthermore, cross-body motion is at the end-range of motion of the glenohumeral joint, where capsular ligaments contribute to stabilization (Harryman et al., 1990; Terry et al., 1991). While anterior glenohumeral ligaments and the coracohumeral ligament were modeled here, anterior glenohumeral ligaments are only engaged when the shoulder is in extension or external rotation (Terry et al., 1991). Cross-body tasks, however, involve flexion and internal rotation where the posterior capsule, not modeled in the present study, undergoes tension (Terry et al., 1991). Including the posterior capsule in future modeling may increase predicted stability of this task target, but the results of the present study suggest that the muscles do have a limited ability to stabilize the reaction for cross-body tasks. In addition to the instability of the cross-body target, the other extreme posture – lateral 0º horizontal target - was significantly less stable than the 45º horizontal target for unimanual pushing. This is consistent with the work of Klemt et al. (2018), who found that cross-body task, where subjects moved from a lateral target to the other extreme, resulted in the least stable reaction of all the activities of daily living tested in their study. In contrast to targets at the horizontal extremes, the applied force direction for the horizontal 45º target is essentially perpendicular to the glenoid; therefore, force production for pushing to this target likely results in a natural increase in compressive reaction forces, thereby making this target particularly stable. Similarly, for both bimanual pushing and pulling, the 45º horizontal target was again the most stable task target. Furthermore, there was no difference in stability for bimanual pushing or pulling at this target, suggesting that this target is stable regardless of exertion direction. This increased stability was present for both unimanual and bimanual pushing and pulling, making it

the ideal target location when considering glenohumeral stability alone. This task target is in mid-range of glenohumeral motion; therefore, stability is provided through active contributions of muscles. Interestingly, a prior study of muscle demand during dynamic pushing and pulling in the same cohort of participants (McFarland et al., In review) reported that this 45º horizontal target was also less demanding than other horizontal targets, as determined from muscle activation. Inherent task stability of this particular target may contribute to the reduced muscle demand. Additional research is needed to fully understand to what degree inherent task stability and required muscled demand are linked.

Prior studies have reported that pushing results in unstable reactions at the glenohumeral joint (Marchi et al., 2014; Nimbarte et al., 2013), whereas pulling results in more stable reactions (Marchi et al., 2014; Vidt et al., In review; Vidt, 2014). In general, the results from this current study agree with these previous studies, with reactions for pushing resulting in less stable reactions for most targets. Of these previous studies, only Marchi et al. (2014) directly compared pushing and pulling, considering targets placed directly in front of the subject. Therefore, their results would be most analogous to our results for the horizontal 90º target, for which pushing was significantly less stable. Another study by Klemt et al. (2018) compared glenohumeral stability during reaching tasks toward and away from the body while holding a thin wooden rod without applied resistance. They report that both these tasks had high shear to compressive force ratios in the directed inferiorly on the glenoid, although the ratio for tasks toward the body were slightly lower than for away. Reported force ratios were above the empirical stability limits reported in Halder et al. (2001) for the inferior direction. In our study, pulling at the horizontal 90º target resulted in net joint reactions that were within experimental stability limits. This difference in reported stability for pulling is likely related to the difference in applied load

between the study by Klemt et al. (2018) and ours due to the increased muscle forces needed to resist the applied load. We did not observe a difference between pushing and pulling for the high sagittal target or 45º horizontal target for bimanual tasks; no other study has compared glenohumeral stability for these particular task targets. The lack of difference between pushing and pulling at these targets may be partially related to statistical power (difference in pushing and pulling approached significance for unimanual tasks at the sagittal 170º target $p=0.0503$) or related to inherent stability of the joint when forces are directly perpendicularly to the glenoid, as in the 45º horizontal target. Since pushing was in general less stable than pulling, designing for stability may see greater benefits from appropriately choosing exertion direction to be a pull rather than attempting to optimize push layout.

Pushing often resulted in stability ratios that were near experimental limits reported by Halder et al. (2001). Subjects in the experimental study, however, did not report pain or instability during the experimental protocol. The experimental limits reported by Halder et al. (2001) were determined through cadaveric studies at low compression loads and may be lower than *in vivo* stability limits at higher compression. Furthermore, concavity compression ratios do depend on posture (Halder et al., 2001), but are typically measured in an abducted posture (Halder et al., 2001; Lippitt et al., 1993). Our push and pull tasks required postures that differ from abducted postures, and stability limits in these postures may therefore differ from the experimental limits determined in abduction. Some translation of the humeral head, however, does occur naturally *in vivo*. During abduction under anterior loading, humeral head translation *in vivo* is on the order of millimeters (Cereatti et al., 2014). Therefore, it is possible that our testing protocol did result in high transverse forces that caused translation of the humeral head within the glenoid fossa.

Bimanual operation did not result in a significant increase in stability, suggesting that there may be limited stability benefit from switching to bimanual operation at low loading. Stability benefits of bimanual operation, however, may exist if loading is increased. Previous work has shown that reducing the applied load reduces the demand on shoulder muscles for isometric tasks (Meszaros et al., 2018) and that bimanual operation reduced demand on the dominant shoulder for dynamic push-pull tasks (McFarland et al., In review). While glenohumeral stability is related to this combined muscular effort balancing the net joint reaction, this reduction in demand does not appear to influence overall stability.

Study limitations should be taken into consideration when interpreting these results. Subject history of upper limb injury was self-reported, and subjects were not screened for presence of an asymptomatic injury. Shoulder injury, such as a rotator cuff tear, can alter kinematic choices and EMG signaling (Hawkes et al., 2012), which could affect joint loading and stability ratios. These injuries, however, are primarily present in older adults (Minagawa et al., 2013), and our population was young healthy adults. Although subjects received instructions regarding approximate trial timing, task speed was not explicitly controlled. However, workers typically perform tasks at a self-selected speed and thus this approach may be more representative of industrial settings. Subjects performed tasks in a seated posture with their torso restrained to isolate the effects of task on shoulder kinematics. However, in an industrial setting, workers are typically unconstrained and may rely more heavily on torso rotation to complete tasks. Incorporating torso rotation into the movement strategy would require less shoulder motion to reach the lateral horizontal targets; therefore, the range of shoulder motion in an industrial setting may be less extreme than the targets evaluated in this study. Strength scaling was limited to measurements collected for shoulder abduction and elbow flexion in one posture

each, and subjects' strength profile in other postures and for other joints was assumed to follow the same relative profile as the default model. Individual strength profiles across postures can vary (Garner and Pandy, 2001; Otis et al., 1990). Strength of individual muscles were scaled with their primary functional group since muscle volume distribution is highly conserved across adults (Holzbaur, Murray et al., 2007; Saul, Vidt et al., 2015; Vidt et al., 2012). If muscle volume distribution in these subjects differed from reported values in the literature, then individual muscle forces would vary correspondingly; however, we did not have imaging data available to evaluate this. Furthermore, strength data of the non-dominant arm and the wrist of the dominant arm were not collected, so strength symmetry was assumed. Finally, in the simulations the applied force was limited to planar directions to correspond to the controlled handle loading and motion in the experiment along a linear track; however, in the experimental study there may have been limited non-planar components of the applied force as well.

Conclusions

While glenohumeral stability has been previously explored for push-pull tasks, whether stability is dependent on the spatial location of the task has been previously unexplored. We found the glenohumeral joint reaction was most stable for all task types (unimanual and bimanual pushing and pulling) when the applied force was directed essentially perpendicular to the glenoid, thereby limiting shear force production. Therefore, placing push-pull tasks near this task target may help reduce degenerative wear to the glenoid. Pushing, in general, was less stable than pulling and had predicted stability ratios nearing empirical stability limits, suggesting that stability benefits may be seen from converting tasks from push to pull tasks. Lastly, there was no

difference in stability between bimanual and unimanual tasks, suggesting limited stability benefit to bimanual operation at low loading.

CHAPTER 4

Comparison of Techniques to Incorporate Glenohumeral Stability Mechanisms into Inherently Stable Musculoskeletal Models (In preparation for *Computer Methods in Biomechanics and Biomedical Engineering*)

Daniel C. McFarland, Alexander G. Brynildsen, and Dr. Katherine R. Saul

Abstract

Most upper extremity musculoskeletal models use an ideal ball-and-socket for the glenohumeral joint however, this joint requires active coordination of muscles to stabilize itself. Several methods have been proposed to incorporate active stabilizing mechanisms into computational simulations and thereby improve predicted outcomes, but direct comparison of these methods on multiple predicted outcomes have not been previously made. A sensitivity analysis of common predicted outcomes (net glenohumeral reaction force, rotator cuff activations, and instability) to different techniques of modeling active stabilizing mechanisms (constraining the direction of the net joint reaction and incorporating surface EMG signals into the optimization) was performed. Both EMG and reaction force constraints were successful at stabilizing the joint, however, the other outcomes were more sensitive to the EMG constraints. Restrictive EMG constraints had a tendency to overconstrain the model leading to poor tracking error and simulation failure. Furthermore, predicted outcomes were contextualized with experimental outcomes reported in the literature which suggests that the sensitivity to EMG constraints may not always improve predicted outcomes. Therefore, force constraints may be more appropriate than EMG constraints as a method to incorporate stability since net joint reaction forces and rotator cuff activations were less sensitive to the force constraints.

Introduction

Modeling the glenohumeral joint is a challenging task because it is the most mobile joint in the human body. *In vivo* motion of the glenohumeral joint involves not only rotational degrees of freedom, but translational motion as well (Cereatti et al., 2014). To simplify this joint for modeling purposes, most musculoskeletal models neglect these translations and model the joint as a ball-and-socket (Chadwick et al., 2009; Dickerson et al., 2007; Holzbaur et al., 2005). This modeling assumption makes the glenohumeral joint inherently stable; however, stabilization *in vivo* is provided through a coordinated cocontracting effort of surrounding muscles to balance the net joint reaction force within the glenoid fossa (Lippitt and Matsen, 1993). This inherent stability of a ball-and-socket joint is primarily an issue when using optimizations to solve for required muscle activations since these optimizations typically attempt to minimize muscular effort (Cholewicki et al., 1995). Solutions with cocontractions are typically avoided as they generally increase muscular effort without contributing to the resulting motion. A consequence of this is that these optimizations can neglect coconstractions necessary for joint stability resulting in poor predicted outcomes for net joint reactions (Nikooyan et al., 2010), rotator cuff forces, and predicted instability. To mediate this issue, researchers have proposed methods of incorporating cocontraction into optimization approaches; two common methods are constraining predicted muscle activations to follow measured surface EMG signals (Nikooyan et al., 2012) or requiring the optimization to balance the net joint reaction force within the glenoid through stability constraints (Blache et al., 2017; Chadwick et al., 2009; Dickerson et al., 2007). Constraining predicted muscle activations to surface EMG signals can be done by either constraining on/off timing or constraining the entire signal within a tolerance (Nikooyan et al., 2012). Nikooyan et al. (2012), however, showed that predictive ability of their model was

dependent on how many muscles were incorporated as constraints. Incorporating the entire set of recorded muscles overconstrained their model and led to poor predictions. On the other hand, force constraints address the balance of the net glenohumeral joint reaction force rather than muscle coordination explicitly using one of two mechanisms by which joint reaction forces are stabilized *in vivo*: concavity compression and scapulohumeral balance (Lippitt and Matsen, 1993). Concavity compression constraints (pressing the humeral head into the glenoid fossa) (Blache et al., 2017; Dickerson et al., 2007; Quental et al., 2015) work by constraining the ratio of transverse to compressive forces to fall within multi-direction dislocation force ratios determined through cadaveric studies (Halder et al., 2001; Lippitt et al., 1993). Scapulohumeral balance constraints (the principle that the humeral head is balanced if the net joint reaction passes through the glenoid fossa) (Chadwick et al., 2009; van der Helm, 1994) require the resultant force to remain within the curvature of the glenoid which is typically modeled as an ellipse.

While the effects of both EMG constraints and stability constraints have been individually evaluated, these evaluations are typically made on only one predicted outcome. For example, Dickerson et al. (2007) evaluated the effects of concavity compression constraints on predicted muscle forces, but not glenohumeral reaction forces, and Nikooyan et al. (2012) evaluated the effect of a ±5% EMG tolerance on predicted net joint reactions, but not predicted muscle forces. Furthermore, while Nikooyan et al. (2012) incorporates both EMG and force constraints, the interaction of these constraints were not evaluated. Direct comparison of these techniques to model stabilizing forces in inherently stable glenohumeral joints for multiple outcomes would provide valuable modeling information for future studies.

Therefore, the objectives of this research were to evaluate the sensitivity of three predicted outcomes (net glenohumeral joint reaction force, calculated rotator cuff activations, and predicted instability) to modeling choices for incorporating stability (EMG constraints and force constraints) Our hypotheses were that (i) inclusion of EMG constraints would lower predicted instability and influence the timing and magnitude of net joint reaction forces and rotator cuff activation curves, but style of EMG constraint would not influence outcomes and (ii) inclusion of force constraints would lower predicted instability and influence the timing and magnitude of net joint reaction forces and rotator cuff activation curves, but style of force constraint would not influence outcomes. This research aims to expand understanding of how musculoskeletal modeling choices influence predicted glenohumeral reactions and rotator cuff activations.

Methods

We compared simulation constraints designed to incorporate active stabilization mechanisms into inherently stable models: specifically, their effects on the variability of three predicted outcomes (net glenohumeral joint reaction force, rotator cuff activations, and instability). Simulation constraints evaluated include muscle excitation constraints that incorporate surface EMG signals and force constraints that control the direction of the net joint reaction force. First, we describe the musculoskeletal model employed. Next, we explain the overall simulation approach for low and high demand abduction and forward flexion tasks. Finally, we detail implementation of each constraint.

Musculoskeletal Modeling

A previously developed and validated unimanual upper extremity musculoskeletal model (Saul et al., 2015) representing a 50th percentile male was used to simulate shoulder tasks in OpenSim (v3.3) (Delp et al., 2007). Shoulder degrees of freedom are defined according to the ISB standards (Wu et al., 2005). Scapular and clavicle movement are constrained to move with scapulohumeral rhythm through regression equations developed by de Groot and Brand (2001). The 15 muscle-tendon units representing the muscles crossing the glenohumeral joint and the 10 muscle-tendon units representing muscles crossing the elbow joint were used in this study, and were implemented using Millard muscle models (Millard et al., 2013) implemented with force-length, force-velocity, and tendon curves adjusted to reflect the relationships described by Binder-Markey and Murray (2017). Tendon compliance of the clavicular component of the pectoralis major muscle model was neglected due to the small ratio of tendon slack length to optimal muscle fiber length (Millard et al., 2013). For each simulation, the model was scaled to subject anthropometry using a static motion capture trial and the scale tool in OpenSim. For weighted tasks, the weight was modeled as a cylinder and added to the hand with a weld constraint. Anthropometrically scaled models were used to obtain joint angle trajectories consistent with observed joint marker position for each task through inverse kinematics. Resultant joint kinematics were filtered with a zero-phase filter in Matlab (The Mathworks, Natick, MA).

Computational Simulations

We performed computed muscle control (CMC) simulations (Thelen et al., 2003; Thelen and Anderson, 2006), augmented to include a variety of stability constraints, of low and high demand abduction and forward flexion tasks. Briefly, the CMC algorithm incorporates error dynamics to determine joint accelerations required to track experimental kinematics, a static optimization to calculate required muscle activations to produce the desired joint accelerations, and an excitation controller to drive a forward dynamic simulation which creates simulated joint kinematics that feedback into the error dynamics. Reserve actuators were permitted to provide up to 10 Nm of joint torque if required to track the kinematics (Hicks et al., 2015). Input kinematics for these simulations were taken from four healthy young adults (2 males/2 females) between the ages of 20 and 25 years. The participants met the following inclusion criteria: 1) no history of injury or pathology of the upper limb, 2) no neuromuscular impairments, and 3) no physical impediments to performing the required physical exertions. All of the subjects were self-reported right-dominant, and the dominant hand was used for all tasks. All subjects provided written informed consent in accordance with North Carolina State University Institutional Review Board. Each subject completed the testing protocol in a single session on a single day. Subjects performed a series of low and high demand abduction and forward flexion trials. For high demand tasks, subjects held a 10lb dumbbell; low demand tasks were performed without weight. The three trials of each task were performed consecutively with 30 seconds of rest between trials to prevent fatigue and task order was randomized. Subjects were instructed to abduct or forward flex to the end of their range of motion at a rate of 2 seconds per movement. Kinematic data were simultaneously collected using 7 motion capture cameras (Motion Analysis Corporation, Santa Rosa, CA) tracking 1 cm retroreflective markers placed on anatomical landmarks (Vidt et al.,

2016). Prior to the testing protocol, a static trial in which all markers were visible to the cameras was collected for scaling purposes. Data were post-processed and smoothed with a 6 Hz Butterworth filter (Cortex, Motion Analysis Corporation, Santa Rose, CA). Unilateral surface electromyographic (EMG) recordings of the anterior, middle, and posterior deltoid, biceps brachii, long head of triceps brachii, latissimus dorsi, clavicular and sternal components of the pectoralis major, and brachioradialis were simultaneously collected. Recordings were made at 2000 Hz using 1-cm Ag/AgCl dual electrodes with 16-channel capacity (Noraxon Telemyo DTS system, Noraxon, Scottsdale, AZ). Electrodes were placed on the skin overlying the muscle belly following the recommendations of Cram and Criswell (2011). Prior to the testing protocol, subjects performed a series of maximum voluntary contractions (MVC) against manually applied resistance following a standard protocol (Meszaros et al. (2018)); the MVC test for biceps brachii was also applied for brachioradialis. Exertions were obtained over 5 seconds and each muscle was tested 3 times with two minutes of rest between trials. The second trial of each task for each participant was post-processed and used to normalize EMG recordings obtained during task performance for use in the EMG constraints.

Simulation Constraints

We evaluated two different methods of incorporating surface EMG signals into the computed muscle control optimization: constraining the on/off timing of excitations and constraining the simulated excitations to be within ±5% of the normalized surface EMG signals (Nikooyan et al., 2012). For the on/off timing constraint, when the EMG signal was below 0.1, the muscle was considered off and calculated excitation was limited to 0.1. Otherwise, the muscle was considered on, and calculated excitation was required to be above 0.1. Nikooyan et

al. (2012) compared EMG-driven simulations of abduction and flexion against experimentally determined net joint reactions measured by an endoprosthesis and reported better tracking of joint reactions when only a subset of muscles was evaluated rather than their entire set. Therefore, simulations were performed with both the entire set of recorded muscles constrained and a subset of the recorded muscles constrained. Subsets of muscles for each task were taken from the best conditions reported by Nikooyan et al. (2012). For abduction, this subset included the sternal component of pectoralis major and triceps long head. For forward flexion, this subset included all components of the deltoid, the clavicular component of pectoralis major and brachioradialis. Altogether we evaluate two styles of EMG constraints at three levels of muscles constrained (all, subset, and none) for a total of 5 EMG conditions per subject per task.

We also evaluated two methods of controlling direction of the net joint reaction force within the glenoid: concavity compression (Blache et al., 2017; Dickerson et al., 2007) and scapulohumeral balance (Chadwick et al., 2009; van der Helm, 1994). An additional penalty term was added to the CMC optimization to force the resultant joint reaction force toward the stability limits and thereby prevent theoretical glenohumeral joint subluxation. For the concavity compression constraint, the net joint reaction was decomposed into compressive and transverse forces, and the ratio of transverse to compressive forces was constrained to fall within experimental limits of stability from cadaveric studies (Halder et al., 2001; Lippitt and Matsen, 1993). These stability limits were determined in multiple directions (e.g anterior-posterior, superior-inferior) by compressing the humeral head into the glenoid and determining the transverse force required to dislocate the joint. In the current study, concavity compression stability ratios (transverse to compressive force ratios) were derived from Halder et al. (2001), who reported average stability ratios measured at 4 different levels of shoulder abduction and 3

different force levels. For the scapulohumeral balance constraint, the glenoid was modeled as an ellipse and the net joint reaction is constrained to remain within the ellipse (Chadwick et al., 2009). The ellipse shape for the scapulohumeral balance constraint was derived from experimental measurements (Lippitt and Matsen, 1993). When the resultant joint reaction was directed beyond these constraint limits, a penalty term proportional to force exceeding the limit was applied to the optimization. The same penalty function was applied for each style of constraint. A total of 15 simulations per task per subject (3 stability constraints and 5 EMG constraints) were performed. In total, we simulated 4 subjects during 4 different tasks for a total of 240 simulations.

Statistical Analysis

For each simulated task, we evaluated the effect of the simulation constraints on predicted instability, calculated net joint reaction force, and calculated rotator cuff activations. Predicted instability is calculated as a percentage of the empirical stability limit determined from cadaveric studies (Halder et al., 2001):

$$\frac{(Transverse\ Force/Compressive\ Force)}{(Empirical\ Stability\ Limit)} * 100,$$

where net glenohumeral reaction force is decomposed into transverse and compressive components, and the empirical stability limit is defined according to the direction of the transverse component. For the outcomes of predicted peak instability, peak net joint reaction force, and the peak sum of rotator cuff activations (supraspinatus, subscapularis, and infraspinatus), a three-way ANOVA ($\alpha<0.05$) (factors: EMG constraints, stability constraints, and task) was performed. When interactions were not present, they were removed from the model and a Tukey's honest significant difference post-hoc test was used to analyze results.

Furthermore, if no interaction was present, data were grouped by each level of each factor and evaluated as a function of thoracohumeral elevation angle. If an interaction was present, a simple main effects test was performed with a one-way ANOVA at each factor level of the interaction. Due to the exploratory nature of the study, we did not adjust α for multiple comparisons. Lastly, if an interaction was present, data were grouped by each level of interaction and evaluated as a function of thoracohumeral elevation angle.

Results

Of the 240 simulations, 6 simulations (2.5%) failed to converge on a solution during the optimization and were removed from the analysis. Three of these were for high demand abduction using the ±5% EMG tolerance constraint. The other two were low demand tasks with the scapulohumeral balance force constraint (1 forward flexion with no EMG constraint and 2 abductions: one with the timing constraint and the other without an EMG constraint). Failed simulations are reported in Table 1. Of the simulations that ran successfully, mean root mean squared (RMS) error between input kinematics and CMC results was less than 1.1º for all degrees of freedom. Twelve simulations resulted in tracking error above 5º. All of these simulations were with the ±5% EMG tolerance constraint during high demand tasks (9 abductions and 3 forward flexions). Maximum tracking error was 7.16º for thoracohumeral elevation during a high demand abduction task using both the concavity compression constraint applied and the ±5% constraint applied to all recorded muscles. Simulations with tracking error above the recommended limit of 5º are reported in Table 2. Reserve torque for each coordinate was limited to a maximum of 10 Nm. Maximum RMS reserve torque used was 9.39 Nm for any of the simulated tasks. This maximum occurred for the elevation plane coordinate during high

demand abduction using both the scapulohumeral balance constraint and the ±5% EMG constraint applied to all recorded muscles. Mean RMS reserve torque was under 2.0 Nm for all degrees of freedom for all trials. To confirm that subjects performed tasks at a consistent speed, the time for motion from 30^o to 90^o thoracohumeral elevation was determined. Task duration was 0.71±0.15 seconds with a range between 0.50 and1.07 seconds.

Table 4.1: Failed simulations.

Removed Task	Subject	Force Constraint	EMG Constraint	Reason
Abduction low demand	M1	scapulohumeral balance	timing subset	optimization did not converge
	M1	scapulohumeral balance	none	optimization did not converge
Flexion low demand	M1	scapulohumeral balance	none	optimization did not converge
Abduction high demand	M2	concavity compression	±5% all	optimization did not converge
	M2	none	±5% all	optimization did not converge
	M2	scapulohumeral balance	±5% all	optimization did not converge

Table 4.2: Simulations with high tracking error.

Removed Task	Subject	Force Constraint	EMG Constraint	Tracking Error
Abduction high demand	F1	concavity compression	±5% all	7.2° for plane of elevation
	F1	none	±5% all	7.2° for plane of elevation
	F1	scapulohumeral balance	±5% all	7.2° for plane of elevation
	F2	concavity compression	±5% all	6.1° for plane of elevation
	F2	none	±5% all	6.1° for plane of elevation
	F2	scapulohumeral balance	±5% all	6.1° for plane of elevation
	M1	concavity compression	±5% all	5.8° for thoracohumeral elevation
	M1	none	±5% all	5.9° for thoracohumeral elevation
	M1	scapulohumeral balance	±5% all	6.0° for thoracohumeral elevation
Flexion high demand	M2	concavity compression	±5% all	5.6° for thoracohumeral elevation
	M2	none	±5% all	5.6° for thoracohumeral elevation
	M2	scapulohumeral balance	±5% all	5.6° for thoracohumeral elevation

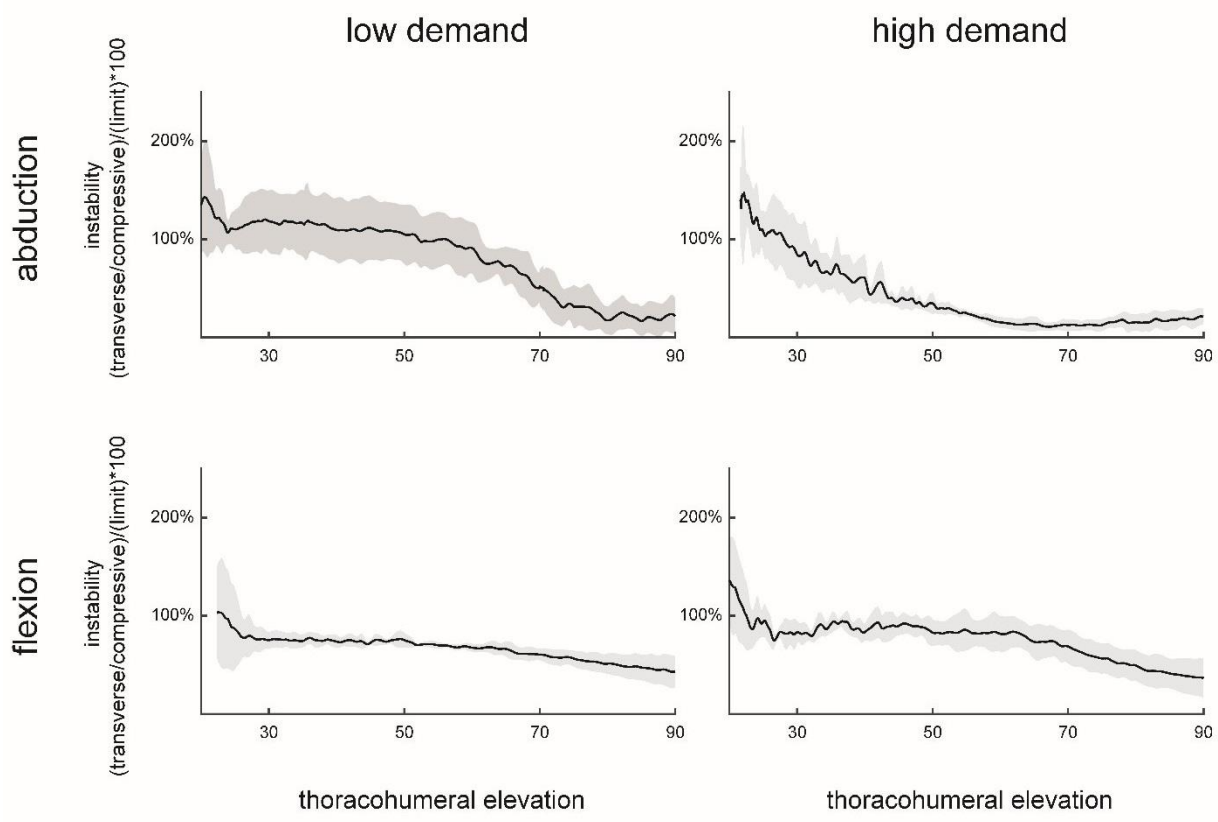

Figure 4.1: Glenohumeral instability during motion.

Mean predicted instability of the subjects when neither force nor EMG constraints are applied is displayed against thoracohumeral elevation. Instability was near empirical stability limits (100%) primarily at low thoracohumeral elevations.

First for each task, average predicted instability was plotted against thoracohumeral elevation for each task to determine elevations where instability would be a concern. Predicted instability neared empirical limits primarily at low thoracohumeral elevations (below 30˚ elevation) (Figure 4.1), so inclusion of stability constraint may only cause variability in other predicted outcomes at low elevations.

EMG constraints, force constraints, and task type were all present as main effects on predicted instability ($p<0.0001$). Furthermore, all interactions of factor were significant ($p<0.05$).

When no force constraints were applied, any EMG constraint significantly lowered predicted instability to be within empirical limits for both flexion tasks ($p<0.0001$) (Figure 4.2). For abduction tasks when no force constraint was applied, only the ±5% tolerance applied to all the recorded muscles significantly lowered predicted instability to be within empirical limits ($p<0.05$) (Figure 4.2). For low demand abduction predicted instability when the timing constraint was applied to all recorded muscles was also within the empirical limits as well, but this reduction in instability was not significant from other EMG conditions. When no EMG constraints were applied, any force constraint significantly lowered predicted instability for high demand abduction and both flexion tasks ($p<0.05$) (Figure 4.2). For low demand abduction, inclusion of a force constraint when no EMG constraints were applied lowered predicted instability, but not significantly ($p=0.1411$ and $p=0.1382$ for concavity compression and scapulohumeral balance respectively). Lowered predicted instability when a force constraint and no EMG constraints were applied were still above empirical stability limits for all task types, but only slightly (all less than 106% of the empirical limit). Using any EMG constraint with a force constraint, lowered predicted instability to be within the empirical stability limits for both flexion tasks, although whether this reduction was significant depended on the interaction between constraints and task type (Figure 4.2). For abduction tasks, using either EMG constraint applied to all the recorded muscles with a force constraint, lowered predicted instability to be within the empirical stability limits for both abduction tasks, although whether this reduction was significant also depended on the interaction between constraints and task type (Figure 4.2). Using the subset of muscles as an EMG constraint with a force constraint did not significantly lower predicted instability for abduction tasks.

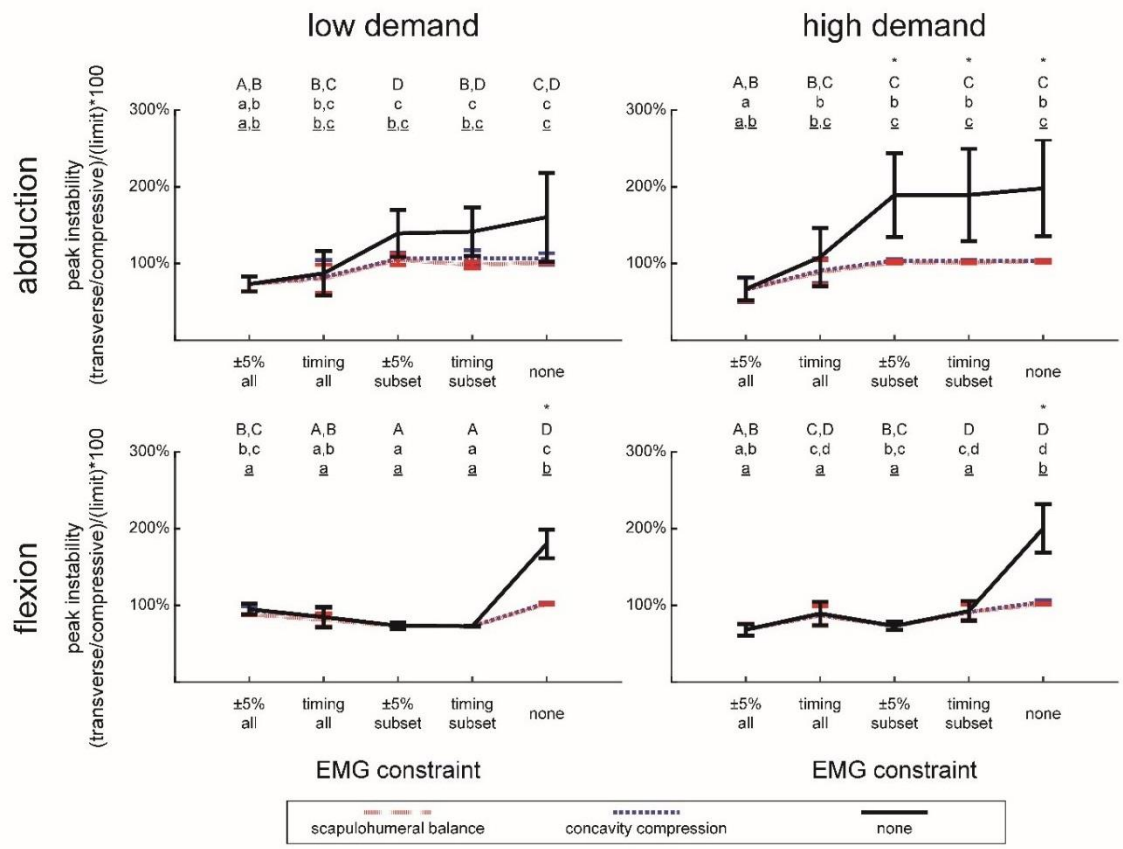

Figure 4.2: Peak glenohumeral instability.

Mean peak predicted instability (percentage of empirical stability limit) is displayed for each task. Predicted instability is grouped by each force constraint and displayed against EMG constraint. For simulations with the scapulohumeral balance constraint, EMG conditions with different capital letters are significantly different. For simulations with the concavity compression constraint, EMG conditions with different lowercase letters are significantly different. For simulations with no force constraint, EMG conditions with different underlined letters are significantly different. Differences in predicted instability among force constraints for a given EMG condition are denoted by *.

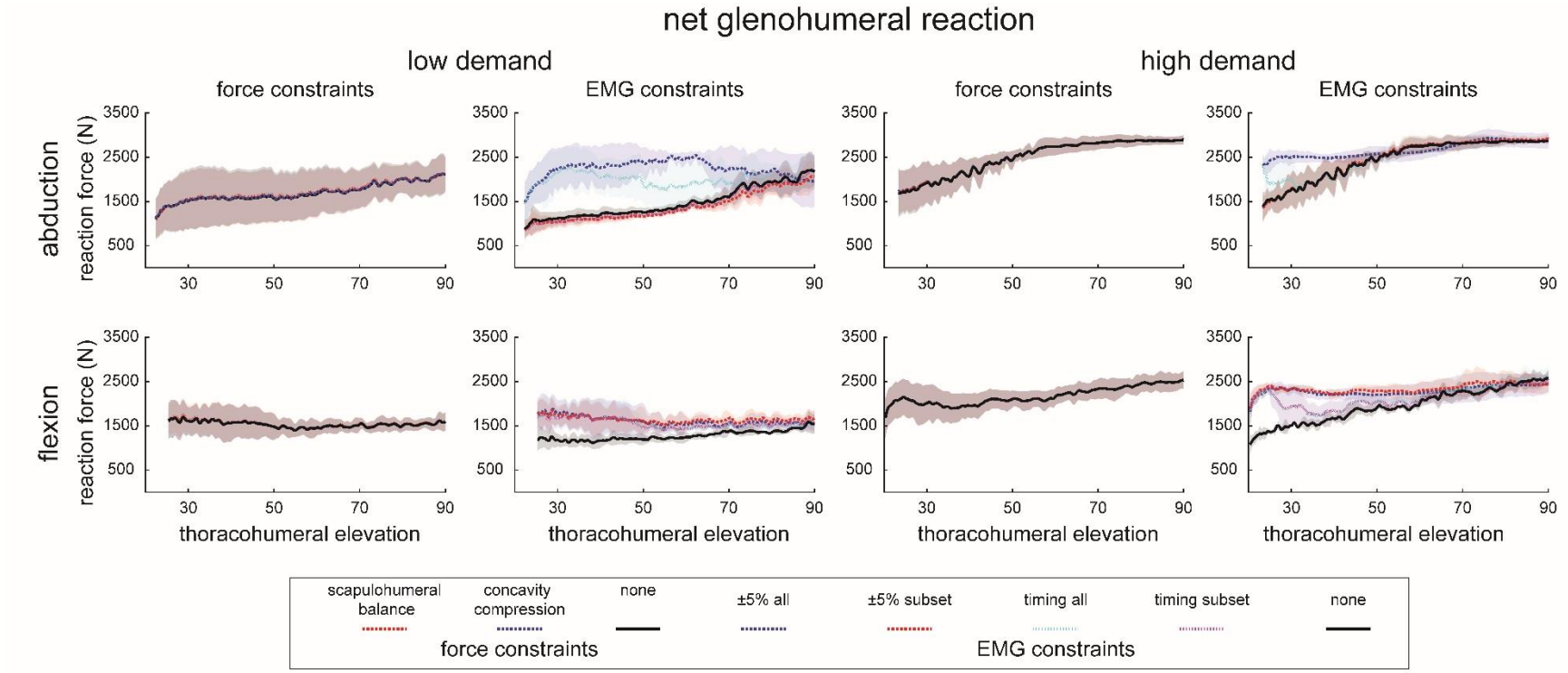

Figure 4.3: Net glenohumeral reaction.

Magnitude of net glenohumeral reaction forces is displayed for all tasks in the testing protocol. Because there was not an interaction between force and EMG constraints, reaction forces are grouped by constraint type, and a plot for each constraint type is displayed for each task.

EMG constraints had a large impact on net joint reaction forces, while force constraints only resulted in subtle differences. EMG constraints and task type were present as main effects ($p<0.0001$), but force constraints were not ($p=0.9995$). Furthermore, there was an interaction between EMG constraint and task type ($p<0.0001$). Post-hoc analysis revealed that only low demand tasks saw differences in peak net joint reaction force from inclusion of EMG constraints ($p<0.0001$). For low demand abduction, constraining the entire set of recorded surface muscles with either the ±5% tolerance or timing constraint resulted in higher peak reaction forces than when the subset or no EMG data was used ($p<0.05$). For low demand forward flexion, including any EMG constraint resulted in significantly higher peak reaction forces than when no EMG constraint was applied ($p<0.0001$), but there were no differences in peak reaction among the types of EMG constraints. Furthermore, for all tasks the type of EMG constraint used impacted the overall timing of the net joint reaction curves (Figure 4.3). For abduction tasks, EMG constraints that used the entire set of recorded muscles had the largest impact on timing causing high reaction forces to develop at low thoracohumeral elevation. Other EMG conditions saw a more gradual build-up of reaction forces. Constraint style (±5% tolerance or timing) had less of an effect on timing, with the EMG timing constraint being more similar to no EMG constraint. For low demand flexion, including any EMG data resulted in high reaction forces developing at low thoracohumeral elevation rather than the gradual build-up of force seen in the no EMG constraint condition. EMG constraint style and number of muscles included, however, had minor impact. For high demand flexion, both styles of EMG constraints resulted in high reaction forces at the start of movement, although the timing constraint saw a decrease in reaction force after the initial peak whereas the ±5% tolerance constraint did not see this reduction. The number of muscles included for high demand flexion, however, had minor influence on curve shape.

Inclusion of the force constraints did not affect the timing or magnitude of reaction force peaks. Only subtle differences were present from using the force constraints, and these differences were typically less than 100N whereas overall reactions were on the order of 1000N. For high demand abduction and low demand flexion differences between force constraints were only present at the start of the motion when reaction forces were near stability limits. Low demand abduction saw differences subtle differences from style of force constraint employed throughout the entire motion.

Predicted rotator cuff activation curves were also most affected by EMG constraints on surface muscles, while inclusion of force constraints only had minor influence. EMG constraints and task type were present as main effects ($p<0.0001$), but force constraints were not ($p=0.9953$). Furthermore, there was an interaction between EMG constraint and task type ($p<0.0001$). Post-hoc analysis revealed that all tasks saw differences in rotator cuff activations from inclusion of EMG constraints ($p<0.001$). For flexion tasks, including any EMG constraint resulted in significantly higher peak activations than when no EMG constraint was applied ($p<0.0001$). There were no differences in peak rotator cuff activations among the types of EMG constraints for high demand flexion, but the ±5% tolerance constraint required higher peak activations for the rotator cuff muscles than the subset constraints ($p<0.05$). Inclusion of EMG data, however, did not have a large impact on overall timing for low demand flexion (Figure 4), but required activations were higher throughout the motion. For high demand flexion, inclusion of EMG data did influence overall timing, and the ±5% tolerance constraint had more of an influence than the timing constraint, regardless of how many muscles were included. However, for both abduction tasks, the number of muscles included had more of an influence on magnitude and timing than constraint style. For low demand abduction, including the entire set of recorded

surface muscles regardless of the EMG constraint style resulted in higher peak activation than including the subset or no EMG data ($p<0.001$). For high demand abduction, including the entire set of recorded muscles for both EMG constraint styles (±5% tolerance and timing) resulted in significantly higher peaks than including no EMG data ($p=0.0028$ and $p=0.0019$ respectively). Including all the recorded surfaces muscles as EMG constraint also influenced activation timing requiring high rotator cuff activations throughout the entire motion. Inclusion of force constraints did not influence peak activations or overall timing for any tasks (Figures 4.4 and 4.5). Only minor differences from inclusion of force constraints were present in the rotator cuff activations, and these differences were primarily present at low thoracohumeral elevations where reaction forces were near empirical stability limits.

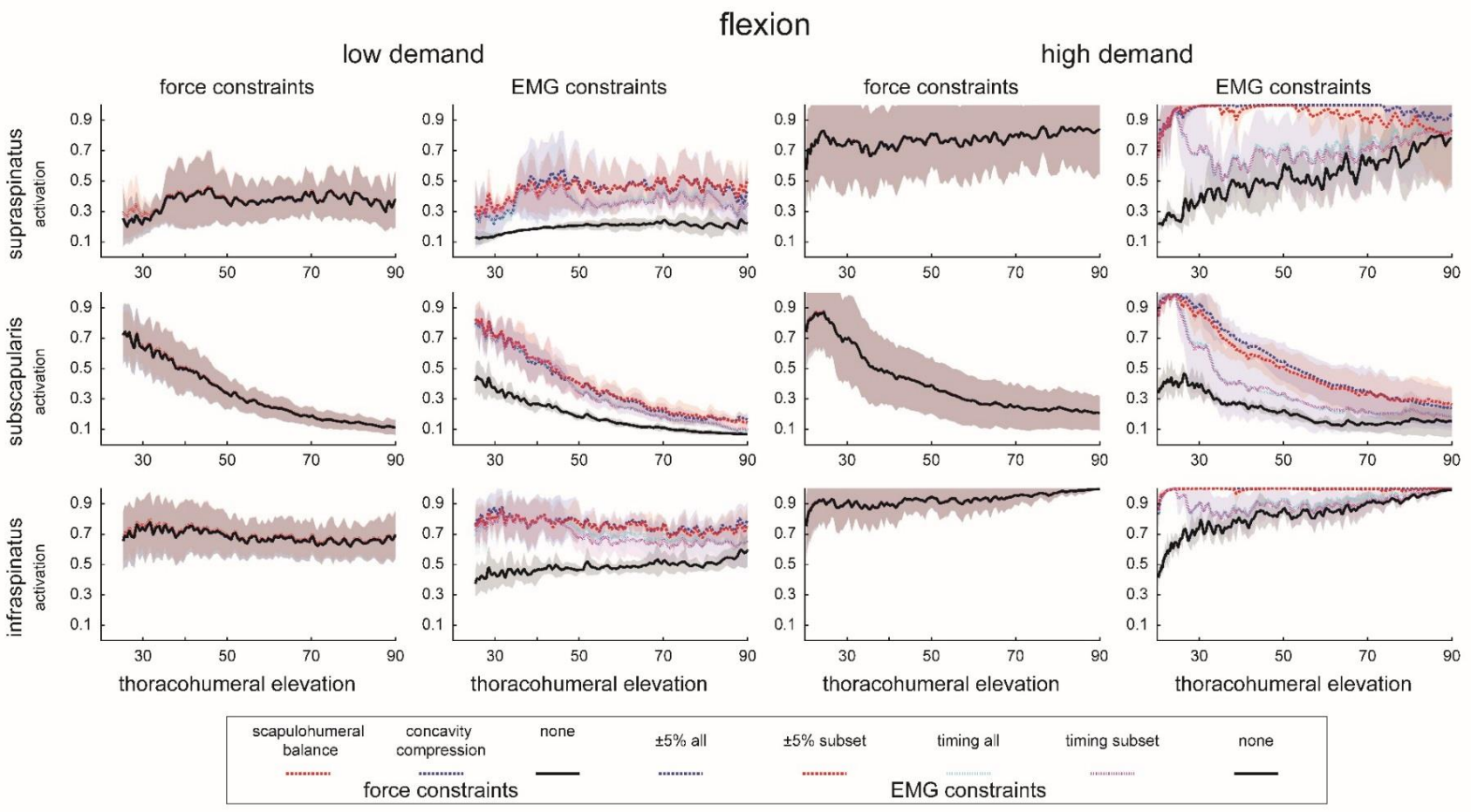

Figure 4.4: Predicted rotator cuff activations during flexion.

Calculated rotator cuff activations for supraspinatus, infraspinatus, and subscapularis are displayed for low and high demand flexion tasks. Because there was not an interaction between force and EMG constraints, activations are grouped by constraint type, and a plot for each constraint type is displayed for each task.

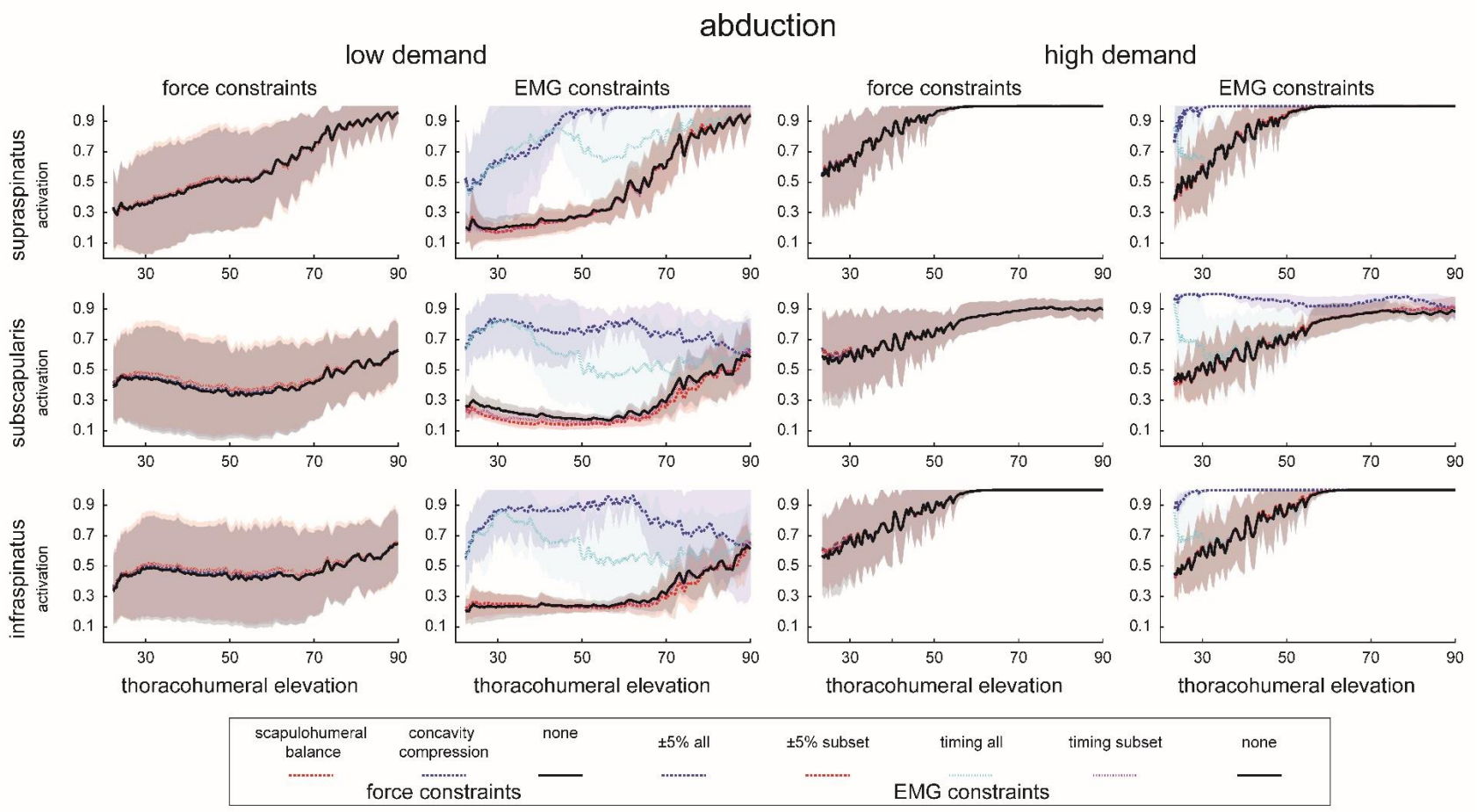

Figure 4.5: Predicted rotator cuff activations during abduction.

Calculated rotator cuff activations for supraspinatus, infraspinatus, and subscapularis are displayed for low and high demand abduction tasks. Because there was not an interaction between force and EMG constraints, activations are grouped by constraint type, and a plot for each constraint type is displayed for each task.

Discussion

We evaluated the effects of force constraints and EMG constraints on predicted glenohumeral instability, net glenohumeral joint reaction forces, and rotator cuff activations during low and high demand abduction and forward flexion. Predicted instability was influenced by the interaction of EMG and force constraints, whereas net joint reaction and rotator cuff activations were influenced by inclusion of surface EMG data, but not by the force constraints. For forward flexion, inclusion of EMG data was sufficient to stabilize the ratio of transverse to compressive joint reaction forces within empirical stability limits reported by Halder et al. (2001). Both force constraints (concavity compression and scapulohumeral balance) were able to stabilize the reaction forces slightly above empirical limits when no EMG data were included; adding EMG constraints on top of stability constraints restored behavior to within empirical limits. Predicted instability values slightly above empirical stability limits are likely acceptable since stability limits vary based on posture (Halder et al., 2001) and some translation of the humeral head occurs *in vivo* (Cereatti et al., 2014). For abduction, only simulations with all recorded muscles constrained resulted in mean peak predicted instability ratios below empirical stability limits. Inclusion of force constraints lowered predicted instability to near empirical stability limits; however, this reduction was not significant for simulations (with EMG constraints applied to either the subset of muscles or no muscles) when compared against simulations without a force constraint applied. It is important to note that different subsets of muscles were used as inputs for the flexion and abduction tasks based off the recommendations by Nikooyan et al. (2012), and the subset for abduction included fewer muscles than the subset used in flexion. Furthermore, the flexion subset included all components of the deltoid which likely impact stability more than the sternal component of pectoralis major and triceps long head

(the abduction subset). Based off predicted instability results for all tasks evaluated in this current study, constraining either the direction of the net glenohumeral reaction force or muscle excitations to surface EMG signals appear to be appropriate methods of incorporating stability. The ability to stabilize the joint with EMG constraints, however, appears to be dependent on which muscles are constrained. Incorporating both EMG constraints and force constraints appears unnecessary since force constraints successfully control the net joint reaction on their own and EMG constraints can successfully control the reaction on their own if enough muscles are incorporated.

Inclusion of surface EMG data as simulation constraints had the largest impact on net glenohumeral reaction forces and predicted rotator cuff activations, however, this impact on magnitude and timing did not always improve consistency with previously reported rotator cuff EMG signals (Heuberer et al., 2015; Wickham et al., 2010) or glenohumeral reaction forces (Nikooyan et al., 2010; Nikooyan et al., 2012). In particular, using the entire set of recorded muscles resulted in high reaction forces developing at low thoracohumeral elevations during both low demand abduction and flexion; however, experimental results show a gradual increase during the entire motion (Nikooyan et al., 2010; Nikooyan et al., 2012). Additionally, using the subset of muscles also resulted in the high reaction forces developing early on during flexion. All predicted net joint reaction forces, however, were much different in magnitude from the experimental measures in Nikooyan et al. (2010; 2012), but these magnitude differences may be due to differences in subject populations since their study involved older adults with an instrumented endoprothesis and ours involved healthy young adults. Furthermore, sensitivity of rotator cuff activations to EMG constraints did not always agree with reported EMG signals. For example, using EMG constraints during low demand flexion did not change timing of predicted

activations, but resulted in higher magnitudes when compared to not using EMG constraints. Experimental results from Heuberer et al. (2015), however, report low EMG signals throughout the motion, and, as a result, supraspinatus activation are more similar to reported EMG signals when no EMG constraints are used. This inconsistency of high predicted rotator cuff activations and low reported EMG signals was also seen in the low demand abduction simulations, but these differences were primarily present when the constraints were applied to the entire set of recorded muscles. Previous work has suggested that more accurate net joint reactions are predicted with a small subset of muscles constrained rather than a larger set (Nikooyan et al., 2012). In the prior study, they recorded 10 muscles and muscle compartments, but when the entire recorded set was used with ±5% EMG tolerance, their simulations failed. Similarly, in the current study for high demand abduction, all simulations with the ±5% tolerance constraint applied to all the recorded muscles resulted in tracking error above 5º or simulation failure (3 simulations). Furthermore, predicted rotator cuff activations during high demand abduction were less similar timing and magnitude when compared to experimental rotator cuff EMG signals (Wickham et al., 2010) when the entire set of recorded surface EMG signals were used as constraints. Wickham et al. (2010) ,however, used a 2.5kg as weighting and such differences in task conditions may contribute to differences seen in timing and magnitude of cuff activations. Therefore, careful consideration of which surface muscles to constrain is needed since overconstraining a model can result in poor predicted outcomes. Constraining muscle excitations to the subset of surface EMG signals (all components of the deltoid, the clavicular component of pectoralis major and brachioradialis) for low demand forward flexion also resulted in less similar timing and magnitude of predicted rotator cuff activation when compared with experimental fine-wire EMG signal (Heuberer et al., 2015) and net joint reaction forces (Nikooyan et al., 2010). In the

previous work of EMG-driven simulations (Nikooyan et al., 2012), the best predicted glenohumeral reaction forces for forward flexion occurred when a subset of 4 muscles rather than the entire recorded set was constrained; however, this best combination of muscles varied from subject to subject. Including the scapular component of the deltoid resulted in poor tracking of experimental reaction forces for one subject in the previous study. In our study, we constrained all components of the deltoid which may explain why every simulation with EMG data included resulted in less similar shapes to the previously reported *in vivo* reactions. Nikooyan et al. (2012) suggest that constraining only one cocontracting muscle may be appropriate and that choice of this muscle should depend on how similar the task evaluated is to forward flexion or abduction. In the current study, constraining the subset (pectoralis major sternal component and triceps medialis) to surface EMG signals for abduction tasks did not result in significantly different peaks for net joint reaction or rotator cuff activations from simulations that included no EMG data. Therefore, incorporating stability through constraining muscle excitations to surface EMG signals may not be worth the risk of overconstraining the model since using a small subset may not significantly change predicted outcomes. Lastly, if EMG constraints are incorporated, a timing constraint may be more appropriate since this style of constraint produced less marked output variability than the tolerance constraint.

Inclusion of constraints to control the direction of the net joint reaction force only had minor influence on the magnitude of net glenohumeral reaction forces and rotator cuff activations, resulting in slightly higher reaction forces and rotator cuff activations. In general, these differences were only present at low thoracohumeral elevations where reaction forces were near empirical stability limits. Since only minor changes in magnitude of reaction forces are seen when force constraints are applied, it is likely that stability in these models is provided through

controlling the direction of the resultant force rather than increasing the magnitude of the compressive force. Blache et al. (2017) compared using a concavity compression constraint to using no constraint and report minor changes in magnitude and timing of shear and compressive forces between conditions. In their study, the shear force is slightly lower, but the compressive force is slightly higher. A trade off of shear forces for compressive forces explains the change in stability without marked change in net joint reaction force magnitude. Additionally, several studies have evaluated the effect of force constraints on muscular effort (Blache et al., 2017; Steenbrink et al., 2009; van Drongelen et al., 2013) and report varying increases in muscular effort to stabilize the reaction. The degree to which force constraints affect muscular effort may be related to the empirical stability limits employed. Empirical stability limits vary (Halder et al., 2001; Lippitt and Matsen, 1993), and several models implement more conservative limits than those we employed (Blache et al., 2017; Dickerson et al., 2007), whereas others use less conservative limits (Chadwick et al., 2009). Dickerson et al. (2007) evaluated a range of stability limits in their study and report increased muscle forces with more conservative stability limits. Overall both force constraints evaluated in the current study had minimal effect on rotator cuff activation and net joint reaction forces and do not appear to be a critical factor when evaluating the overall magnitude or timing of either of these outcomes especially if the motion is known to be particularly stable.

Study limitations should be considered when interpreting these results. Experimental glenohumeral reaction forces and rotator cuff EMG signals were not measured for our subjects; therefore, our analysis was limited to sensitivity of simulation outputs to simulation constraints. Other limitations include the EMG normalization procedure for the EMG constraints used. We normalized our EMG signals using standardized MVC activities (Meszaros et al., 2018);

however, if true peaks were not elicited during these MVC activities, it would artificially increase the applied EMG constraints. Several studies have reported an inablity to capture true peaks during standardized MVC isometric actives (Clarys et al., 1983; Hautier et al., 2000; Jobe et al., 1984; Nikooyan et al., 2012). We evaluated simulation variability for low and high demand abduction and forward flexion between 20º and 90º; however, variability in predicted outcomes from the evaluated constraints may differ for functional tasks or an extended range of motion during these tasks. In addition, we evaluated the variability of predicted outcomes to simulation constraints based on inputs from four healthy young adult subjects; however, simulation outcomes may vary differently when a different sample population are used, i.e. subjects with a rotator cuff tear.

Conclusion

Predicted instability was successfully controlled by either force constraints that controls the direction of the net joint reaction or EMG constraints if several surface muscles were used. Magnitude and timing of the net joint reaction and predicted rotator cuff activations were more sensitive to inclusion of EMG data than force constraints. However, more restrictive EMG constraints, i.e. the ±5% tolerance constraint, had a tendency to overconstrain the model resulting in poor kinematic tracking or simulation failure. Furthermore, outcome sensitivity contextualized with reported experimental outcomes, suggests that EMG constraints may not always improve predictions. Therefore, we recommend including EMG data with caution, and careful consideration of which muscles to include needs to be taken into account. Of the EMG constraints evaluated in this study, an on/off timing constraint may be more appropriate than a tolerance constraint since timing constraints are less likely to overconstrain the model. On the

other hand, force constraints had a large impact on predicted instability , but minor influence on the magnitude and timing of net joint reaction and rotator cuff activation. Style of force constraint had little impact on outcomes and both scapulohumeral balance and concavity compression appear appropriate when evaluating instability. Force constraints may be more appropriate than EMG constraints as a method to incorporate stability since choice of force constraints had minor influence on net joint reaction forces and rotator cuff activations.

CHAPTER 5

Conclusions

Contributions

The first contribution of this work is characterizing the spatial dependency of muscular demand for superficial glenohumeral muscles during dynamic submaximal push and pull tasks. Previous works have characterized the spatial dependency for submaximal isometric exertions including pushing and pulling (McDonald et al., 2014; McDonald et al., 2012; Meszaros et al., 2018; Nadon et al., 2016); however, results from isometric studies are not directly generalizable to dynamic tasks since EMG and force exertion under dynamic conditions frequently differ (Antony and Keir, 2010; Kumar, 1995). This work measured EMG signals to evaluate overall demand of superficial glenohumeral muscles during push-pull tasks to task targets located throughout the reachable workspace. Our results were compared with previous isometric studies to highlight similarities and differences among spatial dependency of muscular demand. Additionally, recommendations were made on workspace design for these dynamic tasks to reduce required muscular demand.

Furthermore, the spatial dependency of glenohumeral stability during these dynamic push-pull tasks is evaluated through computational musculoskeletal simulations. Degenerative wear and previous injuries to the glenohumeral joint can lead to a limited ability to stabilize the joint (Lazarus et al., 1996; Lippitt and Matsen, 1993; Marchi et al., 2014); therefore, preventing initial damage to joint structures is critical. While glenohumeral stability has been evaluated previously for functional tasks (Klemt et al., 2018), this work provides a novel evaluation of how task location impacts glenohumeral stability during pushing and pulling. Peak glenohumeral

stability is reported for several task targets and recommendations on task locations that can reduce glenohumeral joint wear are made.

Lastly, a comparison of modeling techniques to account for active glenohumeral stabilization in inherently stable musculoskeletal models were made. Most musculoskeletal models of the upper extremity use an ideal ball-and-socket for the glenohumeral joint (Chadwick et al., 2009; Dickerson et al., 2007; Quental et al., 2015; Saul et al., 2015; van der Helm, 1994); however, the glenohumeral joint requires active coordination of muscles to limit translations and stabilize the joint. Several methods have been proposed to incorporate active stabilizing mechanisms into computational simulations and thereby improve predicted outcomes. This work compares these techniques and their impact on pertinent predicted outcomes including predicted instability, net joint reaction force, and rotator cuff activations. Recommendations based on our results were made regarding which methods are most appropriate when evaluating each outcome.

Applications

There are several potential applications of the work presented in this dissertation. We found that muscular demand for superficial glenohumeral muscles was primarily dependent on the interaction between thoracohumeral elevation target and task direction, with exertions directed against gravity requiring the most demand. Additionally, we found that glenohumeral stability was spatially dependent during dynamic push-pull tasks; tasks directed along the plane of scaption were the most stable. This information can be used to place dynamic push-pull tasks in low demand locations that are inherently stable when designing workspaces. Industrial workspaces, such as a station on an assembly line, can frequently involve dynamic submaximal

push-pull tasks, and by incorporating the information presented in this dissertation, the risk of developing shoulder musculoskeletal disorders and glenohumeral joint wear can be reduced.

To evaluate the spatial dependency of glenohumeral stability, we developed two custom software applications. The first application uses experimental strength or muscle volume data to strength-scale musculoskeletal models. Strength scaling musculoskeletal models has been shown to improve predicted outcomes for clinical populations (Mogk et al., 2011), and this tool facilitates the scaling procedure. The second application is a custom CMC algorithm (Thelen et al., 2003; Thelen and Anderson, 2006) that requires the net joint reaction to be directed within empirical stability limits (Halder et al., 2001). Including this stability criterion in future studies of glenohumeral stability can help improve predictions of whether tasks pose stability risks. Both of these applications were developed for OpenSim (Delp et al., 2007), an open-source software package that facilitates broad dissemination of these applications to other biomechanics researchers.

Lastly, we evaluated several techniques to model glenohumeral stabilization mechanisms in inherently stable musculoskeletal models. Constraining calculated activations to surface EMG signals had the largest impact on all three predicted outcomes evaluated (glenohumeral stability, net glenohumeral reaction force, and rotator cuff activations). Inclusion of EMG data sometimes overconstrained the musculoskeletal model, resulting in predicted outcomes that agreed less with previously reported experimental results. On the other hand, constraining the direction of net joint reaction impacted glenohumeral stability but had only minor influence over the other predicted outcomes. The information in this dissertation work can be used to inform choices in future computational simulation studies evaluating glenohumeral reaction forces and rotator cuff activations, and thereby improve analysis in future studies.

Future Work

Determine the effect of increased task loading on muscular demand and glenohumeral stability

This dissertation evaluates the spatial dependency of submaximal dynamic push-pull tasks; however, only one task loading condition of 15% of subject's isometric push-pull capacity was evaluated. Evaluating the spatial dependency of both muscular demand and glenohumeral stability at a range of loading conditions could provide additional insight into workspace design. An isometric study has evaluated the effects of increased task loading on muscular demand, reporting that demand increases with loading (Meszaros et al., 2018). It is likely that muscular demand increases with loading for dynamic tasks as well, but spatial dependency of muscular demand may be altered. Additionally, in the current work, we evaluated the effects of switching to bimanual operations and saw no increase in glenohumeral stability; however, stability benefits of bimanual operation may only become apparent at higher task loading.

Determine the spatial dependency of glenohumeral stability for isometric push-pull tasks

While the spatial dependency of muscular demand has been evaluated for isometric tasks (McDonald et al., 2014; McDonald et al., 2012; Meszaros et al., 2018; Nadon et al., 2016), these studies did not evaluate glenohumeral stability. Determining how glenohumeral stability varies with task target during isometric exertions would provide insight into designing workspaces that that reduce glenohumeral joint wear.

Evaluate the spatial dependency of muscular demand for other industrial tasks

Pushing and pulling are some of the most common industrial tasks and were, therefore, chosen for evaluation in this work. Industrial workstations typically involve other tasks as well, such as lifting objects. Previous work has evaluated the effects of height on mechanical muscle work for deep shoulder muscles during an overhead lifting task (Blache et al., 2015), but additional work could extend this evaluation to the entire reachable workspace. Together with the findings presented in this dissertation, this additional work would provide a more complete understanding of appropriate workspace design for workstations that involve multiple types of tasks.

Evaluate the relationship between glenohumeral stability and muscle demand

In this dissertation, we identified 45º plane of elevation as requiring less demand than other horizontal task targets. Additionally, in Chapter 3 we report that this task target was particularly stable. Stabilization of the glenohumeral joint depends on active contributions of muscles to compress the humeral head into the glenoid fossa (Lippitt and Matsen, 1993), and this decrease in demand may, in part, be due to a decreased need to compress the humeral head. Additional research could determine the exact nature of this relationship between muscular demand and glenohumeral stability. If a strong relationship between glenohumeral stability and muscular demand exists, computational simulations can be run with and without the stability constraint applied to determine which muscles contribute to stabilization effort.

Determine the effects of a rotator cuff tear on demand and stability during pushing and pulling

Asymptomatic rotator cuff tears are twice as common as symptomatic tears in the general population (Minagawa et al., 2013). The rotator cuff muscles are the primary active stabilizers of the glenohumeral joint and working with an asymptomatic tear may reduce the ability to stabilize the net joint reaction. Furthermore, muscular demand may increase significantly as a result of attempting to stabilize the net reaction force in the presence of a rotator cuff tear. Rotator cuff tears can be simulated by removing or weakening muscles in a musculoskeletal model (Steenbrink et al., 2009; van Drongelen et al., 2013). The effects of an asymptomatic rotator cuff tear during push-pull tasks can be evaluated by simulating these tasks with and without the simulated tear.

Determine the sensitivity of predicted instability to the number of muscle paths included in a musculoskeletal model

Other musculoskeletal models that evaluate glenohumeral stability use several muscle paths to represent a single muscle (Blache et al., 2017; Chadwick et al., 2009; Dickerson et al., 2007). In Chapter 3, several of our predicted instability ratios were above the empirical stability limits. The current musculoskeletal model may have a limited ability to control the direction of the net joint reaction due to the number of muscle paths in our current model. A sensitivity analysis to determine the appropriate number of muscle paths when analyzing glenohumeral stability could provide valuable insight for future computational simulation studies.

Summary

This dissertation work provides new information characterizing the spatial dependency of muscular demand and glenohumeral stability during dynamic submaximal push-pull tasks. We measured EMG signals of surface glenohumeral muscles and calculated a measure of overall muscular demand. We then used this EMG data to inform computational simulations to predict glenohumeral instability for several of the task targets in the experimental protocol. Lastly, we compared several modeling techniques to incorporate active glenohumeral stabilizing mechanisms into computational simulations and report their effects on several pertinent outcomes.

This work provides evidence that describes how task target and type influence overall muscle demand and glenohumeral loading and stability. In particular, the numerical comparisons between exertion types and targets can be used to inform new workspace design to reduce demand or instability relative to current task placement or task direction. These guidelines are applicable to dynamic workspaces such as assembly line work, where subjects are repetitively performing push-pull tasks that move materials or operate levers. Currently, task loading is typically based on isometric strength from software packages such as 3DSSPP (Chaffin, 1997), but the current work suggests that muscle demand during dynamic tasks may not reflect isometric strength since isometric pull capacity was less than push yet, in general, dynamic push tasks required more demand than pull tasks. Furthermore, the current work shows that during dynamic submaximal tasks the interaction of task direction and task target can result in demand similar to maximal isometric exertions. This highlights the importance of evaluating muscular demand as well, rather than basing task design on isometric capacity alone, since such an interaction may confound fatigue estimates based on isometric strength in isolation. When

muscular fatigue occurs, glenohumeral and scapular kinematics are typically altered (Chen et al., 1999; Chopp et al., 2010; Michener et al., 2003), which can pose risks for shoulder instability or tissue damage that can lead to future instability (Dickerson et al., 2015). For example, induced fatigue of the deltoid or rotator cuff has been shown to lead to increased superior humeral head migration (Chen et al., 1999; Chopp et al., 2010; Michener et al., 2003). Therefore, the novel concept of designing for glenohumeral stability introduced in this work may specifically help counter instability risks from worker fatigue. In particular, the current results suggest that converting dynamic pushing to pulling tasks will not only help reduce the risk of muscular fatigue, but if worker fatigue is induced, then pulling would also protect against further injury due to its inherent overall glenohumeral stability.

While the current analyses and recommendations were developed with push and pull tasks in mind, it is likely that some lessons learned here are applicable to other dynamic tasks such as lifting, although caution should be used. Ergonomists frequently use the best available information to inform task design when information on a specific task is lacking. For example, the ergonomics software 3DSSPP (Chaffin, 1997) is designed to determine static strength capacity, but can be applied to heavy material handling tasks if slow tasks are considered where effects of acceleration and momentum are negligible. Together with future work to determine effects of increased loading, repetition, or the influence of other task movements on demand and stability, this work could be used to develop predictive equations to estimate demand and instability based on task type and location for dynamic tasks. Such a module for dynamic exertions could be a valuable addition to the existing strength capacity software packages (Chaffin, 1997) and isometric submaximal predictive equations (McDonald et al., 2014; McDonald et al., 2012; Nadon et al., 2016) already used by ergonomists.

REFERENCES

Antony, N. T., Keir, P. J., 2010. Effects of posture, movement and hand load on shoulder muscle activity. Journal of Electromyography and Kinesiology 20, 191-198.

Arnold, E. M., Ward, S. R., Lieber, R. L., Delp, S. L., 2010. A model of the lower limb for analysis of human movement. Annals of Biomedical Engineering 38, 269-279.

Arnold, E. M., Hamner, S. R., Seth, A., Millard, M., Delp, S. L., 2013. How muscle fiber lengths and velocities affect muscle force generation as humans walk and run at different speeds. The Journal of Experimental Biology 216, 2150-2160.

Baril-Gingras, G., Lortie, M., 1995. The handling of objects other than boxes: univariate analysis of handling techniques in a large transport company. Ergonomics 38, 905-925.

Bennett, A. I., Todd, A. I., Desai, S. D., 2011. Pushing and pulling, technique and load effects: an electromyographical study. Work (Reading, Mass.) 38, 291-299.

Bhattacharya, A., 2014. Costs of occupational musculoskeletal disorders (MSDs) in the United States. International Journal of Industrial Ergonomics 44, 448-454.

Bigliani, L. U., Kelkar, R., Flatow, E. L., Pollock, R. G., Mow, V. C., 1996. Glenohumeral stability. Biomechanical properties of passive and active stabilizers. Clinical Orthopaedics and Related Research (330), 13-30.

Bigliani, L. U., Pollock, R. G., Soslowsky, L. J., Flatow, E. L., Pawluk, R. J., Mow, V. C., 1992. Tensile properties of the inferior glenohumeral ligament. Journal of Orthopaedic Research : Official Publication of the Orthopaedic Research Society 10, 187-197.

Binder-Markey, B. I., Murray, W. M., 2017. Incorporating the length-dependent passive-force generating muscle properties of the extrinsic finger muscles into a wrist and finger biomechanical musculoskeletal model. Journal of Biomechanics 61, 250-257.

Bjorksten, M., Jonsson, B., 1977. Endurance limit of force in long-term intermittent static contractions. Scandinavian Journal of Work, Environment & Health 3, 23-27.

Blache, Y., Desmoulins, L., Allard, P., Plamondon, A., Begon, M., 2015. Effects of height and load weight on shoulder muscle work during overhead lifting task. Ergonomics 58, 748-761.

Blache, Y., Begon, M., Michaud, B., Desmoulins, L., Allard, P., Dal Maso, F., 2017. Muscle function in glenohumeral joint stability during lifting task. PLoS ONE 12, e0189406.

Boardman, N. D., Debski, R. E., Warner, J. J. P., Taskiran, E., Maddox, L., Imhoff, A. B., Fu, F. H., Woo, S. L., 1996. Tensile properties of the superior glenohumeral and coracohumeral ligaments. Journal of Shoulder and Elbow Surgery 5, 249-254.

Bonato, P., Ebenbichler, G. R., Roy, S. H., Lehr, S., Posch, M., Kollmitzer, J., Della Croce, U., 2003. Muscle fatigue and fatigue-related biomechanical changes during a cyclic lifting task. Spine 28, 1810-1820.

Boocock, M. G., Haslam, R. A., Lemon, P., Thorpe, S., 2006. Initial force and postural adaptations when pushing and pulling on floor surfaces with good and reduced resistance to slipping. Ergonomics 49, 801-821.

Burkart, A. C., Debski, R. E., 2002. Anatomy and function of the glenohumeral ligaments in anterior shoulder instability. Clinical Orthopaedics and Related Research (400), 32-39.

Calé-Benzoor, M., Dickstein, R., Arnon, M., Ayalon, M., 2016a. Dynamic push–pull characteristics at three hand-reach envelopes: Applications for the workplace. Applied Ergonomics 52, 216-221.

Calé-Benzoor, M., Dickstein, R., Arnon, M., Ayalon, M., 2016b. Dynamic push–pull characteristics at three hand-reach envelopes: Applications for the workplace. Applied Ergonomics 52, 216-221.

Cereatti, A., Calderone, M., Buckland, D. M., Buettner, A., Della Croce, U., Rosso, C., 2014. In vivo glenohumeral translation under anterior loading in an open-MRI set-up. Journal of Biomechanics 47, 3771-3775.

Chadwick, E. K., Blana, D., van den Bogert, A J, Kirsch, R. F., 2009. A real-time, 3-D musculoskeletal model for dynamic simulation of arm movements. IEEE Transactions on Bio-Medical Engineering 56, 941-948.

Chaffin, D. B., Andres, R. O., Garg, A., 1983. Volitional postures during maximal push/pull exertions in the sagittal plane. Human Factors 25, 541-550.

Chaffin, D. B., 1997. Development of computerized human static strength simulation model for job design. Human Factors and Ergonomics in Manufacturing 7, 305-322.

Chen, S., Simonian, P. T., Wickiewicz, T. L., Otis, J. C., Warren, R. F., 1999. Radiographic evaluation of glenohumeral kinematics: A muscle fatigue model. Journal of Shoulder and Elbow Surgery 8, 49-52.

Cholewicki, J., McGill, S. M., Norman, R. W., 1995. Comparison of muscle forces and joint load from an optimization and EMG assisted lumbar spine model: Towards development of a hybrid approach. Journal of Biomechanics 28, 321-331.

Chopp, J. N., O'Neill, J. M., Hurley, K., Dickerson, C. R., 2010a. Superior humeral head migration occurs after a protocol designed to fatigue the rotator cuff: A radiographic analysis. Journal of Shoulder and Elbow Surgery 19, 1137-1144.

Chopp, J. N., Fischer, S. L., Dickerson, C. R., 2010b. The impact of work configuration, target angle and hand force direction on upper extremity muscle activity during sub-maximal overhead work. Ergonomics 53, 83-91.

Chopp-Hurley, J. N., Langenderfer, J. E., Dickerson, C. R., 2014. Probabilistic evaluation of predicted force sensitivity to muscle attachment and glenohumeral stability uncertainty. Annals of Biomedical Engineering 42, 1867-1879.

Chow, A. Y., Dickerson, C. R., 2016. Determinants and magnitudes of manual force strengths and joint moments during two-handed standing maximal horizontal pushing and pulling. Ergonomics 59, 534-544.

Chow, A. Y., Dickerson, C. R., 2009. Shoulder strength of females while sitting and standing as a function of hand location and force direction. Applied Ergonomics 40, 303-308.

Chow, A. Y., La Delfa, N. J., Dickerson, C. R., 2017. Muscular Exposures During Standardized Two-Handed Maximal Pushing and Pulling Tasks. IISE Transactions on Occupational Ergonomics and Human Factors 5, 136-147.

Cifrek, M., Medved, V., Tonković, S., Ostojić, S., 2009. Surface EMG based muscle fatigue evaluation in biomechanics. Clinical Biomechanics 24, 327-340.

Clarys, J. P., Massez, C., Van Den Broeck, M., Piette, G., Robeaux, R., 1983. Total telemetric surface of the front crawl. Biomechanics VIII-B.International Series on Biomechanics 4, 951-958.

Cram, J. R., Criswell, E., 2011. Cram's introduction to surface electromyography. Jones and Bartlett, Sudbury, MA, .

Cudlip, A. C., Meszaros, K. A., Dickerson, C. R., 2016. The Influence of Hand Location and Force Direction on Shoulder Muscular Activity in Females During Nonsagittal Multidirectional Overhead Exertions. Human Factors 58, 120-139.

Cudlip, A. C., Callaghan, J. P., Dickerson, C. R., 2015. Effects of sitting and standing on upper extremity physical exposures in materials handling tasks. Ergonomics 58, 1637-1646.

da Costa, B. R., Vieira, E. R., 2010. Risk factors for work-related musculoskeletal disorders: A systematic review of recent longitudinal studies. American Journal of Industrial Medicine 53, 285-323.

Daly, M., Vidt, M. E., Eggebeen, J. D., Simpson, W. G., Miller, M. E., Marsh, A. P., Saul, K. R., 2012. Upper Extremity Muscle Volumes and Functional Strength After Resistance Training in Older Adults. Journal of Aging and Physical Activity 21, 186-207.

Das, B., Wang, Y., 2004. Isometric pull-push strengths in workspace: 1. Strength profiles. International Journal of Occupational Safety and Ergonomics : JOSE 10, 43-58.

Das, B., Sengupta, A. K., 1996. Industrial workstation design: A systematic ergonomics approach. Applied Ergonomics 27, 157-163.

de Groot, J. H., Brand, R., 2001. A three-dimensional regression model of the shoulder rhythm. Clinical Biomechanics 16, 735-743.

Delp, S. L., Anderson, F. C., Arnold, A. S., Loan, P., Habib, A., John, C. T., Guendelman, E., Thelen, D. G., 2007. OpenSim: open-source software to create and analyze dynamic simulations of movement. IEEE Transactions on Bio-Medical Engineering 54, 1940-1950.

Dickerson, C. R., Chaffin, D. B., Hughes, R. E., 2007. A mathematical musculoskeletal shoulder model for proactive ergonomic analysis. Computer Methods in Biomechanics and Biomedical Engineering 10, 389-400.

Dickerson, C. R., Meszaros, K. A., Cudlip, A. C., Chopp-Hurley, J., Langenderfer, J. E., 2015. The influence of cycle time on shoulder fatigue responses for a fixed total overhead workload. Journal of Biomechanics 48, 2911-2918.

Dickerson, C. R., Hughes, R. E., Chaffin, D. B., 2008. Experimental evaluation of a computational shoulder musculoskeletal model. Clinical Biomechanics 23, 886-894.

Drake, J. D. M., Callaghan, J. P., 2006. Elimination of electrocardiogram contamination from electromyogram signals: An evaluation of currently used removal techniques. Journal of Electromyography and Kinesiology 16, 175-187.

Dunning, K. K., Davis, K. G., Cook, C., Kotowski, S. E., Hamrick, C., Jewell, G., Lockey, J., 2010. Costs by industry and diagnosis among musculoskeletal claims in a state workers compensation system: 1999-2004. American Journal of Industrial Medicine 53, 276-284.

Felli, L., Biglieni, L., Fiore, M., Coviello, M., Borri, R., Cutulo, M., 2012. Functional study of glenohumeral ligaments. Journal of Orthopaedic Science 17, 634-637.

Fischer, S. L., Picco, B. R., Wells, R. P., Dickerson, C. R., 2013. The roles of whole body balance, shoe-floor friction and joint strength during maximum exertions: searching for the "weakest link". Journal of Applied Biomechanics 29, 1-11.

Flatow, E. L., Soslowsky, L. J., Ateshian, G. A., Ark, J. W., Pawluk, R. J., Bigliani, L. U., Mow, V. C., 1991. Shoulder joint anatomy and the effect of subluxations and size mismatch on patterns of glenohumeral contact. Orthop Trans 15, 803-804.

Fredriksson, K., Alfredsson, L., Ahlberg, G., Josephson, M., Kilbom, A., Wigaeus, H., Wiktorin, C., Vingard, E., 2002. Work environment and neck and shoulder pain: the influence of exposure time. Results from a population based case-control study. Occupational and Environmental Medicine 59, 182-188.

Garg, A., Beller, D., 1990. One-handed dynamic pulling strength with special reference to speed, handle height and angles of pulling. International Journal of Industrial Ergonomics 6, 231-240.

Garner, B. A., Pandy, M. G., 2001. Musculoskeletal model of the upper limb based on the visible human male dataset. Computer Methods in Biomechanics and Biomedical Engineering 4, 93-126.

Gerber, C., Costouros, J. G., Sukthankar, A., Fucentese, S. F., 2009. Static posterior humeral head subluxation and total shoulder arthroplasty. Journal of Shoulder and Elbow Surgery 18, 505-510.

Grieve, J., Dickerson, C., 2008. Overhead work: Identification of evidence-based exposure guidelines. pp. 53-66.

Hagberg, M., 1981. Muscular endurance and surface electromyogram in isometric and dynamic exercise. Journal of Applied Physiology: Respiratory, Environmental and Exercise Physiology 51, 1-7.

Hagberg, M., Wegman, D. H., 1987. Prevalence rates and odds ratios of shoulder-neck diseases in different occupational groups. British Journal of Industrial Medicine 44, 602-610.

Halder, A. M., Kuhl, S. G., Zobitz, M. E., Larson, D., An, K. N., 2001. Effects of the glenoid labrum and glenohumeral abduction on stability of the shoulder joint through concavity-compression : an in vitro study. The Journal of Bone and Joint Surgery.American Volume 83-A, 1062-1069.

Harryman, D. T.,2nd, Sidles, J. A., Clark, J. M., McQuade, K. J., Gibb, T. D., Matsen, F. A.,3rd, 1990. Translation of the humeral head on the glenoid with passive glenohumeral motion. The Journal of Bone and Joint Surgery.American Volume 72, 1334-1343.

Hauret, K. G., Jones, B. H., Bullock, S. H., Canham-Chervak, M., Canada, S., 2010. Musculoskeletal Injuries: Description of an Under-Recognized Injury Problem Among Military Personnel. American Journal of Preventive Medicine 38, S70.

Hautier, C. A., Arsac, L. M., Deghdegh, K., Souquet, J., Belli, A., Lacour, J. R., 2000. Influence of fatigue on EMG/force ratio and cocontraction in cycling. Medicine and Science in Sports and Exercise 32, 839-843.

Hawkes, D. H., Alizadehkhaiyat, O., Kemp, G. J., Fisher, A. C., Roebuck, M. M., Frostick, S. P., 2015. Electromyographic assessment of muscle fatigue in massive rotator cuff tear. Journal of Electromyography and Kinesiology 25, 93-99.

Hawkes, D. H., Alizadehkhaiyat, O., Kemp, G. J., Fisher, A. C., Roebuck, M. M., Frostick, S. P., 2012. Shoulder muscle activation and coordination in patients with a massive rotator cuff

tear: an electromyographic study. Journal of Orthopaedic Research : Official Publication of the Orthopaedic Research Society 30, 1140-1146.

Heuberer, P., Kranzl, A., Laky, B., Anderl, W., Wurnig, C., 2015. Electromyographic analysis: shoulder muscle activity revisited. Archives of Orthopaedic and Trauma Surgery 135, 549-563.

Hicks, J. L., Uchida, T. K., Seth, A., Rajagopal, A., Delp, S. L., 2015. Is my model good enough? Best practices for verification and validation of musculoskeletal models and simulations of movement. Journal of Biomechanical Engineering 137, 020905.

Hill, A. V., 1938. The heat of shortening and the dynamic constants of muscle. Proc.R.Soc.Lond.B 126, 136-195.

Hodder, J. N., Keir, P. J., 2013. Obtaining maximum muscle excitation for normalizing shoulder electromyography in dynamic contractions. Journal of Electromyography and Kinesiology 23, 1166-1173.

Hof, A. L., 1991. Errors in frequency parameters of EMG power spectra. IEEE Transactions on Bio-Medical Engineering 38, 1077-1088.

Holzbaur, K. R., Murray, W. M., Delp, S. L., 2005. A model of the upper extremity for simulating musculoskeletal surgery and analyzing neuromuscular control. Annals of Biomedical Engineering 33, 829-840.

Holzbaur, K. R., Delp, S. L., Gold, G. E., Murray, W. M., 2007. Moment-generating capacity of upper limb muscles in healthy adults. Journal of Biomechanics 40, 2442-2449.

Holzbaur, K. R., Murray, W. M., Gold, G. E., Delp, S. L., 2007. Upper limb muscle volumes in adult subjects. Journal of Biomechanics 40, 742-749.

Hoozemans, M. J., van der Beek, A J, Frings-Dresen, M. H., van der Woude, L H, van Dijk, F. J., 2002. Pushing and pulling in association with low back and shoulder complaints. Occupational and Environmental Medicine 59, 696-702.

Hoozemans, M. J., van der Beek, A J, Frings-Dresen, M. H., van Dijk, F. J., van der Woude, L H, 1998. Pushing and pulling in relation to musculoskeletal disorders: a review of risk factors. Ergonomics 41, 757-781.

Howell, S. M., Galinat, B. J., 1989. The glenoid-labral socket. A constrained articular surface. Clinical Orthopaedics and Related Research (243), 122-125.

Howell, S. M., Galinat, B. J., Renzi, A. J., Marone, P. J., 1988. Normal and abnormal mechanics of the glenohumeral joint in the horizontal plane. The Journal of Bone and Joint Surgery.American Volume 70, 227-232.

Imrhan, S. N., Ramakrishnan, U., 1992. The effects of arm elevation, direction of pull and speed of pull on isokinetic pull strength. International Journal of Industrial Ergonomics 9, 265-273.

Jobe, F. W., Moynes, D. R., Tibone, J. E., Perry, J., 1984. An EMG analysis of the shoulder in pitching. A second report. The American Journal of Sports Medicine 12, 218-220.

Kao, H. C., Lin, C. J., Lee, Y. H., Chen, S. H., 2015. The Effects of Direction of Exertion, Path, and Load Placement in Nursing Cart Pushing and Pulling Tasks: An Electromyographical Study. PloS One 10, e0140792.

Kelly, B. T., Williams, R. J., Cordasco, F. A., Backus, S. I., Otis, J. C., Weiland, D. E., Altchek, D. W., Craig, E. V., Wickiewicz, T. L., Warren, R. F., 2005. Differential patterns of muscle activation in patients with symptomatic and asymptomatic rotator cuff tears. Journal of Shoulder and Elbow Surgery 14, 165-171.

Kim, H. M., Teefey, S. A., Zelig, A., Galatz, L. M., Keener, J. D., Yamaguchi, K., 2009. Shoulder strength in asymptomatic individuals with intact compared with torn rotator cuffs. The Journal of Bone and Joint Surgery.American Volume 91, 289-296.

Klemt, C., Prinold, J. A., Morgans, S., Smith, S. H. L., Nolte, D., Reilly, P., Bull, A. M. J., 2018. Analysis of shoulder compressive and shear forces during functional activities of daily life. Clinical Biomechanics 54, 34-41.

Knaflitz, M., Merletti, R., De Luca, C. J., 1990. Inference of motor unit recruitment order in voluntary and electrically elicited contractions. Journal of Applied Physiology (Bethesda, Md.: 1985) 68, 1657-1667.

Knapik, G. G., Marras, W. S., 2009. Spine loading at different lumbar levels during pushing and pulling. Ergonomics 52, 60-70.

Kumar, S., Narayan, Y., Bacchus, C., 1995. Symmetric and asymmetric two-handed pull-push strength of young adults. Human Factors 37, 854-865.

Kumar, S., 1995. Upper body push-pull strength of normal young adults in sagittal plane at three heights. International Journal of Industrial Ergonomics 15, 427-436.

La Delfa, N. J., Freeman, C. C., Petruzzi, C., Potvin, J. R., 2014. Equations to predict female manual arm strength based on hand location relative to the shoulder. Ergonomics 57, 254-261.

La Delfa, N. J., Potvin, J. R., 2016. Multidirectional manual arm strength and its relationship with resultant shoulder moment and arm posture. Ergonomics 59, 1625-1636.

Langenderfer, J., Jerabek, S. A., Thangamani, V. B., Kuhn, J. E., Hughes, R. E., 2004. Musculoskeletal parameters of muscles crossing the shoulder and elbow and the effect of

sarcomere length sample size on estimation of optimal muscle length. Clinical Biomechanics 19, 664-670.

Laursen, B., Schibye, B., 2002. The effect of different surfaces on biomechanical loading of shoulder and lumbar spine during pushing and pulling of two-wheeled containers. Applied Ergonomics 33, 167-174.

Lazarus, M. D., Sidles, J. A., Harryman, D. T.,2nd, Matsen, F. A.,3rd, 1996. Effect of a chondral-labral defect on glenoid concavity and glenohumeral stability. A cadaveric model. The Journal of Bone and Joint Surgery.American Volume 78, 94-102.

Leigh, J. P., Cone, J. E., Harrison, R., 2001. Costs of Occupational Injuries and Illnesses in California. Preventive Medicine 32, 393-406.

Lett, K. K., McGill, S. M., 2006. Pushing and pulling: personal mechanics influence spine loads. Ergonomics 49, 895-908.

Lin, C., Chen, M., Wei, Y., Wang, M. J., 2010. The evaluation of force exertions and muscle activities when operating a manual guided vehicle. Applied Ergonomics 41, 313-318.

Lin, J., McGorry, R. W., Chang, C., 2012. Effects of handle orientation and between-handle distance on bi-manual isometric push strength. Applied Ergonomics 43, 664-670.

Lin, J., McGorry, R. W., Maynard, W., 2013. One-handed standing pull strength in different postures: Normative data. Applied Ergonomics 44, 603-608.

Lind, C. M., 2018. Pushing and pulling: an assessment tool for occupational health and safety practitioners. International Journal of Occupational Safety and Ergonomics : JOSE 24, 14-26.

Lippitt, S. B., Matsen, F., 1993. Mechanisms of glenohumeral joint stability. Clinical Orthopaedics and Related Research (291), 20-28.

Lippitt, S. B., Vanderhooft, J. E., Harris, S. L., Sidles, J. A., Harryman, D. T., Matsen, F. A., 1993. Glenohumeral stability from concavity-compression: A quantitative analysis. Journal of Shoulder and Elbow Surgery 2, 27-35.

MacKinnon, S. N., Vaughan, C. L., 2005. Effect of the reach distance on the execution of one-handed submaximal pull forces. Occupational Ergonomics 5, 161-172.

MacKinnon, S. N., 1998. Isometric pull forces in the sagittal plane. Applied Ergonomics 29, 319-324.

Marchi, J., Blana, D., Chadwick, E. K., 2014. Glenohumeral stability during a hand-positioning task in previously injured shoulders. Medical & Biological Engineering & Computing 52, 251-256.

McDonald, A. C., Brenneman, E. C., Cudlip, A. C., Dickerson, C. R., 2014. The spatial dependency of shoulder muscle demands for seated lateral hand force exertions. Journal of Applied Biomechanics 30, 1-11.

McDonald, A. C., Picco, B. R., Belbeck, A. L., Chow, A. Y., Dickerson, C. R., 2012. Spatial dependency of shoulder muscle demands in horizontal pushing and pulling. Applied Ergonomics 43, 971-978.

McFarland, D. C., Poppo, M. N., McCain, E. M., Saul, K. R., 2017. Spatial dependency of shoulder muscle demand during dynamic unimanual pushing and pulling. In 41st Annual American Society of Biomechanics. Boulder, CO.

McFarland, D. C., Poppo, M. N., McCain, E. M., Saul, K. R., Spatial dependency of shoulder muscle demand during dynamic unimanual and bimanual pushing and pulling. Applied Ergonomics.

Meszaros, K. A., Vidt, M. E., Dickerson, C. R., 2018. The effects of hand force variation on shoulder muscle activation during submaximal exertions. International Journal of Occupational Safety and Ergonomics 24, 100-110.

Michener, L. A., McClure, P. W., Karduna, A. R., 2003. Anatomical and biomechanical mechanisms of subacromial impingement syndrome. Clinical Biomechanics 18, 369-379.

Millard, M., Uchida, T., Seth, A., Delp, S. L., 2013. Flexing computational muscle: modeling and simulation of musculotendon dynamics. Journal of Biomechanical Engineering 135, 021005.

Minagawa, H., Yamamoto, N., Abe, H., Fukuda, M., Seki, N., Kikuchi, K., Kijima, H., Itoi, E., 2013. Prevalence of symptomatic and asymptomatic rotator cuff tears in the general population: From mass-screening in one village. Journal of Orthopaedics 10, 8-12.

Mital, A., Kopardekar, P., Motorwala, A., 1995. Isokinetic pull strengths in the vertical plane: effects of speed and arm angle. Clinical Biomechanics 10, 110-112.

Mogk, J. P. M., Johanson, M. E., Hentz, V. R., Saul, K. R., Murray, W. M., 2011. A simulation analysis of the combined effects of muscle strength and surgical tensioning on lateral pinch force following brachioradialis to flexor pollicis longus transfer. Journal of Biomechanics 44, 669-675.

Nadon, A. L., Vidt, M. E., Chow, A. Y., Dickerson, C. R., 2016. The spatial dependency of shoulder muscular demands during upward and downward exertions. Ergonomics 59, 1294-1306.

National Academy of Science, 2001. Musculoskeletal Disorders and the Workplace: Low Back and Upper Extremities. The National Academies Press, Washington, DC, .

Nikooyan, A. A., Veeger, H. E. J., Westerhoff, P., Bolsterlee, B., Graichen, F., Bergmann, G., van der Helm, F C T, 2012. An EMG-driven musculoskeletal model of the shoulder. Human Movement Science 31, 429-447.

Nikooyan, A. A., Veeger, H. E. J., Westerhoff, P., Graichen, F., Bergmann, G., van der Helm, F C T, 2010. Validation of the Delft Shoulder and Elbow Model using in-vivo glenohumeral joint contact forces. Journal of Biomechanics 43, 3007-3014.

Nimbarte, A. D., Sun, Y., Jaridi, M., Hsiao, H., 2013. Biomechanical loading of the shoulder complex and lumbosacral joints during dynamic cart pushing task. Applied Ergonomics 44, 841-849.

Okunribido, O. O., Haslegrave, C. M., 2008. Ready steady push--a study of the role of arm posture in manual exertions. Ergonomics 51, 192-216.

Otis, J. C., Warren, R. F., Backus, S. I., Santner, T. J., Mabrey, J. D., 1990. Torque production in the shoulder of the normal young adult male. The interaction of function, dominance, joint angle, and angular velocity. The American Journal of Sports Medicine 18, 119-123.

Pagnani, M. J., Warren, R. F., 1994. Stabilizers of the glenohumeral joint. Journal of Shoulder and Elbow Surgery 3, 173-190.

Potvin, J. R., Bent, L. R., 1997. A validation of techniques using surface EMG signals from dynamic contractions to quantify muscle fatigue during repetitive tasks. Journal of Electromyography and Kinesiology 7, 131-139.

Quental, C., Folgado, J., Ambrosio, J., Monteiro, J., 2015. Critical analysis of musculoskeletal modelling complexity in multibody biomechanical models of the upper limb. Computer Methods in Biomechanics and Biomedical Engineering 18, 749-759.

Quental, C., Folgado, J., Ambrósio, J., Monteiro, J., 2016. A new shoulder model with a biologically inspired glenohumeral joint. Medical Engineering & Physics 38, 969-977.

Rajaratnam, B. S., Goh, J., Kumar, V. P., 2014. A Comparison of EMG signals from surface and fine-wire electrodes during shoulder abduction. International Journal of Physical Medicine & Rehabilitation.

Rancourt, D., Hogan, N., 2001. Dynamics of pushing. Journal of Motor Behavior 33, 351-362.

Resnick, M. L., Chaffin, D. B., 1995. An ergonomic evaluation of handle height and load in maximal and submaximal cart pushing. Applied Ergonomics 26, 173-178.

Rohmert, W., 1973. Problems in determining rest allowances: Part 1: Use of modern methods to evaluate stress and strain in static muscular work. Applied Ergonomics 4, 91-95.

Roman-Liu, D., Tokarski, T., 2005. Upper limb strength in relation to upper limb posture. International Journal of Industrial Ergonomics 35, 19-31.

Roquelaure, Y., Ha, C., Rouillon, C., Fouquet, N., Leclerc, A., Descatha, A., Touranchet, A., Goldberg, M., Imbernon, E., Members of Occupational Health Services of the Pays de la Loire Region, 2009. Risk factors for upper-extremity musculoskeletal disorders in the working population. Arthritis and Rheumatism 61, 1425-1434.

Rowe, C. R., Patel, D., Southmayd, W. W., 1978. The Bankart procedure: a long-term end-result study. The Journal of Bone and Joint Surgery.American Volume 60, 1-16.

Saper, M. G., Milchteim, C., Zondervan, R. L., Andrews, J. R., Ostrander, R. V., 2017. Outcomes After Arthroscopic Bankart Repair in Adolescent Athletes Participating in Collision and Contact Sports. Orthopaedic Journal of Sports Medicine 5, 2325967117697950.

Saul, K. R., Hu, X., Goehler, C. M., Vidt, M. E., Daly, M., Velisar, A., Murray, W. M., 2015. Benchmarking of dynamic simulation predictions in two software platforms using an upper limb musculoskeletal model. Computer Methods in Biomechanics and Biomedical Engineering 18, 1445-1458.

Saul, K. R., Vidt, M. E., Gold, G. E., Murray, W. M., 2015. Upper Limb Strength and Muscle Volume in Healthy Middle-Aged Adults. Journal of Applied Biomechanics 31, 484-491.

Seo, N. J., Armstrong, T. J., 2009. Biomechanical analysis for handle stability during maximum push and pull exertions. Ergonomics 52, 1568-1575.

Seo, N. J., Armstrong, T. J., Young, J. G., 2010. Effects of handle orientation, gloves, handle friction and elbow posture on maximum horizontal pull and push forces. Ergonomics 53, 92-101.

Shair, E. F., Ahmad, S. A., Marhaban, M. H., Mohd Tamrin, S. B., Abdullah, A. R., 2017. EMG Processing Based Measures of Fatigue Assessment during Manual Lifting. BioMed Research International 2017, 3937254.

Snook, S. H., Ciriello, V. M., 1991. The design of manual handling tasks: revised tables of maximum acceptable weights and forces. Ergonomics 34, 1197-1213.

Sonnabend, D. H., Young, A. A., 2009. Comparative anatomy of the rotator cuff. The Journal of Bone and Joint Surgery.British Volume 91, 1632-1637.

Soslowsky, L. J., Malicky, D. M., Blasier, R. B., 1997. Active and passive factors in inferior glenohumeral stabilization: a biomechanical model. Journal of Shoulder and Elbow Surgery 6, 371-379.

Steenbrink, F., de Groot, J. H., Veeger, H. E., van der Helm, F C, Rozing, P. M., 2009. Glenohumeral stability in simulated rotator cuff tears. Journal of Biomechanics 42, 1740-1745.

Terry, G. C., Hammon, D., France, P., Norwood, L. A., 1991. The stabilizing function of passive shoulder restraints. The American Journal of Sports Medicine 19, 26-34.

Thelen, D. G., Anderson, F. C., 2006. Using computed muscle control to generate forward dynamic simulations of human walking from experimental data. Journal of Biomechanics 39, 1107-1115.

Thelen, D. G., Anderson, F. C., Delp, S. L., 2003. Generating dynamic simulations of movement using computed muscle control. Journal of Biomechanics 36, 321-328.

Thiehoff, R., 2002. Economic significance of work disability caused by musculoskeletal disorders. Der Orthopade 31, 949-956.

van der Helm, F., 1994a. A finite element musculoskeletal model of the shoulder mechanism. Journal of Biomechanics 27, 551-569.

van der Helm, F., 1994b. A finite element musculoskeletal model of the shoulder mechanism. Journal of Biomechanics 27, 551-569.

van Drongelen, S., Schlussel, M., Arnet, U., Veeger, D., 2013. The influence of simulated rotator cuff tears on the risk for impingement in handbike and handrim wheelchair propulsion. Clinical Biomechanics (Bristol, Avon) 28, 495-501.

Vidt, M. E., Daly, M., Miller, M. E., Davis, C. C., Marsh, A. P., Saul, K. R., 2012. Characterizing upper limb muscle volume and strength in older adults: A comparison with young adults. Journal of Biomechanics 45, 334-341.

Vidt, M. E., Santago II, A. C., Marsh, A. P., Hegedus, E. J., Tuohy, C. J., Poehling, G. G., Freehill, M. T., Miller, M. E., Saul, K. R., Analysis of activities of daily living for older adults with a rotator cuff tear using individualized computational models. Journal of Biomechanics.

Vidt, M. E., Santago, A. C., Marsh, A. P., Hegedus, E. J., Tuohy, C. J., Poehling, G. G., Freehill, M. T., Miller, M. E., Saul, K. R., 2016. The effects of a rotator cuff tear on activities of daily living in older adults: A kinematic analysis. Journal of Biomechanics 49, 611-617.

Vidt, M. E., 2014. Muscle structure and function in older adults with a rotator cuff tear. ProQuest Dissertations Publishing.

Warwick, D., Novak, G., Schultz, A., Berkson, M., 1980. Maximum voluntary strengths of male adults in some lifting, pushing and pulling activities. Ergonomics 23, 49-54.

Weston, E. B., Aurand, A., Dufour, J. S., Knapik, G. G., Marras, W. S., 2017. Biomechanically determined hand force limits protecting the low back during occupational pushing and pulling tasks. Ergonomics, 1-13.

Wickham, J., Pizzari, T., Stansfeld, K., Burnside, A., Watson, L., 2010. Quantifying 'normal' shoulder muscle activity during abduction. Journal of Electromyography and Kinesiology 20, 212-222.

Wiker, S. F., Chaffin, D. B., Langolf, G. D., 1989. Shoulder posture and localized muscle fatigue and discomfort. Ergonomics 32, 211-237.

Wu, G., van der Helm, Frans C T, (DirkJan) Veeger, H E J, Makhsous, M., Van Roy, P., Anglin, C., Nagels, J., Karduna, A. R., McQuade, K., Wang, X., Werner, F. W., Buchholz, B., 2005. ISB recommendation on definitions of joint coordinate systems of various joints for the reporting of human joint motion—Part II: shoulder, elbow, wrist and hand. Journal of Biomechanics 38, 981-992.

Yang, C., Goto, A., Sahara, W., Yoshikawa, H., Sugamoto, K., 2010. In vivo three-dimensional evaluation of the functional length of glenohumeral ligaments. Clinical Biomechanics 25, 137-141.

Zajac, F. E., 1989. Muscle and tendon: properties, models, scaling, and application to biomechanics and motor control. Critical Reviews in Biomedical Engineering 17, 359-411.

APPENDICES

Appendix A: Anthropometric Data for Chapters 2 and 3

This appendix contains the subject codes and anthropometric data (height, weight, etc.) of subjects who participated in the experimental protocol for Chapters 2 and 3. Left-handed subjects and subjects with incomplete isometric moments were not simulated for Chapter 3; therefore, these subjects do not have codes for Chapter 3. One subject did not have MVC data for one of the isometric trials and was, therefore, excluded from the analysis in Chapter 2. This subject was still included in Chapter 3 as EMG normalization for this chapter was just determining on/off timing.

Chapter 2 Subject Code	Chapter 3 Subject Code	Height (cm)	Weight (lbs)	Dominant Arm	Age	Chest Circumference (cm)	Bicep Circumference		Torso Length (cm)	Humerus Length		Forearm Length	
							Left (cm)	Right (cm)		Left (cm)	Right (cm)	Left (cm)	Right (cm)
M1	M1	188	198	R	32	99	35	35.5	52	40	40	28	28
M2	-	180	155	R	31	92	30	31	61.2	37.5	38	30	29.5
M3	-	176	171	L	24	101	31	30	51	39	39	26	26
M4	M2	181	174	R	23	96	37	39	56	35	35	29.5	30
M5	M3	183	197	R	20	98	35.5	35.5	59	37.5	38	26	27
M6	M4	176	210	R	24	103	32	33.5	53	32	31	28	28
M7	M5	178	191	R	21	99	34	35	51	34	34	29	28
M8	M6	183	212	R	24	107	36	38	55	37	37	30	30
-	F1	167	125	R	28	85	27	27	48	36	36	25	25
F1	F2	168	133	R	20	88	27	27	52	32	32	23	23
F2	F3	179	166	R	27	92	28	27	63	37	37	27	27
F3	-	165	199	R	23	118.5	38	39	56	33.5	33.5	25	25
F4	F4	176	177	R	25	96.5	32	32	57	33	33	26	26
F5	-	179	138	L	24	85	27.5	28	54	38	37	26	26
F6	F5	168	167	R	22	99	31	31	54	32	32	25	25
F7	F6	155	140	R	22	91	30	30	53	31	31	21	22
F8	F7	166	151	R	22	92	29	29	52	35	35	25	25
F9	F8	170	167	R	24	96	34.5	35	56	34	34	26	26

Appendix B: Strength Capacity and Dynamic Loading

This appendix contains the subject codes and strength data (elbow flexion isometric joint moment, shoulder abduction joint moment, isometric push-pull capacity, and task loading) of subjects who participated in the experimental protocol for Chapters 2 and 3. Left-handed subjects and subjects with incomplete isometric moments were not simulated for Chapter 3; therefore, these subjects do not have codes for Chapter 3. One subject did not have MVC data for one of the isometric trials and was, therefore, excluded from the analysis in Chapter 2. This subject was still included in Chapter 3 as EMG normalization for this chapter was just determining on/off timing.

Chapter 2 Subject Code	Chapter 3 Subject Code	Elbow Flexion (ft-lbs)	Shoulder Abduction (ft-lbs)	Push Capacity (lbs)	Pull Capacity (lbs)	Dynamic Loading (lbs)
M1	M1	56.7	43.1	146.8	111.5	22.5
M2	-	-	33	109.6	69.9	16.75
M3	-	37.2	41.3	97.3	103.1	16.25
M4	M2	56.7	43.6	109.9	95.5	17
M5	M3	59.3	52.6	176.1	124.6	26.75
M6	M4	33.1	17.8	109.4	57.8	16.25
M7	M5	49.6	35.9	122	102.8	18.5
M8	M6	51.6	48.2	119.9	88.7	18.5
-	F1	23.6	19.4	98.1	50.7	15
F1	F2	17.5	10.6	59.6	48.6	8.75
F2	F3	27.7	11.1	69.6	65.1	10.75
F3	-	-	24.8	71.7	50	10.75
F4	F4	32.5	21.1	76.1	59.4	11.75
F5	-	30.3	24.9	91.3	80.8	14
F6	F5	22.2	16.4	74.3	51	11.25
F7	F6	18.1	11.4	64.6	36.1	9.75
F8	F7	27.1	23.6	79.5	64.6	13.25
F9	F8	35.1	24.4	113.8	73.8	17
Male AVG		47.9±9.3	39.0±9.7	119.3±25.7	88.9±23.4	18.8±3.3
Female AVG		26.0±6.1	18.8±6.0	79.9±16.6	58.0±13.3	12.2±2.5
Total AVG		37.0±13.6	28.9±13.0	99.6±29.2	73.5±24.4	15.5±4.4

Appendix C: Custom Push-pull Device Parts List, Manufacturing, and Assembly

This appendix contains a parts list of required components for the custom device as well as manufacturing drawings for custom components. This appendix also contains information on device assembly.

Parts List

Component	Part	Quantity
Handle	1' x 1/2" Ø Cylinder Handle	1
	Handle to Carriage Attachment	1
	M5 x 0.8mm Screws for Handle Attachment	4
	Ball Bearing Carriage	1
	Carabiner	2
Mount to PowerTec	Base Mount	1
	Side Sheet for Mount	2
	1/4" x1/2" Screws	4
Rail	20mm x 1000mm Guide Rail	1
	3/16" Ø, 2-1/2" Outer Ø Pulley	2
	M5 x 4mm Screws for Rail Mounting	2
	M5 Nuts	2
	1/2" Bolts 4.5" for Axis Mounting	3
	1/2" Nuts	3
	Spacer, 1" Outer Ø, 1" Long, for 1/2" Screw	1
	Spacers, 1" Outer Ø, 1/4" Long	2
	Rotating Axis	1
Pulley Attachment	3/16" Diameter, 2-1/2" Outer Ø Pulley	1
	1/2" Nut	1
	1/2” Bolt	1
	M5 x 4mm Screws for Rail Mounting	2
	M5 Nuts	2
	Pulley Attachment	1

Handle

The handle to carriage attachment screws into the ball bearing carriage with 4 M5 x 0.8mm screws. The 1' x 1/2" Ø cylinder handle is placed through the handle to carriage attachment, and two carabiners are attached to the carriage attachment to attach wire ropes of the PowerTec.

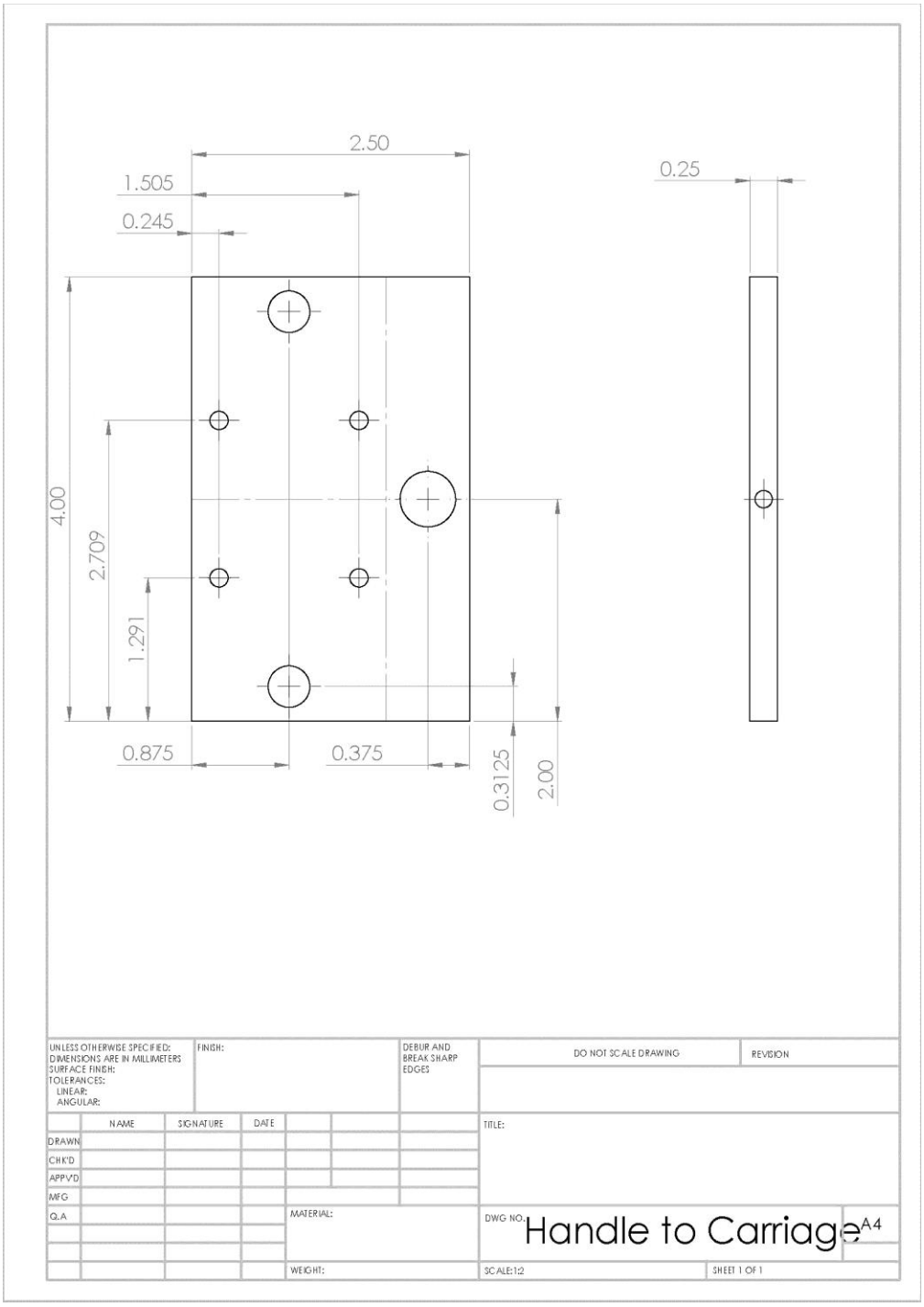

Mount to PowerTec

The slide sheets for the mount are attached to the base mount with 4 1/4" x1/2" screws

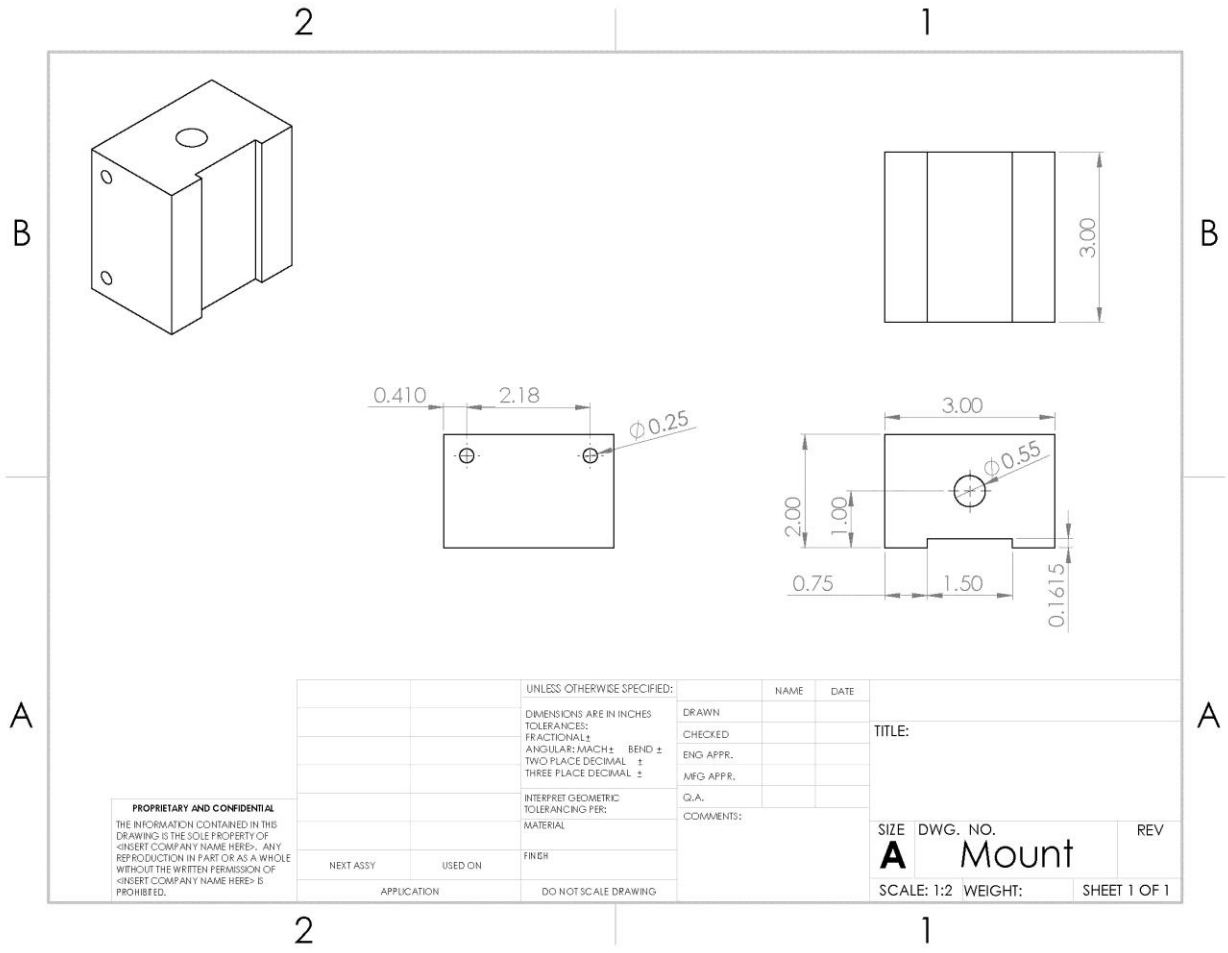

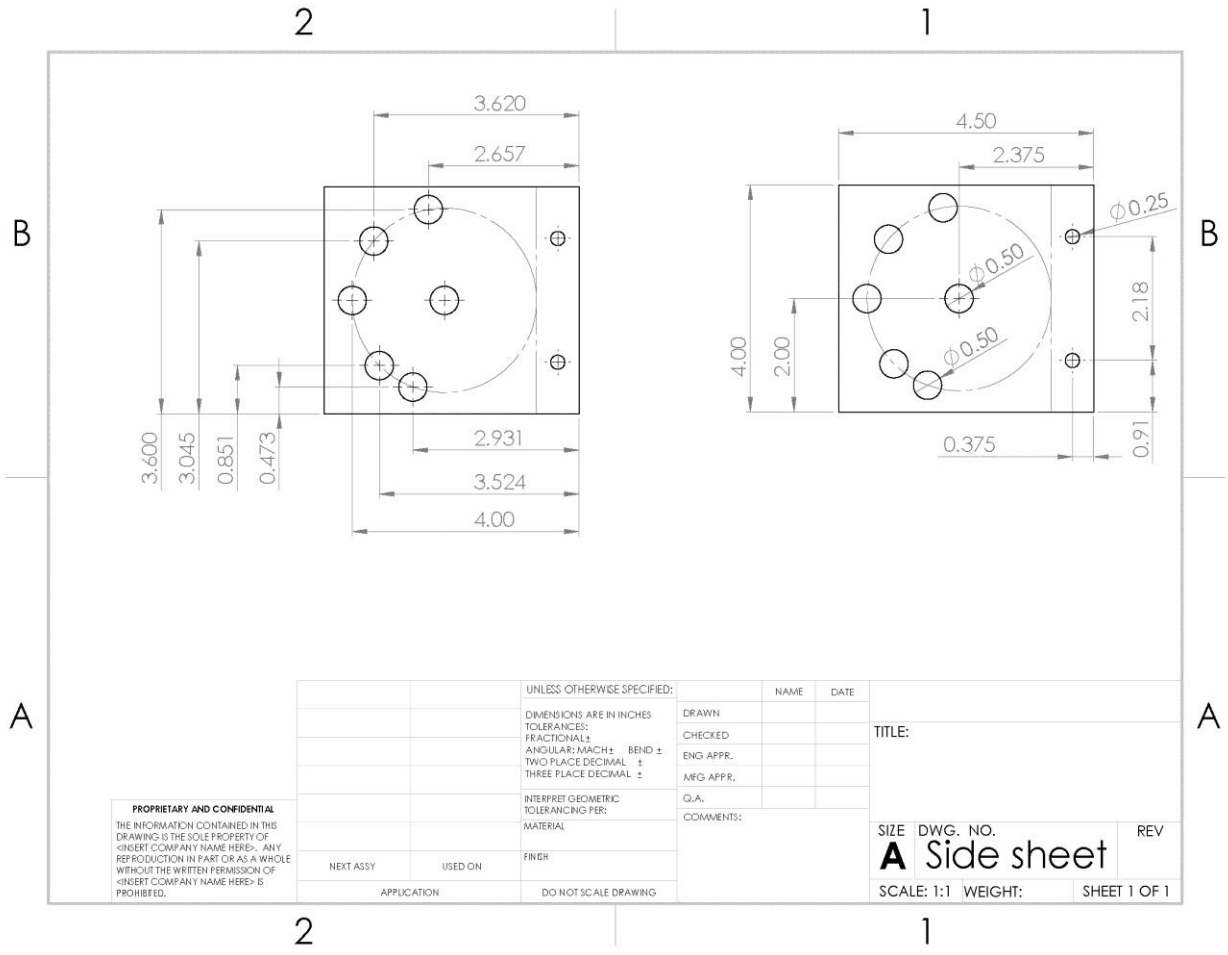
2
1
B
A
3.620
2.657
3.600
3.045
0.851
0.473
2.931
3.524
4.00
4.50
2.375
Ø0.25
Ø0.50
Ø0.50
4.00
2.00
2.18
0.375
0.91
PROPRIETARY AND CONFIDENTIAL
THE INFORMATION CONTAINED IN THIS DRAWING IS THE SOLE PROPERTY OF <INSERT COMPANY NAME HERE>. ANY REPRODUCTION IN PART OR AS A WHOLE WITHOUT THE WRITTEN PERMISSION OF <INSERT COMPANY NAME HERE> IS PROHIBITED.
UNLESS OTHERWISE SPECIFIED:
DIMENSIONS ARE IN INCHES
TOLERANCES:
FRACTIONAL ±
ANGULAR: MACH ± BEND ±
TWO PLACE DECIMAL ±
THREE PLACE DECIMAL ±
INTERPRET GEOMETRIC TOLERANCING PER:
MATERIAL
FINISH
NAME
DATE
DRAWN
CHECKED
ENG APPR.
MFG APPR.
Q.A.
COMMENTS:
TITLE:
SIZE
A
DWG. NO.
Side sheet
REV
SCALE: 1:1
WEIGHT:
SHEET 1 OF 1
NEXT ASSY
USED ON
APPLICATION
DO NOT SCALE DRAWING

Rail

The handle assembly slides onto the 20mm x 1000mm guide rail. The guide rail then attaches to the rotating axis via 2 M5 x 4mm screws and nuts. The 1st 1/2” hole on the rotating axis attaches the handle to the mount to the PowerTec with a 1/2" bolt 4.5" in length. The 1” long spacer is placed on the 1/2” bolt on one side of the rotating axis whereas on the other side is the pulley in between the 2 1/4" spaces. The other 1/2” bolt and nut are used to attach the other pulley to the hole on top of the rotating axis.

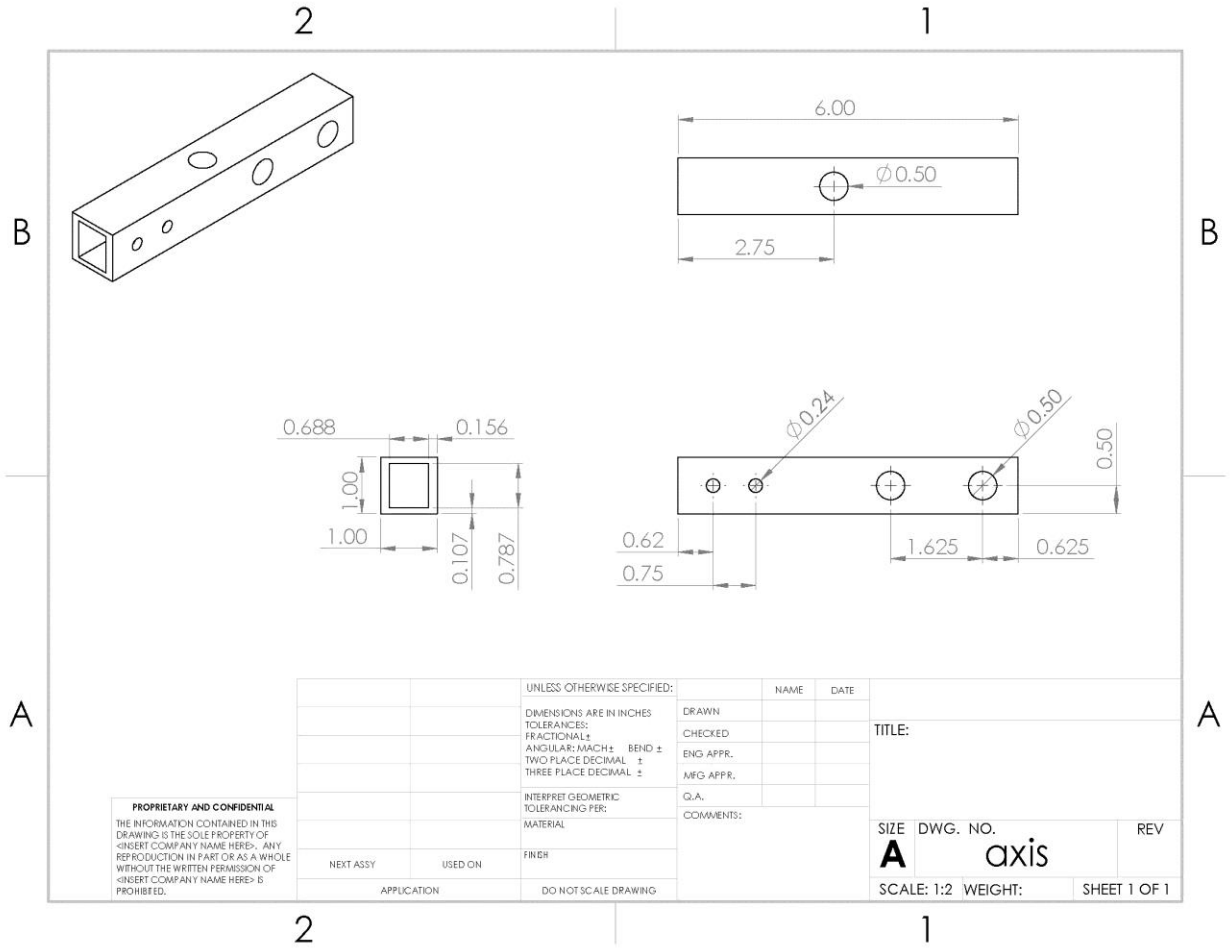

Pulley Attachment

The pulley is attached to the pulley attachment with the 1/2" bolt and nut. The pulley attachment is then attached to the end of the rail with the 2 M5 screws and nut.

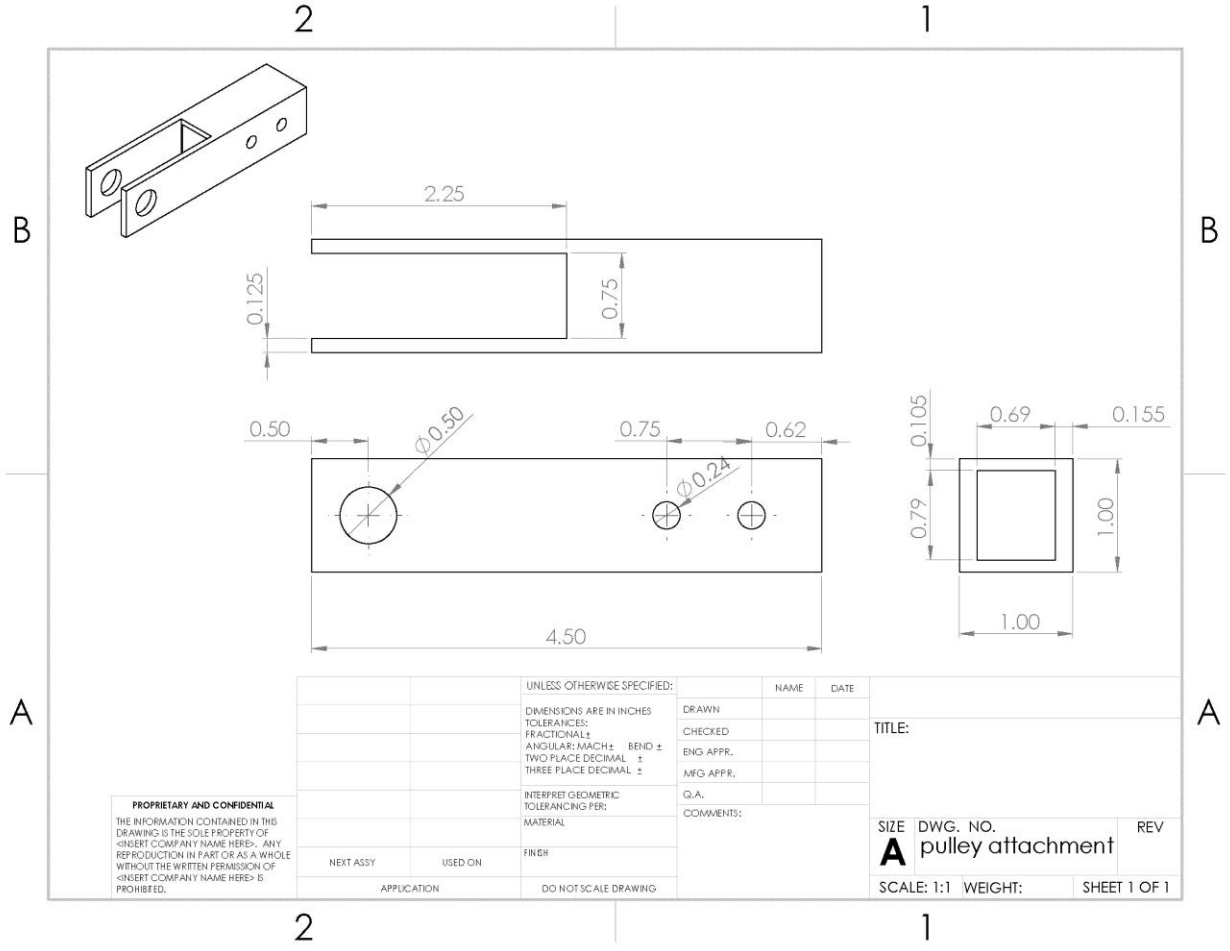

Assembly Views of the Device

The power tech wires are routed via the pulleys to change direction of the applied load. A bolt is used to lock the desired sagittal (thoracohumeral elevation) target on mount portion of the device.

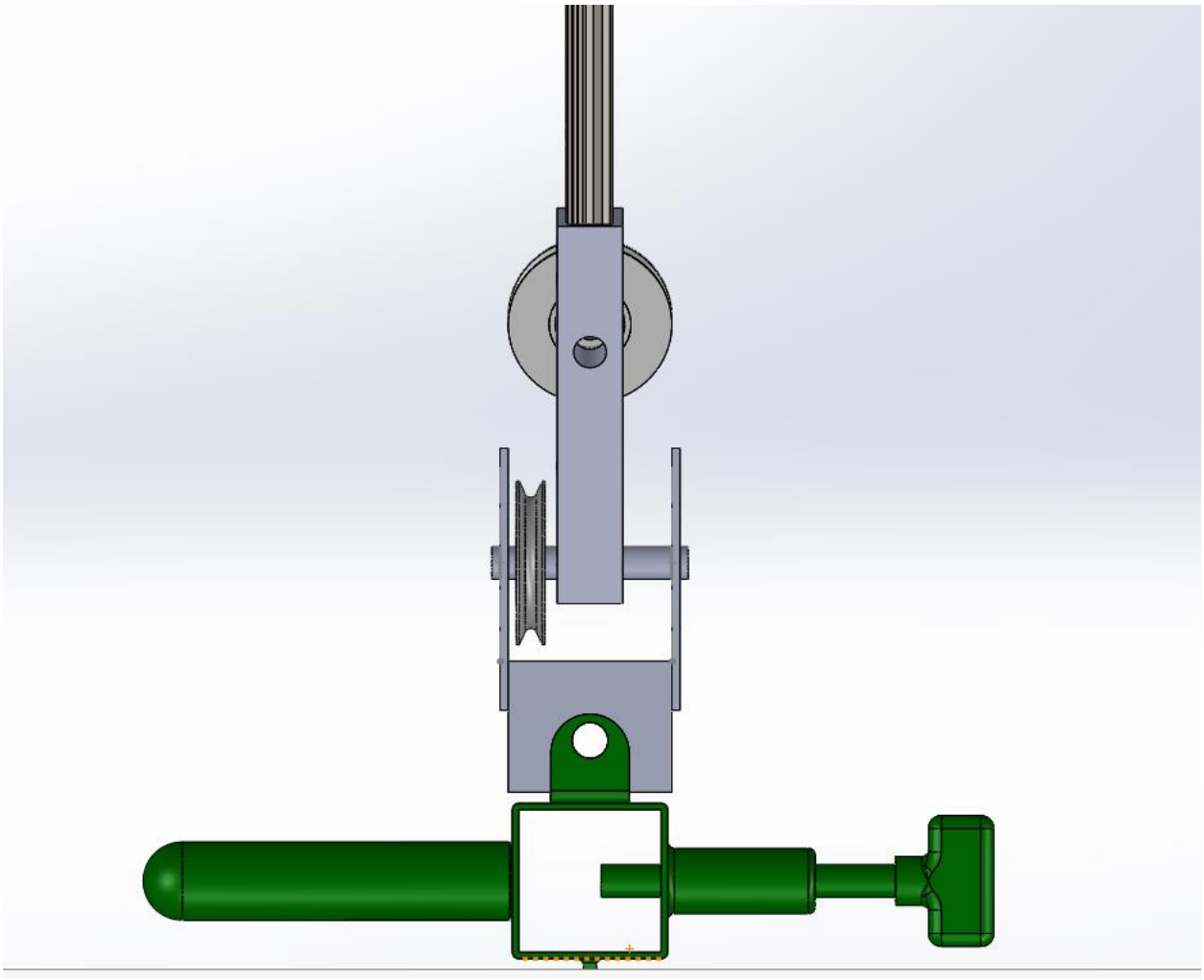

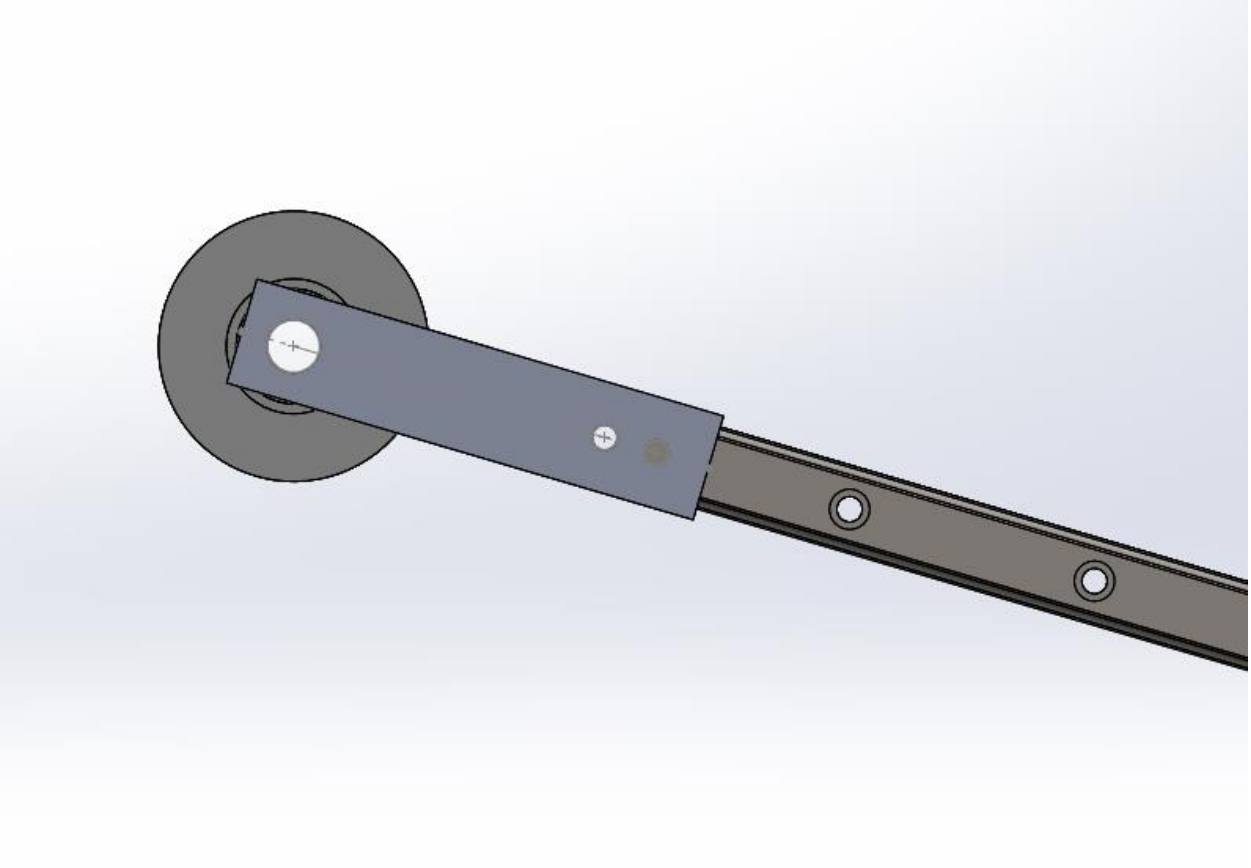

Appendix D: Muscle Demand for Chapter 2

This appendix contains each subject's muscle demand for each task target used in Chapter 2. Data are presented in 4 tables, one for each task type (unimanual pulling, unimanual pushing, bimanual pulling, and bimanual pushing). Subject F5 could not complete the 170˚ elevation and 135˚ plane of elevation unimanual push at 15% of their isometric push-pull capacity; therefore, this data is missing. Only the return motion was captured for subject M5 performing the unimanual pull task to the 170˚ elevation and 135˚ plane of elevation; therefore, this data is missing.

Elevation	Plane of Elevation	Unimanual Pushing																
		Subject Codes																
		M1	M2	M3	M4	M5	M6	M7	M8	F1	F2	F3	F4	F5	F6	F7	F8	F9
20°	0°	0.332	0.264	0.325	0.388	0.157	0.283	0.290	0.34	0.548	0.617	0.301	0.301	0.356	0.439	0.252	0.380	0.295
	45°	0.334	0.259	0.232	0.326	0.159	0.237	0.308	0.120	0.485	0.353	0.233	0.372	0.335	0.398	0.235	0.312	0.224
	90°	0.335	0.387	0.284	0.240	0.210	0.327	0.375	0.316	0.420	0.393	0.274	0.479	0.328	0.422	0.280	0.336	0.219
	135°	0.322	0.358	0.294	0.172	0.254	0.293	0.350	0.305	0.533	0.372	0.326	0.467	0.488	0.462	0.298	0.370	0.289
90°	0°	0.292	0.347	0.275	0.362	0.195	0.439	0.366	0.251	0.516	0.384	0.285	0.383	0.356	0.449	0.399	0.469	0.495
	45°	0.249	0.339	0.273	0.312	0.190	0.503	0.412	0.261	0.377	0.383	0.273	0.407	0.343	0.429	0.383	0.444	0.333
	90°	0.299	0.364	0.290	0.397	0.238	0.439	0.397	0.311	0.288	0.454	0.270	0.377	0.370	0.410	0.354	0.378	0.389
	135°	0.354	0.437	0.252	0.328	0.285	0.415	0.570	0.399	0.390	0.290	0.412	0.317	0.356	0.521	0.421	0.531	0.408
170°	0°	0.453	0.415	0.487	0.538	0.125	0.857	0.631	0.451	0.682	0.691	0.432	0.542	0.485	0.699	0.477	0.527	0.555
	45°	0.391	0.419	0.456	0.531	0.140	0.602	0.560	0.502	0.483	0.711	0.417	0.524	0.488	0.647	0.514	0.467	0.485
	90°	0.447	0.526	0.399	0.649	0.150	0.582	0.610	0.414	0.496	0.701	0.409	0.562	0.619	0.659	0.461	0.447	0.526
	135°	0.492	0.584	0.464	0.625	0.232	0.701	0.678	0.501	0.769	0.811	0.505	0.583	-	0.813	0.556	0.529	0.549

Elevation	Plane of Elevation	Unimanual Pulling																
		Subject Codes																
		M1	M2	M3	M4	M5	M6	M7	M8	F1	F2	F3	F4	F5	F6	F7	F8	F9
20°	0°	0.296	0.231	0.438	0.383	0.254	0.596	0.246	0.285	0.664	0.733	0.300	0.284	0.410	0.536	0.510	0.374	0.477
	45°	0.201	0.167	0.346	0.328	0.249	0.800	0.333	0.155	0.529	0.659	0.299	0.213	0.427	0.564	0.583	0.407	0.316
	90°	0.235	0.335	0.366	0.569	0.235	0.703	0.335	0.261	0.398	0.593	0.318	0.245	0.467	0.688	0.653	0.374	0.336
	135°	0.146	0.404	0.316	0.408	0.317	0.689	0.347	0.292	0.553	0.711	0.287	0.196	0.362	0.649	0.608	0.347	0.322
90°	0°	0.140	0.240	0.227	0.212	0.141	0.266	0.281	0.179	0.470	0.241	0.321	0.255	0.167	0.316	0.328	0.245	0.211
	45°	0.127	0.197	0.115	0.186	0.112	0.176	0.285	0.146	0.331	0.209	0.223	0.173	0.148	0.216	0.261	0.165	0.235
	90°	0.084	0.148	0.113	0.116	0.078	0.147	0.308	0.102	0.309	0.195	0.198	0.120	0.117	0.187	0.227	0.158	0.161
	135°	0.087	0.150	0.130	0.192	0.092	0.118	0.242	0.119	0.283	0.254	0.169	0.113	0.143	0.202	0.183	0.156	0.137
170°	0°	0.127	0.178	0.124	0.120	0.067	0.183	0.202	0.169	0.292	0.367	0.201	0.165	0.100	0.226	0.265	0.184	0.162
	45°	0.095	0.168	0.101	0.175	0.161	0.125	0.246	0.109	0.249	0.347	0.192	0.147	0.159	0.216	0.187	0.219	0.181
	90°	0.100	0.219	0.093	0.145	0.100	0.146	0.160	0.114	0.231	0.256	0.217	0.207	0.330	0.257	0.174	0.224	0.203
	135°	0.194	0.240	0.130	0.198	-	0.138	0.246	0.126	0.255	0.194	0.195	0.184	0.273	0.218	0.161	0.313	0.164

Elevation	Plane of Elevation	Bimanual Pushing																
		Subject Codes																
		M1	M2	M3	M4	M5	M6	M7	M8	F1	F2	F3	F4	F5	F6	F7	F8	F9
20°	0°	0.172	0.206	0.233	0.261	0.119	0.184	0.187	0.214	0.485	0.344	0.254	0.178	0.210	0.259	0.202	0.264	0.232
	45°	0.185	0.209	0.125	0.235	0.088	0.173	0.188	0.080	0.381	0.255	0.206	0.202	0.196	0.274	0.244	0.216	0.122
	90°	0.184	0.261	0.126	0.181	0.127	0.196	0.202	0.177	0.375	0.226	0.182	0.221	0.160	0.218	0.219	0.267	0.172
	135°	0.169	0.238	0.126	0.246	0.171	0.200	0.202	0.127	0.356	0.273	0.186	0.148	0.191	0.144	0.199	0.341	0.117
90°	0°	0.206	0.249	0.268	0.262	0.131	0.437	0.316	0.280	0.431	0.317	0.291	0.215	0.264	0.342	0.318	0.389	0.220
	45°	0.186	0.267	0.170	0.282	0.191	0.309	0.292	0.289	0.269	0.331	0.242	0.200	0.287	0.313	0.239	0.275	0.203
	90°	0.269	0.276	0.181	0.355	0.170	0.298	0.311	0.217	0.278	0.380	0.238	0.192	0.261	0.268	0.269	0.268	0.239
	135°	0.245	0.320	0.099	0.221	0.142	0.283	0.358	0.179	0.258	0.117	0.313	0.170	0.179	0.359	0.355	0.465	0.217
170°	0°	0.315	0.374	0.527	0.617	0.091	0.518	0.524	0.327	0.421	0.706	0.420	0.380	0.381	0.737	0.524	0.422	0.414
	45°	0.361	0.383	0.414	0.430	0.084	0.449	0.458	0.378	0.365	0.490	0.408	0.354	0.368	0.440	0.441	0.414	0.441
	90°	0.350	0.409	0.225	0.453	0.099	0.407	0.549	0.294	0.328	0.655	0.303	0.331	0.303	0.407	0.423	0.389	0.436
	135°	0.276	0.394	0.251	0.416	0.173	0.388	0.485	0.288	0.326	0.594	0.349	0.394	0.294	0.648	0.409	0.432	0.387

Elevation	Plane of Elevation	Bimanual Pulling																
		Subject Codes																
		M1	M2	M3	M4	M5	M6	M7	M8	F1	F2	F3	F4	F5	F6	F7	F8	F9
20°	0°	0.127	0.147	0.206	0.153	0.198	0.378	0.173	0.202	0.459	0.308	0.245	0.164	0.146	0.471	0.344	0.246	0.251
	45°	0.102	0.115	0.105	0.093	0.192	0.595	0.219	0.085	0.398	0.442	0.233	0.184	0.339	0.436	0.310	0.200	0.166
	90°	0.146	0.203	0.167	0.416	0.093	0.275	0.213	0.160	0.362	0.477	0.225	0.122	0.307	0.505	0.385	0.224	0.153
	135°	0.083	0.200	0.261	0.137	0.062	0.215	0.176	0.171	0.403	0.450	0.202	0.140	0.109	0.466	0.496	0.235	0.199
90°	0°	0.071	0.093	0.101	0.106	0.082	0.130	0.163	0.166	0.240	0.122	0.212	0.165	0.068	0.177	0.117	0.147	0.105
	45°	0.068	0.084	0.075	0.106	0.053	0.095	0.195	0.074	0.257	0.183	0.140	0.121	0.069	0.152	0.145	0.102	0.167
	90°	0.059	0.096	0.092	0.090	0.048	0.107	0.226	0.082	0.209	0.194	0.150	0.082	0.096	0.117	0.144	0.110	0.150
	135°	0.062	0.101	0.066	0.098	0.061	0.104	0.188	0.092	0.174	0.077	0.176	0.091	0.067	0.139	0.167	0.125	0.128
170°	0°	0.067	0.075	0.084	0.117	0.055	0.154	0.172	0.123	0.154	0.207	0.195	0.132	0.107	0.171	0.193	0.154	0.130
	45°	0.098	0.091	0.117	0.159	0.045	0.170	0.144	0.079	0.157	0.334	0.212	0.100	0.124	0.190	0.158	0.103	0.092
	90°	0.073	0.112	0.100	0.091	0.058	0.129	0.164	0.117	0.181	0.189	0.150	0.121	0.105	0.196	0.149	0.116	0.100
	135°	0.096	0.100	0.075	0.134	0.047	0.130	0.181	0.101	0.153	0.200	0.160	0.119	0.127	0.188	0.167	0.165	0.088

Appendix E: CMC Code Unimanual Concavity Compression

This appendix contains the section of CMC code in which the concavity compression style of constraint is applied to control the direction of the net joint reaction force. This code is used for the unimanual simulations in Chapter 3 and the concavity compression simulations in Chapter 4.

```
int ActuatorForceTarget::
objectiveFunc(const Vector &aF, const bool new_coefficients, Real& rP) const
{
	// Define Variables
	double penalty=0;
	double angle, constraint;
	SimTK::State s=_saveState;
	SimTK::Vec3 JRF;
	Vec3 DC_r1,DC_r2,DC_r3,Glenoid_reaction,JRF_reaction;
	const Set<Actuator> &fSet = _controller->getActuatorSet();
	Body &ground = _controller->getModel().getSimbodyEngine().getGroundBody();
	Body& scapula = _controller->getModel().getBodySet().get(3);
	int numBodies=_controller->getModel().getNumBodies();
	Vector_<Vec3> allForcesVec2(numBodies);
	Vector_<Vec3> allMomentsVec2(numBodies);

	for(int i=0;i<fSet.getSize();i++) { //override forces so we can use computeReactions
	// function
		 Actuator& act = fSet.get(i);
		act.setOverrideForce(s, aF[i]);
		act.overrideForce(s,true);
	}

	_controller->getModel().getMultibodySystem().realize(s, SimTK::Stage::Acceleration );
	_controller->getModel().getSimbodyEngine().computeReactions(s, allForcesVec2,
	allMomentsVec2);
	JRF=allForcesVec2[5]; // get JRF at scapula expressed in ground

	////////////TRANSFORM TO GLENOID/////////////////////////////////////////
	_controller->getModel().getSimbodyEngine().transform(s, ground,-JRF,scapula,JRF);

	//Direction Cosine to rotate to glenoid
	DC_r1[0]=0.866025;
	DC_r1[1]=0.0;
	DC_r1[2]=-.5;
	DC_r2[0]=0.0;
	DC_r2[1]=1.0;
	DC_r2[2]=0.0;
	DC_r3[0]=0.5;
	DC_r3[1]=0.0;
	DC_r3[2]=0.866025;
	Glenoid_reaction[0]=dot(DC_r1,JRF);
	Glenoid_reaction[1]=dot(DC_r2,JRF);
	Glenoid_reaction[2]=dot(DC_r3,JRF);
```

```
////////////CALCULATE CONSTRAINT/////////////////////////////////////////////
// Calculate angle of transverse force

if(Glenoid_reaction.get(1)==0&&Glenoid_reaction.get(0)==0){
        angle=0;
}
else if(Glenoid_reaction.get(1)>0&&Glenoid_reaction.get(0)>=0){
        angle=atan(Glenoid_reaction.get(0)/Glenoid_reaction.get(1));
}
else if(Glenoid_reaction.get(1)<=0&&Glenoid_reaction.get(0)>0){
        angle=atan(-Glenoid_reaction.get(1)/Glenoid_reaction.get(0))+1.57079632679;
}
else if(Glenoid_reaction.get(1)<0&&Glenoid_reaction.get(0)<=0){
        angle=atan(Glenoid_reaction.get(0)/Glenoid_reaction.get(1))+3.14159265359;
}
else if(Glenoid_reaction.get(1)>=0&&Glenoid_reaction.get(0)<0){
        angle=atan(Glenoid_reaction.get(1)/(-
                1*Glenoid_reaction.get(0)))+4.71238898038;
}


// Calculate constraint in direction of transverse force
if(angle>=0&&angle<0.78539816339){
        constraint=(.443-.561)/(0.78539816339)*angle+.561;
}
else if (angle>=0.78539816339&&angle<1.57079632679){
        constraint=(.366-.443)/(0.78539816339)*(angle-0.78539816339)+.443;
}
else if (angle>=1.57079632679&&angle<2.35619449019){
        constraint=(.504-.366)/(0.78539816339)*(angle-1.57079632679)+.366;
}
else if (angle>=2.35619449019&&angle<3.14159265359){
        constraint=(.598-.504)/(0.78539816339)*(angle-2.35619449019)+.504;
}
else if (angle>=3.14159265359&&angle<3.92699081699){
        constraint=(.482-.598)/(0.78539816339)*(angle-3.14159265359)+.598;
}
else if (angle>=3.92699081699&&angle<4.71238898038){
        constraint=(.32-.482)/(0.78539816339)*(angle-3.92699081699)+.482;
}
else if (angle>=4.71238898038&&angle<5.49778714378){
        constraint=(.437-.32)/(0.78539816339)*(angle-4.71238898038)+.32;
}
else if (angle>=5.49778714378){
        constraint=(.561-.437)/(0.78539816339)*(angle-5.49778714378)+.437;
}
```

```
        double limit=-1*Glenoid_reaction[2]*constraint;
        double glenoid_jrf =
        sqrt(Glenoid_reaction[0]*Glenoid_reaction[0]+Glenoid_reaction[1]*Glenoid_reaction[1]
        );

        // calculate penalty force
        if(limit<glenoid_jrf){
                penalty=.05*(glenoid_jrf-limit);//10+.01*atan((glenoid_jrf-limit)/(-
        1*Glenoid_reaction[2]));
        }

        // reset the actuator control
        for(int i=0;i<fSet.getSize();i++) {
                Actuator& act = fSet.get(i);
                act.overrideForce(s,false);
        }



        const CMC_TaskSet& tset=_controller->getTaskSet();
        rP = (_accelPerformanceMatrix * aF + _accelPerformanceVector).normSqr() +
        (_forcePerformanceMatrix * aF + _forcePerformanceVector).normSqr();

        rP=rP+penalty;// Add in penalty term
        return(0);
}
```

Appendix F: CMC Code Unimanual Scapulohumeral Balance

This appendix contains the section of CMC code in which the scapulohumeral balance style of constraint is applied to control the direction of the net joint reaction force. This code is used for the scapulohumeral balance simulations in Chapter 4.

```
int ActuatorForceTarget::
objectiveFunc(const Vector &aF, const bool new_coefficients, Real& rP) const
{
	// Define Variables
	double penalty=0;
	double phi,theta;
	SimTK::State s=_saveState;
	SimTK::Vec3 JRF;
	Vec3 DC_r1,DC_r2,DC_r3,Glenoid_reaction;
	const Set<Actuator> &fSet = _controller->getActuatorSet();
	Body &ground = _controller->getModel().getSimbodyEngine().getGroundBody();
	Body& scapula = _controller->getModel().getBodySet().get(3);
	int numBodies=_controller->getModel().getNumBodies();
	Vector_<Vec3> allForcesVec2(numBodies);
	Vector_<Vec3> allMomentsVec2(numBodies);

	for(int i=0;i<fSet.getSize();i++) { //override forces so we can use computeReactions
	// function
		Actuator& act = fSet.get(i);
		act.setOverrideForce(s, aF[i]);
		act.overrideForce(s,true);
	}

	_controller->getModel().getMultibodySystem().realize(s, SimTK::Stage::Acceleration );
	_controller->getModel().getSimbodyEngine().computeReactions(s, allForcesVec2,
	allMomentsVec2);
	JRF=allForcesVec2[5]; // get JRF at scapula expressed in ground

	////////////TRANSFORM TO GLENOID/////////////////////////////////////////
	_controller->getModel().getSimbodyEngine().transform(s, ground,-JRF,scapula,JRF);

	//Direction Cosine to rotate to glenoid
	DC_r1[0]=0.866025;
	DC_r1[1]=0.0;
	DC_r1[2]=-.5;
	DC_r2[0]=0.0;
	DC_r2[1]=1.0;
	DC_r2[2]=0.0;
	DC_r3[0]=0.5;
	DC_r3[1]=0.0;
	DC_r3[2]=0.866025;
	Glenoid_reaction[0]=dot(DC_r1,JRF);
	Glenoid_reaction[1]=dot(DC_r2,JRF);
	Glenoid_reaction[2]=dot(DC_r3,JRF);
```

```
////////////CALCULATE CONSTRAINT/////////////////////////////////////////////
// Calculate angle of transverse force
if(Glenoid_reaction.get(0)>=0){
        phi=atan(Glenoid_reaction.get(0)/(-1*Glenoid_reaction.get(2)));
        phi=phi*(180/3.14159265359);
}
else if(Glenoid_reaction.get(0)<0){
        phi=atan((-1*Glenoid_reaction.get(0))/(-1*Glenoid_reaction.get(2)));
        phi=phi*(180/3.14159265359);
}
if(Glenoid_reaction.get(1)>=0){
        theta=atan(Glenoid_reaction.get(1)/(-1*Glenoid_reaction.get(2)));
        theta=theta*(180/3.14159265359);
}
else if(Glenoid_reaction.get(1)<0){
        theta=atan((-1*Glenoid_reaction.get(1))/(-1*Glenoid_reaction.get(2)));
        theta=theta*(180/3.14159265359);
}

// Calculate constraint in direction of transverse force
double constraint=(theta/28.5)*(theta/28.5)+(phi/18.5)*(phi/18.5);

///CALCULATE TRANSVERSE ANGLE//////////////////////////////////////
double X, Y, Z, TANtheta;
if(Glenoid_reaction.get(1)>0&&Glenoid_reaction.get(0)>=0){
        TANtheta=(Glenoid_reaction.get(0)/Glenoid_reaction.get(1));
        X=(28.5*18.5*TANtheta)/sqrt(18.5*18.5+((28.5*28.5)*TANtheta*TANtheta));
        Y=(28.5*18.5)/sqrt(18.5*18.5+((28.5*28.5)*TANtheta*TANtheta));
}
else if(Glenoid_reaction.get(1)<=0&&Glenoid_reaction.get(0)>0){
        TANtheta=(-Glenoid_reaction.get(1)/Glenoid_reaction.get(0));
        Y=(28.5*18.5*TANtheta)/sqrt(28.5*28.5+((18.5*18.5)*TANtheta*TANtheta));
        X=(28.5*18.5)/sqrt(28.5*28.5+((18.5*18.5)*TANtheta*TANtheta));
}
else if(Glenoid_reaction.get(1)<0&&Glenoid_reaction.get(0)<=0){
        TANtheta=(Glenoid_reaction.get(0)/Glenoid_reaction.get(1));
        X=(28.5*18.5*TANtheta)/sqrt(18.5*18.5+((28.5*28.5)*TANtheta*TANtheta));
        Y=(28.5*18.5)/sqrt(18.5*18.5+((28.5*28.5)*TANtheta*TANtheta));
}
else if(Glenoid_reaction.get(1)>=0&&Glenoid_reaction.get(0)<0){
        TANtheta=(Glenoid_reaction.get(1)/(-1*Glenoid_reaction.get(0)));
        Y=(28.5*18.5*TANtheta)/sqrt(28.5*28.5+((18.5*18.5)*TANtheta*TANtheta));
        X=(28.5*18.5)/sqrt(28.5*28.5+((18.5*18.5)*TANtheta*TANtheta));
}

Z=sqrt(X*X+Y*Y);
```

```
        Z=Z*(3.14159265359/180);
        double limit=-1*Glenoid_reaction[2]*tan(Z);
        double glenoid_jrf =
        sqrt(Glenoid_reaction[0]*Glenoid_reaction[0]+Glenoid_reaction[1]*Glenoid_reaction[1]
        );

        //calculate penalty
        if(constraint>1&&glenoid_jrf>limit){
                penalty=.05*(glenoid_jrf-limit);
        }

        // reset the actuator control
        for(int i=0;i<fSet.getSize();i++) {
                Actuator& act = fSet.get(i);
                act.overrideForce(s,false);
        }

        const CMC_TaskSet& tset=_controller->getTaskSet();
        rP = (_accelPerformanceMatrix * aF + _accelPerformanceVector).normSqr() +
        (_forcePerformanceMatrix * aF + _forcePerformanceVector).normSqr();

        rP=rP+penalty;// Add in penalty term
        return(0);
}
```

Appendix G: CMC Code Bimanual Concavity Compression

This appendix contains the section of CMC code in which the concavity compression style of constraint is applied to control the direction of the net joint reaction force for bimanual simulations. This code is used for the bimanual simulations in Chapter 3.

```
int ActuatorForceTarget::
objectiveFunc(const Vector &aF, const bool new_coefficients, Real& rP) const
{
	//Define Variabel
	SimTK::State s=_saveState;
	int numBodies=_controller->getModel().getNumBodies();
	Vector_<Vec3> allForcesVec2(numBodies);
	Vector_<Vec3> allMomentsVec2(numBodies);
	const Set<Actuator> &fSet = _controller->getActuatorSet();
	Body &ground = _controller->getModel().getSimbodyEngine().getGroundBody();

	//Right Shoulder////////////////////////////////////////////////////////////////////////////////////////////
	double penalty_r=0;
	double angle_r,constraint_r;
	SimTK::Vec3 JRF_r;
	Vec3 DC_r1_r,DC_r2_r,DC_r3_r,Glenoid_reaction_r,JRF_reaction_r;
	Body& scapula_r = _controller->getModel().getBodySet().get(3);

	//Left Shoulder/////////////////////////////////////////////////////////////////////////////////////////////
	double penalty_l=0;
	double angle_l,constraint_l;
	SimTK::Vec3 JRF_l;
	Vec3 DC_r1_l,DC_r2_l,DC_r3_l,Glenoid_reaction_l,JRF_reaction_l;
	Body& scapula_l = _controller->getModel().getBodySet().get(14);

	for(int i=0;i<fSet.getSize();i++) { //override forces so we can use computeReactions
	// function
		Actuator& act = fSet.get(i);
		act.setOverrideForce(s, aF[i]);
		act.overrideForce(s,true);
	}

	_controller->getModel().getMultibodySystem().realize(s, SimTK::Stage::Acceleration );
	_controller->getModel().getSimbodyEngine().computeReactions(s, allForcesVec2,
	allMomentsVec2);
	JRF_r=allForcesVec2[5]; // get JRF_r at scapula expressed in ground
	JRF_l=allForcesVec2[16]; // get JRF_l at scapula expressed in ground
```

```
////////////TRANSFORM TO GLENOID ////////////////////////////////////////////
//Right shoulder
_controller->getModel().getSimbodyEngine().transform(s, ground,-
JRF_r,scapula_r,JRF_r);

//Direction Cosine to rotate to glenoid
DC_r1_r[0]=0.866025;
DC_r1_r[1]=0.0;
DC_r1_r[2]=-0.5;
DC_r2_r[0]=0.0;
DC_r2_r[1]=1.0;
DC_r2_r[2]=0.0;
DC_r3_r[0]=0.5;
DC_r3_r[1]=0.0;
DC_r3_r[2]=0.866025;
Glenoid_reaction_r[0]=dot(DC_r1_r,JRF_r);
Glenoid_reaction_r[1]=dot(DC_r2_r,JRF_r);
Glenoid_reaction_r[2]=dot(DC_r3_r,JRF_r);


////////////CALCULATE CONSTRAINT////////////////////////////////////////////
if(Glenoid_reaction_r.get(1)==0&&Glenoid_reaction_r.get(0)==0){
        angle_r=0;
}
else if(Glenoid_reaction_r.get(1)>0&&Glenoid_reaction_r.get(0)>=0){
        angle_r=atan(Glenoid_reaction_r.get(0)/Glenoid_reaction_r.get(1));
}
else if(Glenoid_reaction_r.get(1)<=0&&Glenoid_reaction_r.get(0)>0){
        angle_r=atan(-Glenoid_reaction_r.get(1)/Glenoid_reaction_r.get(0))+1.570796;
}
else if(Glenoid_reaction_r.get(1)<0&&Glenoid_reaction_r.get(0)<=0){
        angle_r=atan(Glenoid_reaction_r.get(0)/Glenoid_reaction_r.get(1))+ 3.141592;
}
else if(Glenoid_reaction_r.get(1)>=0&&Glenoid_reaction_r.get(0)<0){
        angle_r=atan(Glenoid_reaction_r.get(1)/(-Glenoid_reaction_r.get(0)))+4.712388;
}
```

```
//Calculate constraint in the direction of transverse force
if(angle_r>=0&&angle_r<0.78539816339){
	constraint_r=(.443-.561)/(0.78539816339)*angle_r+.561;
}
else if (angle_r>=0.78539816339&&angle_r<1.57079632679){
	constraint_r=(.366-.443)/(0.78539816339)*(angle_r-0.78539816339)+.443;
}
else if (angle_r>=1.57079632679&&angle_r<2.35619449019){
	constraint_r=(.504-.366)/(0.78539816339)*(angle_r-1.57079632679)+.366;
}
else if (angle_r>=2.35619449019&&angle_r<3.14159265359){
	constraint_r=(.598-.504)/(0.78539816339)*(angle_r-2.35619449019)+.504;
}
else if (angle_r>=3.14159265359&&angle_r<3.92699081699){
	constraint_r=(.482-.598)/(0.78539816339)*(angle_r-3.14159265359)+.598;
}
else if (angle_r>=3.92699081699&&angle_r<4.71238898038){
	constraint_r=(.32-.482)/(0.78539816339)*(angle_r-3.92699081699)+.482;
}
else if (angle_r>=4.71238898038&&angle_r<5.49778714378){
	constraint_r=(.437-.32)/(0.78539816339)*(angle_r-4.71238898038)+.32;
}
else if (angle_r>=5.49778714378){
	constraint_r=(.561-.437)/(0.78539816339)*(angle_r-5.49778714378)+.437;
}


double limit_r=-Glenoid_reaction_r[2]*constraint_r;
double glenoid_jrf_r =
sqrt(Glenoid_reaction_r[0]*Glenoid_reaction_r[0]+Glenoid_reaction_r[1]*Glenoid_react
ion_r[1]);

//calculate penalty force
if(limit_r<glenoid_jrf_r){
	penalty_r=.05*(glenoid_jrf_r-limit_r);
}
```

```
////////////TRANSFORM TO GLENOID ////////////////////////////////////////////
//Left shoulder
_controller->getModel().getSimbodyEngine().transform(s, ground,-
JRF_l,scapula_l,JRF_l);

//Direction Cosine to rotate to glenoid
DC_r1_l[0]=0.866025;
DC_r1_l[1]=0.0;
DC_r1_l[2]=0.5;
DC_r2_l[0]=0.0;
DC_r2_l[1]=1.0;
DC_r2_l[2]=0.0;
DC_r3_l[0]=-0.5;
DC_r3_l[1]=0.0;
DC_r3_l[2]=0.866025;
Glenoid_reaction_l[0]=dot(DC_r1_l,JRF_l);
Glenoid_reaction_l[1]=dot(DC_r2_l,JRF_l);
Glenoid_reaction_l[2]=dot(DC_r3_l,JRF_l);


////////////CALCULATE CONSTRAINT////////////////////////////////////////////
// Calculate angle of transverse force

if(Glenoid_reaction_l.get(1)==0&&Glenoid_reaction_l.get(0)==0){
        angle_l=0;
}
else if(Glenoid_reaction_l.get(1)>0&&Glenoid_reaction_l.get(0)>=0){
        angle_l=atan(Glenoid_reaction_l.get(0)/Glenoid_reaction_l.get(1));
}
else if(Glenoid_reaction_l.get(1)<=0&&Glenoid_reaction_l.get(0)>0){
        angle_l=atan(-Glenoid_reaction_l.get(1)/Glenoid_reaction_l.get(0))+1.570796;
}
else if(Glenoid_reaction_l.get(1)<0&&Glenoid_reaction_l.get(0)<=0){
        angle_l=atan(Glenoid_reaction_l.get(0)/Glenoid_reaction_l.get(1))+3.141592;
}
else if(Glenoid_reaction_l.get(1)>=0&&Glenoid_reaction_l.get(0)<0){
        angle_l=atan(Glenoid_reaction_l.get(1)/(-*Glenoid_reaction_l.get(0)))+4.712388;
}
```

```
	// Calculate constraint in the direction of transverse force
	if(angle_l>=0&&angle_l<0.78539816339){
		constraint_l=(.443-.561)/(0.78539816339)*angle_l+.561;
	}
	else if (angle_l>=0.78539816339&&angle_l<1.57079632679){
		constraint_l=(.366-.443)/(0.78539816339)*(angle_l-0.78539816339)+.443;
	}
	else if (angle_l>=1.57079632679&&angle_l<2.35619449019){
		constraint_l=(.504-.366)/(0.78539816339)*(angle_l-1.57079632679)+.366;
	}
	else if (angle_l>=2.35619449019&&angle_l<3.14159265359){
		constraint_l=(.598-.504)/(0.78539816339)*(angle_l-2.35619449019)+.504;
	}
	else if (angle_l>=3.14159265359&&angle_l<3.92699081699){
		constraint_l=(.482-.598)/(0.78539816339)*(angle_l-3.14159265359)+.598;
	}
	else if (angle_l>=3.92699081699&&angle_l<4.71238898038){
		constraint_l=(.32-.482)/(0.78539816339)*(angle_l-3.92699081699)+.482;
	}
	else if (angle_l>=4.71238898038&&angle_l<5.49778714378){
		constraint_l=(.437-.32)/(0.78539816339)*(angle_l-4.71238898038)+.32;
	}
	else if (angle_l>=5.49778714378){
		constraint_l=(.561-.437)/(0.78539816339)*(angle_l-5.49778714378)+.437;
	}

	double limit_l=Glenoid_reaction_l[2]*constraint_l;
	double glenoid_jrf_l =
	sqrt(Glenoid_reaction_l[0]*Glenoid_reaction_l[0]+Glenoid_reaction_l[1]*Glenoid_reacti
	on_l[1]);

	//calculate penalty term
	if(limit_l<glenoid_jrf_l){
		penalty_l=.05*(glenoid_jrf_l-limit_l);
	}
	// reset the actuator control
	for(int i=0;i<fSet.getSize();i++) {
		Actuator& act = fSet.get(i);
		act.overrideForce(s,false);
	}
	const CMC_TaskSet& tset=_controller->getTaskSet();
	rP = (_accelPerformanceMatrix * aF + _accelPerformanceVector).normSqr() +
	(_forcePerformanceMatrix * aF + _forcePerformanceVector).normSqr();
	rP=rP+penalty_r+penalty_l;// Add in penalty term
	return(0);
}
```

Appendix H: Strength Scaling Code

This appendix contains the code for the strength scaling application used in Chapter 3. This application optimizes a model's maximum isometric forces so that peak joint moment is the same as experimental moment. Muscles are grouped according to which moment they are associated with and scaled as a group with a single scale factor. Muscles not assigned to any group are scaled to an average of the other scale factors.

```
#include <OpenSim/OpenSim.h>
#include <ctime>  // clock(), clock_t, CLOCKS_PER_SEC
#include <vector>
#include <dirent.h>
using namespace OpenSim;
using namespace SimTK;
using namespace std;
// Global Variables
int stepCount=0;
double bestSoFar=Infinity;
Vector scale_factor(1,0.0); // Vector of scale factors
int StrengthScaling(string setup);

class StrengthOptimize : public OptimizerSystem {
  public:
        StrengthOptimize(int numParameters, State& s, Model& aModel):
        numKnobs(numParameters), OptimizerSystem(numParameters), si(s),
        osimModel(aModel){}

int objectiveFunc(  const Vector &newControls, bool new_coefficients, Real& f ) const {
        State s = si; // make a copy of initial states

        //Update the maximum isometric force
        const Set<Muscle> &muscleSet = osimModel.getMuscles();
        for(int j=0; j<Datasets;j++){
                for(int i=0;i< muscleSet.getSize(); i++ ){
                        if (Mgroup[i]==j+1){
                        muscleSet.get(i).setMaxIsometricForce(newControls[j]*maxISO[i]);
                        }
                }
        }

        double MusForce,MomentArm,moment;
        Vector SumMoment(Datasets,0.0);
        const CoordinateSet& coords = osimModel.getCoordinateSet();
        f=0;
        for(int j=0; j<Datasets;j++){ //Set coordinate for moment
                for(int i=0;i<coords.getSize();i++){
                        if(coordIdx[i+coords.getSize()*j]!=-1){
                                coords.get(i).setValue(s,coordV[i+coords.getSize()*j]);
                        }
                        else{
                                coords.get(i).setValue(s,coords.get(i).getDefaultValue());
                        }
                }
                moment=0;
```

```
                SumMoment[j]=0.0;
                osimModel.equilibrateMuscles(s);
                for(int i=0;i< muscleSet.getSize(); i++ ){ //calculate muscle force & moment arm
                        MusForce=muscleSet.get(i).getForce(s);
                        MomentArm = uscleSet.get(i).computeMomentArm
                                        (s,osimModel.getCoordinateSet().get(Jidx[j]) );
                        if (direction[j]>0){ // only add in moments that increase value
                                moment=MusForce*MomentArm;
                        }
                        else{
                                moment=-1*MusForce*MomentArm;
                        }
                        if (moment>0){
                                SumMoment[j]=SumMoment[j]+moment;
                        }
                }
                f=f+(exMoment[j]-SumMoment[j])*(exMoment[j]-SumMoment[j]);
        }

        stepCount++;
        if( f < bestSoFar){
                bestSoFar = f;
                for(int j=0; j<Datasets;j++){
                        scale_factor[j+1]=newControls[j];
                }
        }
    return(0);
  }
        int setCoordIdx(Vector coord_index){ coordIdx=coord_index; return(0);}
        int setCoordValue(Vector coord_value){ coordV=coord_value; return(0);}
        int setJointIndex(Vector Jindex){ Jidx=Jindex; return(0);}
        int setDirection(Vector Dir){ direction=Dir; return(0); }
        int setExperimentalMoment(Vector EXMO){         exMoment=EXMO; return(0); }
        int setMaximumIsometric(Vector MaxIsoForce){ maxISO=MaxIsoForce; return(0);}
        int setMuscleGroup(Vector muscleGroup){   Mgroup=muscleGroup; return(0);}
        int setNumberOfDataSets(int datasets){Datasets=datasets; return(0);}

private:
   int numKnobs,Datasets;
        State& si;
        Model& osimModel;
        Vector coordIdx,coordV,Jidx,direction,Mgroup,exMoment,maxISO;
};
```

```
//////////////////MAIN PROGRAM////////////////////////////////////////////////////////////////////////////////
 // Imports all files in the current directory and calls the strength scaling function if .xml
int main()
{
try{
	struct dirent *pDirent;
	DIR *pDir;
	pDir = opendir (".."); // Look in current directory
	string setup="";
	while ((pDirent = readdir(pDir)) != NULL) {// Loop through all files
		setup=pDirent->d_name;
		if (setup.find(".xml") != std::string::npos) {
			Xml::Document doc(setup);
			Xml::Element root = doc.getRootElement();
			for (Xml::element_iterator p=root.element_begin(); p !=
			root.element_end(); ++p){
				if (p->getElementTag()=="StrengthScaleTool"){
					stepCount=0; // Reset step count
					bestSoFar=Infinity; // Reset objective value
					StrengthScaling(setup); // Call strength scaling
				}
			}
		}
	 }
	closedir (pDir);
}
catch (const std::exception& ex){ std::cout << ex.what() << std::endl; return 1;}
	return 0;
}

////////////////////////////// Strength scaling function//////////////////////////////////////////////////////
// Reads the tags in the setup file and scales the model
int StrengthScaling(string setup){
try {

std::clock_t startTime = std::clock();  //Start Clock

// Initialize Variables
string Mdl="";
string OutputName="";
string str="";
string avg_scale="";
string ant="";
string scale_file="";
int num=-1; // index variable for vectors
int flag; // flag for error handeling
```

```
int flag_2; // second flag for error handeling
int PCSA_n=0; // number of PCSA tags in the setup file
int volume_n=0; //number of volume tags in the setup file
int datasets=0; // number of experimental moments in the model
double temporary=0.0; // variable used for the temporary storage of doubles
Xml::Document doc(setup); // Read in Setup File
Xml::Element root = doc.getRootElement();

// Run through XML tags to get Model and Number of Datasets
for (Xml::element_iterator p=root.element_begin(); p != root.element_end(); ++p){
        if (p->getElementTag()=="StrengthScaleTool"){
                for (Xml::element_iterator q=p->element_begin(); q != p->element_end(); ++q){
                        if(q->getElementTag()=="Model"){ Mdl = q->getValueAs<string>();}
                        else if (q->getElementTag()=="Moment"){ datasets=datasets+1; }
                        else if (q->getElementTag()=="OutputName"){OutputName= q-
                                >getValueAs<string>();}
                }
        }
}
//Load Model and define variables that depend on the model
Model osimModel(Mdl);
const Set<Muscle> &muscleSet = osimModel.getMuscles();
int numMus=muscleSet.getSize();
State& si = osimModel.initSystem();
const CoordinateSet& coords = osimModel.getCoordinateSet();
Vector EXMO(datasets,0.0); // Vector of experimental moment values
Vector Dir(datasets,1);   // Vector of the direction of experimental moment
Vector Jindex(datasets,1);   // Vector of joint index for which experimental moment is about
Vector coord_index(datasets*coords.getSize(),-1); // Vector of index  of the coordinate
Vector coord_value(datasets*coords.getSize(),0.0); // Vector of posture coordinates
Vector MaxIsoForce(numMus,0.0); // vector that stores original MaxIsoForce of each muscle
Vector muscleGroup(numMus,0.0); // vector of which group each muscle belongs to
scale_factor.resize(datasets+1);

for (Xml::element_iterator p=root.element_begin(); p != root.element_end(); ++p){
  if (p->getElementTag()=="StrengthScaleTool"){
        for (Xml::element_iterator q=p->element_begin(); q != p->element_end(); ++q){
                if (q->getElementTag()=="Moment"){
                        num=num+1;
                        for (Xml::element_iterator w=q->element_begin(); w !=
                        q->element_end(); ++w){
                                if (w->getElementTag()=="Direction"){
                                Dir[num]=w->getValueAs<int>();}
                                else if (w->getElementTag()=="Value"){
                                EXMO[num]= w->getValueAs<double>();}
                                else if (w->getElementTag()=="Joint"){
```

```
                    flag=0;
                    str=w->getValueAs<string>();
                    for(int j=0;j< coords.getSize();j++){
                        if(coords.get(j).getName()==str){
                            Jindex[num]=j;
                            flag=1;
                        }
                    }
                }
                else if (w->getElementTag()=="Muscles"){
                    flag=0;
                    str=w->getValueAs<string>();
                    for(int j=0;j< numMus;j++){
                        if(muscleSet.get(j).getName()==str){
                            flag=1;
                            muscleGroup[j]=num+1;
                        }
                    }
                }
                else if (w->getElementTag()=="Coordinates"){
                    flag=0;
                    for (Xml::element_iterator x=w->element_begin(); x !=
                    w->element_end(); ++x){
                        if (x->getElementTag()=="Name"){
                            str=x->getValueAs<string>();
                            flag=1;
                        }
                        else if (x->getElementTag()=="Number"){
                            flag_2=0;
                            temporary=x->getValueAs<double>();
                            // coordinate value
                            for(int j=0;j< coords.getSize();j++){
                                if(coords.get(j).getName()==str){
                                temporary =
                            convertDegreesToRadians(temporary);
                            coord_value[coords.getSize()*num+j] =
                            temporary;
                            coord_index[coords.getSize()*num+j]=j;
                            flag_2=1;
                                }
                            }
                        }
                    }
                }
            }
        }
```

```
        }
    }
}

// Set muscle activations
for(int i=0; i< numMus; i++ ){
        muscleSet[i].setActivation(si, 1);
        MaxIsoForce[i]=muscleSet.get(i).getMaxIsometricForce();
}
osimModel.equilibrateMuscles(si);
//Optimization
StrengthOptimize sys(datasets, si, osimModel);
sys.setCoordIdx(coord_index);
sys.setCoordValue(coord_value);
sys.setJointIndex(Jindex);
sys.setDirection(Dir);
sys.setExperimentalMoment(EXMO);
sys.setMaximumIsometric(MaxIsoForce);
sys.setMuscleGroup(muscleGroup);
sys.setNumberOfDataSets(datasets);
/* Define initial values and bounds for the controls to optimize */
Real f = NaN;
Vector controls(datasets, 1.05); // 1.05 for start seems to get stuck if 1 is start point
Optimizer opt(sys, SimTK::BestAvailable);
opt.setConvergenceTolerance(0.0001);
opt.useNumericalGradient(true);
opt.setMaxIterations(2000);
opt.setLimitedMemoryHistory(500);
f = opt.optimize(controls); // Optimize it!
// Create an average scale factor for muscles in group 0 that do not get scaled by optimization
scale_factor[0]=0.0;
temporary=0.0;
for(int j=0; j<datasets+1;j++){ temporary=temporary+scale_factor[j];}
scale_factor[0] = temporary / ((double)datasets);
// Apply scale factors to base model
for(int i=0; i< numMus; i++ ){
        for(int j=0; j< datasets+1; j++ ){
                if (muscleGroup[i]==j){
                        muscleSet.get(i).setMaxIsometricForce(scale_factor[j]*MaxIsoForce[i]);
                }
        }
}
osimModel.print(OutputName);
}
  catch (const std::exception& ex){std::cout << ex.what() << std::endl; return 1; }
return(0); }
```

Appendix I: Stability for Chapter 3

This appendix contains each subject's calculated stability (percent of the empirical stability limit in the direction of the transverse force) for each task target used in Chapter 3. Data are presented in 2 tables, one for unimanual and one for bimanual. Missing data in these tables are for the simulations that were removed because the optimization failed to converge or tracking error was over 5˚ (see Tables 3.1). Furthermore, 0˚ target was not simulated for bimanual tasks since these tasks resulted in extremely restricted handle motion and joint rotations.

Subject Code	Unimanual											
	Pulling Task Targets						Pushing Task Targets					
	20°	0°	45°	90°	135°	170°	20°	0°	45°	90°	135°	170°
M1	101.316	62.608	32.447	58.481	60.008	90.471	104.632	101.498	79.059	111.717	135.047	74.325
M2	88.006	103.666	101.260	54.136	77.580	75.300	92.129	110.601	42.111	74.995	126.897	73.054
M3	63.824	102.824	29.820	33.202	47.597	80.557	101.352	113.651	104.072	65.497	82.305	43.616
M4	101.854	53.411	28.193	56.261	59.239	67.203	-	106.510	75.435	100.811	116.464	100.830
M5	-	57.007	38.955	44.047	40.820	69.246	103.528	110.014	100.754	114.855	100.972	101.547
M6	38.438	101.898	39.741	49.949	66.310	57.744	101.498	101.974	50.566	76.184	101.880	67.993
F1	85.060	41.357	39.728	33.242	100.318	101.463	104.403	108.365	48.610	97.132	116.688	108.885
F2	101.231	29.141	60.386	65.249	74.622	101.047	103.523	107.438	101.884	146.732	155.208	101.921
F3	102.561	100.841	60.329	42.145	73.533	79.580	140.066	103.338	102.364	101.715	100.953	100.989
F4	112.236	100.342	39.560	61.958	106.266	67.483	103.170	101.699	102.683	100.570	138.916	104.788
F5	72.074	39.554	40.833	44.089	49.462	76.977	137.752	105.368	102.414	100.326	125.719	102.102
F6	63.745	51.736	52.320	51.643	57.855	75.650	101.938	102.713	63.122	69.241	140.167	100.989
F7	75.945	-	48.588	50.515	51.714	67.976	94.981	106.523	102.078	99.989	107.555	100.438
F8	80.114	43.293	37.362	42.360	48.033	88.609	100.494	112.141	96.818	91.711	123.815	76.244

Subject Code	Bimanual											
	Pulling Task Targets						Pushing Task Targets					
	20°	0°	45°	90°	135°	170°	20°	0°	45°	90°	135°	170°
M1	72.495	-	28.241	55.782	99.525	71.783	99.676	-	59.097	117.172	104.924	86.371
M2	65.940	-	24.963	55.193	-	79.261	90.999	-	30.510	99.443	76.976	93.123
M3	50.806	-	34.634	52.470	71.873	74.150	101.212	-	34.300	99.944	101.227	50.117
M4	-	-	33.070	43.080	73.423	83.647	98.723	-	59.852	94.719	109.541	102.024
M5	83.861	-	39.711	51.886	67.471	90.973	101.732	-	55.980	108.048	116.374	120.349
M6	91.960	-	33.034	60.442	75.751	54.270	94.157	-	54.903	91.367	74.558	55.558
F1	78.842	-	61.379	45.533	84.022	100.968	-	-	43.428	66.836	92.388	114.023
F2	-	-	-	62.487	89.973	95.785	102.866	-	-	136.328	135.571	-
F3	103.416	-	65.230	100.075	101.637	75.914	81.940	-	53.351	84.833	84.350	81.917
F4	-	-	84.158	81.805	100.682	83.750	-	-	102.552	111.779	126.765	125.680
F5	59.615	-	58.914	75.388	80.880	80.209	100.701	-	71.999	101.559	100.458	76.419
F6	80.380	-	57.699	80.370	59.255	60.607	95.293	-	31.367	77.688	89.483	100.042
F7	100.970	-	63.132	64.098	53.777	102.410	-	-	100.714	118.281	100.096	90.266
F8	89.740	-	47.337	79.192	96.783	46.370	95.271	-	33.943	115.950	99.937	60.743

Appendix J: Anthropometric Data for Chapter 4

This appendix contains the subject codes and anthropometric data (height, weight, etc.) of subjects who participated in the experimental protocol for Chapter 4.

Subject Code	Height (cm)	Weight (lbs)	Age
M1	175.3	165.4	25
M2	179.7	215.2	20
F1	158.8	134.4	20
F2	167.6	165.0	25

Appendix K: Stability for Chapter 4

This appendix contains each subject's calculated stability (percent of the empirical stability limit in the direction of the transverse force) for each simulation condition in Chapter 4. Data are divided into 4 tables, two for abduction (low and high demand) and two for flexion (low and high demand). Missing data in these tables are for the simulations that were removed because the optimization failed to converge (see Tables 4.1).

Force Constraint	EMG Constraint	Abduction Low Demand			
		Subject Codes			
		M1	M2	F1	F2
Concavity Compression	±5% All	71.022	72.477	62.921	86.887
	Timing All	102.436	67.718	59.154	100.068
	±5% Subset	117.360	102.931	100.100	104.169
	Timing Subset	122.632	102.822	99.850	103.734
	None	117.272	102.703	101.136	103.239
Scapulohumeral Balance	±5% All	71.022	72.652	62.867	86.592
	Timing All	95.997	67.962	60.618	95.926
	±5% Subset	115.722	101.943	98.756	103.977
	Timing Subset	-	101.020	93.126	100.598
	None	-	100.745	100.503	102.761
one	±5% All	71.022	72.598	62.860	86.644
	Timing All	117.915	67.862	57.560	105.365
	±5% Subset	175.183	138.579	100.134	142.985
	Timing Subset	181.128	139.063	104.373	141.709
	None	245.853	139.869	117.174	138.766

Force Constraint	EMG Constraint	Abduction High Demand			
		Subject Codes			
		M1	M2	F1	F2
Concavity Compression	±5% All	54.573	-	59.346	83.811
	Timing All	88.864	68.663	102.819	102.803
	±5% Subset	102.672	103.807	102.698	105.868
	Timing Subset	102.338	103.907	102.366	104.600
	None	102.977	103.154	102.366	105.053
Scapulohumeral Balance	±5% All	55.722	-	59.313	83.81
	Timing All	81.978	68.609	101.553	101.144
	±5% Subset	100.024	103.291	101.016	102.967
	Timing Subset	101.126	102.519	100.445	102.464
	None	102.000	103.679	100.445	102.832
None	±5% All	57.063	-	59.261	83.747
	Timing All	83.456	68.620	140.082	141.884
	±5% Subset	270.795	160.349	165.528	160.673
	Timing Subset	279.148	157.505	167.717	153.225
	None	291.627	160.521	167.717	172.087

Force Constraint	EMG Constraint	Flexion Low Demand			
		Subject Codes			
		M1	M2	F1	F2
Concavity Compression	±5% All	88.827	90.363	100.339	96.527
	Timing All	84.228	84.622	100.232	68.983
	±5% Subset	67.032	77.024	73.978	75.703
	Timing Subset	71.597	72.955	73.046	73.726
	None	104.012	102.964	102.888	103.092
Scapulohumeral Balance	±5% All	87.777	88.490	87.378	88.817
	Timing All	84.283	84.743	87.110	68.875
	±5% Subset	67.209	75.437	73.975	75.455
	Timing Subset	71.869	72.983	73.136	73.700
	None	-	101.068	101.434	102.805
None	±5% All	89.018	90.309	104.276	96.563
	Timing All	84.282	84.752	101.717	68.572
	±5% Subset	66.939	77.189	74.362	75.446
	Timing Subset	71.732	72.959	73.099	73.440
	None	168.677	160.182	198.031	194.166

Force Constraint	EMG Constraint	Flexion High Demand			
		Subject Codes			
		M1	M2	F1	F2
Concavity Compression	±5% All	61.108	71.946	76.511	63.405
	Timing All	82.097	72.988	92.778	101.928
	±5% Subset	65.597	78.568	75.593	72.507
	Timing Subset	84.597	80.217	99.577	100.544
	None	102.566	107.161	104.300	105.071
Scapulohumeral Balance	±5% All	61.069	71.983	77.555	63.562
	Timing All	80.978	73.062	93.167	100.160
	±5% Subset	65.664	78.586	75.573	72.383
	Timing Subset	85.148	80.047	99.119	100.146
	None	100.937	102.689	101.738	102.100
None	±5% All	61.113	71.826	77.148	63.253
	Timing All	82.535	73.045	92.831	109.304
	±5% Subset	66.007	78.579	75.597	72.490
	Timing Subset	82.671	80.248	100.446	107.226
	None	154.323	203.738	220.346	223.125

Appendix L: Joint Reaction Forces for Chapter 4

This appendix contains each subjects' peak joint reaction force (N) for each simulation condition in Chapter 4. Data are divided into 4 tables, two for abduction (low and high demand) and two for flexion (low and high demand). Missing data in these tables are for the simulations that were removed because the optimization failed to converge (see Tables 4.1).

Force Constraint	EMG Constraint	Abduction Low Demand			
		Subject Codes			
		M1	M2	F1	F2
Concavity Compression	±5% All	2853.95	2651.88	2629.18	2822.56
	Timing All	2864.05	2614.33	2607.81	2646.57
	±5% Subset	2094.34	2544.48	1732.98	2232.07
	Timing Subset	2218.40	2555.65	1757.25	2580.40
	None	2541.15	2525.82	1799.34	2536.68
Scapulohumeral Balance	±5% All	2867.36	2651.06	2626.90	2822.22
	Timing All	2864.29	2609.95	2607.29	2662.25
	±5% Subset	2149.02	2536.17	1733.59	2296.44
	Timing Subset	-	2541.33	1730.26	2576.76
	None	-	2568.84	1800.55	2579.55
None	±5% All	2867.40	2646.96	2627.54	2822.64
	Timing All	2863.12	2610.37	2613.50	2666.31
	±5% Subset	2113.46	2540.85	1745.48	2233.59
	Timing Subset	2126.07	2540.43	1784.37	2596.71
	None	2471.68	2541.86	1810.50	2527.92

Force Constraint	EMG Constraint	Abduction High Demand			
		Subject Codes			
		M1	M2	F1	F2
Concavity Compression	±5% All	2729.94	-	3160.36	3053.83
	Timing All	2908.46	2834.76	3152.57	3001.62
	±5% Subset	2879.87	2902.63	3084.22	3095.68
	Timing Subset	2915.86	2897.48	3104.80	2987.59
	None	2918.68	2899.21	3104.80	2909.52
Scapulohumeral Balance	±5% All	2684.29	-	3159.32	3056.25
	Timing All	2895.19	2827.17	3172.77	3005.84
	±5% Subset	2887.65	2898.26	3079.00	3060.19
	Timing Subset	2891.50	2913.15	3105.20	3006.75
	None	2913.86	2901.27	3105.20	2913.67
None	±5% All	2719.65	-	3184.21	3063.61
	Timing All	2912.35	2841.04	3158.15	3013.46
	±5% Subset	2873.25	2900.54	3082.86	3082.85
	Timing Subset	2882.82	2897.50	3104.81	2982.11
	None	2925.34	2893.32	3104.81	2893.32

Force Constraint	EMG Constraint	Flexion Low Demand			
		Subject Codes			
		M1	M2	F1	F2
Concavity Compression	±5% All	2377.13	1966.12	2431.61	2093.07
	Timing All	2367.31	1933.71	2408.58	1807.33
	±5% Subset	2283.11	2058.30	2286.75	1914.44
	Timing Subset	2287.55	2040.31	2256.34	1876.35
	None	1552.06	1992.74	1561.47	1513.60
Scapulohumeral Balance	±5% All	2373.52	1971.30	2407.16	2012.17
	Timing All	2365.88	1921.21	2474.49	1799.41
	±5% Subset	2265.37	2084.44	2292.44	1919.78
	Timing Subset	2291.00	2046.99	2256.11	1890.04
	None	-	1958.61	1562.44	1510.27
None	±5% All	2375.57	1964.27	2419.79	2090.41
	Timing All	2359.44	1929.21	2415.74	1793.07
	±5% Subset	2271.75	2057.37	2297.11	1928.10
	Timing Subset	2289.52	2039.49	2257.95	1880.40
	None	1560.59	1946.75	1560.58	1495.43

Force Constraint	EMG Constraint	Flexion High Demand			
		Subject Codes			
		M1	M2	F1	F2
Concavity Compression	±5% All	2448.48	2425.22	2896.61	2499.54
	Timing All	2492.31	2742.37	3024.37	2563.74
	±5% Subset	2509.75	2598.68	3040.48	2467.19
	Timing Subset	2519.56	2805.14	2888.28	2471.84
	None	2651.04	2793.83	2795.16	2407.78
Scapulohumeral Balance	±5% All	2441.34	2438.72	2895.55	2492.37
	Timing All	2469.51	2748.02	3021.11	2605.84
	±5% Subset	2515.18	2602.79	3003.48	2464.02
	Timing Subset	2471.99	2802.36	2894.65	2476.24
	None	2638.83	2797.94	2789.47	2375.06
None	±5% All	2464.71	2427.71	2904.98	2508.36
	Timing All	2488.73	2745.50	3035.90	2591.95
	±5% Subset	2529.91	2592.36	3004.64	2469.56
	Timing Subset	2502.13	2803.69	2937.92	2468.18
	None	2648.10	2807.94	2804.20	2409.53

Appendix M: Rotator Cuff Activations for Chapter 4

This appendix contains each subject's peak rotator cuff activations for supraspinatus (Ssp), infraspinatus (Isp), subscapularis (Ssc) and the sum of these muscle for each simulation condition in Chapter 4. Concavity compression is abbreviated as CC and scapulohumeral balance is abbreviated as SB. Data are divided into 4 tables, two for abduction (low and high demand) and two for flexion (low and high demand). Missing data in these tables are for the simulations that were removed because the optimization failed to converge (see Tables 4.1).

Force	EMG	Abduction Low Demand															
		Subject Codes															
		M1				M2				F1				F2			
		Ssp	Isp	Ssc	Sum	Ssp	Isp	Ssc	Sum	Ssp	Isp	Ssc	Sum	Ssp	Isp	Ssc	Sum
CC	±5% All	1.00	1.00	0.97	2.97	1.00	1.00	0.95	2.95	1.00	1.00	0.80	2.79	1.00	1.00	1.00	2.99
	Timing All	1.00	1.00	0.97	2.97	1.00	1.00	0.95	2.95	0.99	0.93	0.81	2.73	0.99	0.94	1.00	2.92
	±5% Subset	0.99	0.65	0.79	2.43	0.99	0.9.0	0.72	2.62	0.87	0.52	0.40	1.79	0.98	0.61	0.72	2.32
	Timing Subset	0.99	0.70	0.81	2.50	0.99	0.90	0.73	2.62	0.87	0.53	0.41	1.81	0.98	0.75	0.86	2.59
	None	0.99	0.75	0.73	2.47	0.98	0.83	0.77	2.58	0.87	0.55	0.42	1.84	0.98	0.73	0.84	2.55
SB	±5% All	1.00	1.00	0.97	2.97	1.00	1.00	0.95	2.95	1.00	1.00	0.8	2.79	1.00	1.00	1.00	2.99
	Timing All	1.00	1.00	0.97	2.97	1.00	1.00	0.95	2.95	0.99	0.92	0.81	2.72	0.99	0.94	1.00	2.93
	±5% Subset	0.99	0.66	0.80	2.46	0.99	0.9.0	0.73	2.62	0.87	0.52	0.40	1.79	0.98	0.64	0.74	2.37
	Timing Subset	-	-	-	-	0.99	0.90	0.73	2.62	0.87	0.52	0.40	1.78	0.98	0.75	0.86	2.58
	None	-	-	-	-	0.98	0.84	0.78	2.60	0.87	0.55	0.42	1.84	0.98	0.76	0.86	2.60
None	±5% All	1.00	1.00	0.97	2.97	1.00	1.00	0.95	2.95	1.00	1.00	0.80	2.79	1.00	1.00	1.00	2.99
	Timing All	1.00	1.00	0.97	2.97	1.00	1.00	0.95	2.95	0.99	0.94	0.81	2.74	0.99	0.94	1.00	2.93
	±5% Subset	0.99	0.66	0.80	2.45	0.99	0.91	0.73	2.62	0.86	0.53	0.41	1.81	0.98	0.60	0.72	2.30
	Timing Subset	0.99	0.66	0.79	2.45	0.99	0.90	0.73	2.62	0.86	0.55	0.42	1.83	0.98	0.76	0.86	2.60
	None	0.99	0.72	0.70	2.41	0.98	0.83	0.77	2.58	0.87	0.55	0.43	1.85	0.98	0.73	0.84	2.55

Force	EMG	Abduction High Demand															
		Subject Codes															
		M1				M2				F1				F2			
		Ssp	Isp	Ssc	Sum	Ssp	Isp	Ssc	Sum	Ssp	Isp	Ssc	Sum	Ssp	Isp	Ssc	Sum
CC	±5% All	1.00	1.00	1.00	3.00	-	-	-	-	1.00	1.00	1.00	3.00	1.00	1.00	1.00	3.00
	Timing All	1.00	1.00	1.00	3.00	1.00	1.00	1.00	3.00	1.00	1.00	1.00	3.00	1.00	1.00	0.99	2.99
	±5% Subset	1.00	1.00	1.00	3.00	1.00	1.00	0.87	2.87	1.00	1.00	1.00	3.00	1.00	1.00	0.95	2.95
	Timing Subset	1.00	1.00	1.00	3.00	1.00	1.00	0.87	2.87	1.00	1.00	1.00	3.00	1.00	1.00	0.93	2.93
	None	1.00	1.00	0.91	2.91	1.00	1.00	0.87	2.87	1.00	1.00	1.00	3.00	1.00	1.00	0.93	2.93
SB	±5% All	1.00	1.00	1.00	3.00	-	-	-	-	1.00	1.00	1.00	3.00	1.00	1.00	1.00	3.00
	Timing All	1.00	1.00	1.00	3.00	1.00	1.00	1.00	3.00	1.00	1.00	1.00	3.00	1.00	1.00	0.99	2.99
	±5% Subset	1.00	1.00	1.00	3.00	1.00	1.00	0.87	2.87	1.00	1.00	1.00	3.00	1.00	1.00	0.95	2.95
	Timing Subset	1.00	1.00	1.00	3.00	1.00	1.00	0.87	2.87	1.00	1.00	1.00	3.00	1.00	1.00	0.93	2.93
	None	1.00	1.00	0.91	2.91	1.00	1.00	0.87	2.87	1.00	1.00	1.00	3.00	1.00	1.00	0.93	2.93
None	±5% All	1.00	1.00	1.00	3.00	-	-	-	-	1.00	1.00	1.00	3.00	1.00	1.00	1.00	3.00
	Timing All	1.00	1.00	1.00	3.00	1.00	1.00	1.00	3.00	1.00	1.00	1.00	3.00	1.00	1.00	0.99	2.99
	±5% Subset	1.00	1.00	1.00	3.00	1.00	1.00	0.86	2.86	1.00	1.00	1.00	3.00	1.00	1.00	0.94	2.94
	Timing Subset	1.00	1.00	1.00	3.00	1.00	1.00	0.87	2.87	1.00	1.00	1.00	3.00	1.00	1.00	0.93	2.93
	None	1.00	1.00	0.91	2.91	1.00	1.00	0.87	2.87	1.00	1.00	1.00	3.00	1.00	1.00	0.94	2.94

Force	EMG	Flexion Low Demand															
		Subject Codes															
		M1				M2				F1				F2			
		Ssp	Isp	Ssc	Sum	Ssp	Isp	Ssc	Sum	Ssp	Isp	Ssc	Sum	Ssp	Isp	Ssc	Sum
CC	±5% All	0.93	1.00	0.87	2.79	0.99	0.97	0.89	2.85	0.98	0.99	0.98	2.95	0.99	0.89	0.99	2.87
	Timing All	0.95	1.00	0.84	2.79	0.98	0.94	0.79	2.71	0.97	0.99	0.98	2.93	0.96	0.77	0.98	2.71
	±5% Subset	0.83	0.99	0.91	2.73	0.94	0.94	0.83	2.71	0.93	0.96	0.98	2.88	0.90	0.81	0.97	2.68
	Timing Subset	0.84	0.98	0.90	2.72	0.91	0.93	0.80	2.64	0.92	0.95	0.98	2.85	0.85	0.80	0.96	2.61
	None	0.42	0.55	0.39	1.36	0.37	0.78	0.52	1.66	0.28	0.58	0.58	1.44	0.27	0.59	0.58	1.45
SB	±5% All	0.93	1.00	0.87	2.79	0.99	0.98	0.89	2.86	0.98	0.99	0.98	2.95	0.99	0.91	0.99	2.89
	Timing All	0.95	1.00	0.84	2.79	0.97	0.94	0.79	2.70	0.96	0.99	0.97	2.91	0.96	0.78	0.98	2.73
	±5% Subset	0.82	0.99	0.91	2.72	0.94	0.94	0.83	2.71	0.93	0.96	0.98	2.87	0.89	0.82	0.97	2.67
	Timing Subset	0.86	0.98	0.90	2.74	0.90	0.94	0.80	2.64	0.92	0.95	0.98	2.85	0.86	0.79	0.95	2.60
	None	-	-	-	-	0.35	0.77	0.52	1.64	0.28	0.58	0.58	1.44	0.30	0.59	0.57	1.46
None	±5% All	0.93	1.00	0.87	2.79	0.99	0.98	0.89	2.85	0.98	0.99	0.99	2.96	0.99	0.88	1.00	2.87
	Timing All	0.95	1.00	0.84	2.79	0.97	0.94	0.80	2.72	0.97	0.99	0.98	2.94	0.96	0.78	0.98	2.71
	±5% Subset	0.83	0.99	0.91	2.73	0.93	0.94	0.83	2.70	0.93	0.97	0.98	2.88	0.92	0.81	0.97	2.69
	Timing Subset	0.84	0.98	0.90	2.72	0.90	0.93	0.80	2.64	0.92	0.95	0.98	2.85	0.85	0.80	0.95	2.60
	None	0.42	0.56	0.34	1.32	0.35	0.77	0.52	1.64	0.25	0.58	0.58	1.41	0.24	0.59	0.57	1.41

Force	EMG	Flexion High Demand															
		Subject Codes															
		M1				M2				F1				F2			
		Ssp	Isp	Ssc	Sum	Ssp	Isp	Ssc	Sum	Ssp	Isp	Ssc	Sum	Ssp	Isp	Ssc	Sum
CC	±5% All	1.00	1.00	0.98	2.98	1.00	1.00	1.00	3.00	1.00	1.00	1.00	3.00	1.00	1.00	1.00	3.00
	Timing All	1.00	1.00	0.98	2.98	1.00	1.00	1.00	3.00	1.00	1.00	1.00	3.00	1.00	1.00	1.00	3.00
	±5% Subset	1.00	1.00	0.98	2.98	1.00	1.00	1.00	3.00	1.00	1.00	1.00	3.00	1.00	1.00	1.00	3.00
	Timing Subset	1.00	1.00	0.99	2.98	1.00	1.00	1.00	3.00	1.00	1.00	1.00	3.00	0.99	1.00	1.00	2.99
	None	1.00	1.00	0.47	2.47	0.93	1.00	0.55	2.48	0.99	1.00	0.59	2.58	0.70	0.97	0.63	2.30
SB	±5% All	1.00	1.00	0.98	2.98	1.00	1.00	1.00	3.00	1.00	1.00	1.00	3.00	1.00	1.00	1.00	3.00
	Timing All	1.00	1.00	0.98	2.98	1.00	1.00	1.00	3.00	1.00	1.00	1.00	3.00	1.00	1.00	1.00	3.00
	±5% Subset	1.00	1.00	0.98	2.98	1.00	1.00	1.00	3.00	1.00	1.00	1.00	3.00	1.00	1.00	1.00	3.00
	Timing Subset	1.00	1.00	0.98	2.98	1.00	1.00	1.00	3.00	1.00	1.00	1.00	3.00	0.99	1.00	1.00	2.99
	None	1.00	1.00	0.48	2.48	0.94	1.00	0.55	2.48	0.99	1.00	0.59	2.58	0.68	0.98	0.64	2.29
None	±5% All	1.00	1.00	0.98	2.98	1.00	1.00	1.00	3.00	1.00	1.00	1.00	3.00	1.00	1.00	1.00	3.00
	Timing All	1.00	1.00	0.98	2.98	1.00	1.00	1.00	3.00	1.00	1.00	1.00	3.00	1.00	1.00	1.00	3.00
	±5% Subset	1.00	1.00	0.98	2.98	1.00	1.00	1.00	3.00	1.00	1.00	1.00	3.00	1.00	1.00	1.00	2.99
	Timing Subset	1.00	1.00	0.98	2.98	1.00	1.00	1.00	3.00	1.00	1.00	1.00	3.00	1.00	1.00	1.00	2.99
	None	1.00	1.00	0.47	2.47	0.94	1.00	0.55	2.49	0.99	1.00	0.58	2.57	0.67	0.97	0.62	2.26